

IMPACT OF IONIC AND POLAR INTERACTION BETWEEN HEAVY CRUDE OIL
AND SURFACTANTS DURING SURFACTANT-STEAM FLOODING PROCESSES

A Dissertation

by

MURTDHA ALI I ALSHAIKH

Submitted to the Office of Graduate and Professional Studies of
Texas A&M University
in partial fulfillment of the requirements for the degree of

DOCTOR OF PHILOSOPHY

Chair of Committee,	Berna Hascakir
Committee Members,	Anthony Knap
	Hadi Nasrabadi
	Sara Abedi
Head of Department,	Jeff Spath

May 2020

Major Subject: Petroleum Engineering

Copyright 2020 Murtdha Ali I Alshaikh

ABSTRACT

Surfactant injection as additives to steam injection is a concept that has great potential to enhance oil recovery efficiency of heavy oil and bitumen. Steam injection enhances oil recovery by introducing heat to the reservoir, decreasing oil viscosity, reducing residual oil, and distillation process of light oil fractions. Although steam has been successfully applied to enhance oil recovery, it has many challenges including heat losses, steam gravity override and channeling which decrease the oil recovery efficiency and can raise the cost above the economic limit. Steam injection is, also, harmful to the environment due to greenhouse gases (GHG) emission, water pollution, and contamination of groundwater aquifers. To overcome these challenges, surfactants have been suggested to be co-injected with steam to enhance microscopic displacement, reduce steam usage, and increase oil recovery.

The microscopic oil recovery enhancement comes from the different electrostatic interactions during surfactant-steam process. Surfactant literature is in general built on light/medium oil reservoirs, which are form mostly by nonpolar hydrocarbon. For high-viscosity crudes, the situation can be different due to the high-polarity components of crude oil. Asphaltene and resins are known as polar components of crude oils, while saturates and aromatics are nonpolar. It is not very well-known how surfactants interact with those crude oil components in the presence of steam. Importantly, the mutual interactions between crude oil components, water, and surfactant examination are essential to determine the surfactant candidate for steam-surfactant flood. The focus of this research

is to study the microscopic interactions during enhance oil recovery process of surfactant-steam flooding and investigate the role of polar-polar interaction and ionic interaction.

Based on coreflood experimental results, the addition of surfactants improves the oil recovery of steam injection. The analyses suggest that polarity magnitude of crude oil is controlled by the mutual interaction of its polar fractions via dipole-dipole interaction and not by their quantities. The mutual interaction of crude oil fractions with surfactants in the presence of steam was visualized by optical microscopy and showed the negative impact of asphaltenes as emulsion inhibitor. During surfactant-steam flood, it appears that the surfactants interacted with the asphaltenes fractions via ion-ion or/and ion-dipole interactions, enhancing asphaltenes stability which is evident by its high content in the recovered oil of coreflood experiments and the high absolute values of the asphaltenes' zeta potential. Finally, the resulted addition of nonionic surfactants makes the separation of water-in-oil emulsion processes easier. In addition to this advantage, the economic analysis revealed that the nonionic surfactants are the most economical to use as steam additives.

DEDICATION

To my parents, my siblings, my wife, my daughter, and my friends.

ACKNOWLEDGMENTS

I want to express my thanks to Dr. Berna Hascakir for providing me with the opportunity to conduct research under her supervision. I am grateful for having her as my advisor and mentor. I appreciate her continuous guidance, support, and encouragement that she provided me throughout the course of this research.

I would also like to extend my gratitude to Dr. Anthony Knap, Dr. Hadi Nasrabadi, and Dr. Sara Abedi for serving on my research committee and providing their valuable inputs towards improving my research. I also want to acknowledge Saudi Aramco, which sponsored me as a PhD student.

CONTRIBUTORS AND FUNDING SOURCES

Contributors

This work was supervised by a dissertation committee consisting of Professor Berna Hascakir, Professor Sara Abedi, and Professor Hadi Nasrabadi of the Department of Petroleum Engineering and Professor Anthony Knap of the Department of Oceanography.

The biomarker determination data and gas chromatography results were conducted in part by Ibrahim Al Atwah and Stephen Sweet of Geochemical and Environmental Research Group.

All other work conducted for the dissertation was completed by the student, independently.

Funding Sources

I acknowledge the financial support for my research to complete my Ph.D. and the opportunity provided by the Heavy Oil, Oil shales, Oil sands, & Carbonate Analysis and Recovery Methods (HOCAM) Research Team at Texas A&M University, Petroleum Engineering Department.

I would like to thank my employer, Saudi Aramco, for sponsoring my education.

NOMENCLATURE

API	American Petroleum Institute
ASTM	American Society for Testing and Materials
EOR	Enhanced Oil Recovery
FTIR	Fourier Transform InfraRed
SARA	Saturates, Aromatics, Resins, and Asphaltenes
w.t.%	Weight percent
ρ	Density, g/cm ³
μ	Viscosity, cP
IFT	Interfacial Tension
cP	Centipoise
SDS	Sodium Dodecyl Sulfate
SDeS	Sodium Decyl Sulphate
SOS	Sodium Octyl Sulfate
CTAB	Hexadecyltrimethylammonium Bromide
MTAB	Myristyltrimethylammonium Bromide
DTAB	Dodecyltrimethylammonium Bromide
X-100	Triton™ X-100
X-114	Triton™ X-114
X-45	Triton™ X-45
TGA	Thermal Gravimetric Analyzer
DSC	Differential Scanning Calorimetry

IFT	Interfacial Tension
EOR	Enhanced Oil Recovery
ΔE	Difference in Atoms Electronegativities

TABLE OF CONTENTS

	Page
ABSTRACT	ii
DEDICATION.....	iv
ACKNOWLEDGMENTS.....	v
CONTRIBUTORS AND FUNDING SOURCES	vi
NOMENCLATURE	vii
TABLE OF CONTENTS	ix
LIST OF FIGURES	xi
LIST OF TABLES.....	xiv
1. INTRODUCTION	1
2. STATEMENT OF THE PROBLEM	13
3. MATERIALS AND METHODS.....	14
3.1 Materials	14
3.1.1 Crude Oil Characterization	14
3.1.2 Surfactant Characterization.....	17
3.2 Methods	20
3.2.1 Procedure for Tube Tests	20
3.2.2 Procedure for Optical Microscopic Tests	20
3.2.3 Procedure for Core Flood Tests	21
4. RESULTS AND DISCUSSION.....	26
4.1 Crude Oil Characterization.....	26
4.2 Thermal Stability of Surfactants	35
4.3 Bottle Test Results	37
4.4 Visualization of Water-Surfactant-Oil Interactions Under Optical Microscopy ...	44
4.5 Coreflood Experiments Results	52
4.5.1 Characterization of emulsion in Produced Oil Samples	56
4.5.2 Produced Water Analysis.....	59
4.5.3 Residual Oil Analysis and Spent Rock Inspection.....	61
4.6 Analysis of Residual and Produced Oil's Asphaltenes	65

4.6.1 Dielectric Constant Measurements (Dipole-Dipole Interaction)	71
4.6.2 Zeta Potential Measurements	74
4.6.3 Economic Analysis.....	77
5. CONCLUSION AND FUTURE WORK.....	78
5.1 Conclusions.....	78
5.2 Future Work.....	79
REFERENCES	81
APPENDIX A	95
APPENDIX B.....	97
APPENDIX C.....	100
APPENDIX D	114
APPENDIX E.....	118
APPENDIX F	125
APPENDIX G	127

LIST OF FIGURES

	Page
Figure 1.1—Steam injection zones and their temperature profiles, modified from (Prats 1982).	2
Figure 1.2—Illustration schematic of intermolecular electrostatic interactions and van der Waals between molecules.	9
Figure 1.3—Illustration of the electrical double layer around negativity charged solid and zeta potential, modified from (Kaszuba et al. 2010).	12
Figure 3.1—Schematic of the experimental setup for steam and surfactant-steam flooding experiments, reprinted with permission from (Alshaikh et al. 2019).	21
Figure 4.1—Temperature dependence of viscosity for Oil 1 and Oil 2.....	27
Figure 4.2—FTIR spectra for (A) initial oils and (B) their asphaltenes, modified with permission from (Al-Atwah et al. 2018).	30
Figure 4.3—GC-FID chromatograms showing overall normal alkane’s distribution, Pr: pristane, Ph: phytane, UCM: unresolved complex mixture, reprinted with permission from (Al-Atwah et al. 2018).	32
Figure 4.4—TGA results for surfactant solutions indicating the thermal stability temperature of surfactants. The red dashed line represents coreflood experimental temperature. All TGA/DSC curves are provided in Appendix B.....	36
Figure 4.5—Fourier Transform InfraRed (FTIR) spectra of (A) anionic, (B) cationic, and (C) nonionic surfactants, modified with permission from (Alshaikh et al. 2018).....	37
Figure 4.6—Visualization of bottle test results for oil-surfactant blends for Oil 1 (top) and Oil 2 (bottom).....	38
Figure 4.7—FTIR spectra of oil phase after mixing surfactant solution, modified with permission from (Alshaikh et al. 2019).	39
Figure 4.8—FTIR spectra of water phase after mixing surfactant solution with crude oils (bottle test) showing water and oil signatures, modified with permission from (Alshaikh et al. 2019).	41

Figure 4.9—Dielectric constants of water phase (A) and oil phase (B) of surfactant-crude oil blends taken from bottle tests.	42
Figure 4.10—Surfactant-crude oil interaction before and after steam exposure at 100x magnification; oil samples were exposed to steam at 150°C for 10 minutes at atmospheric pressure, modified with permission from (Alshaikh et al. 2018).	45
Figure 4.11—Anionic (top), cationic (middle), and nonionic (bottom) surfactant-resin fraction of crude oil and surfactant-asphaltene fraction of crude oil interactions before and after steam exposure at 100x magnification; oil samples were exposed to steam at 150°C for 10 minutes at atmospheric pressure, modified with permission from (Alshaikh et al. 2018).	46
Figure 4.12—Anionic surfactant-[resins+asphaltenes+aromatics+saturates fraction of crude oil] interaction before and after steam exposure at 100x magnification; oil samples were exposed to steam at 150°C for 10 minutes at atmospheric pressure, modified with permission from (Alshaikh et al. 2018).	48
Figure 4.13—Cationic surfactant-[resins+asphaltenes+aromatics+saturates fraction of crude oil] interaction before and after steam exposure at 100x magnification; oil samples were exposed to steam at 150°C for 10 minutes at atmospheric pressure.	48
Figure 4.14—Nonionic surfactant-[resins+asphaltenes+aromatics+saturates fraction of crude oil] interaction before and after steam exposure at 100x magnification; oil samples were exposed to steam at 150°C for 10 minutes at atmospheric pressure.	49
Figure 4.15— Anionic (top), cationic (middle), and nonionic (bottom) surfactant-[resins+aromatics+saturates fraction of crude oil] interaction before and after steam exposure at 100x magnification; oil samples were exposed to steam at 150°C for 10 minutes at atmospheric pressure.	51
Figure 4.16—Cumulative oil recovery from steam and surfactant-steam coreflood results.	55
Figure 4.17—Produced oil samples weight loss with time spent on the oven at 60°-70° C showing the difficulty of separating water-in-oil emulsions.	57
Figure 4.18—Ions concentration of produced water showing surfactants retention for three produced water samples that are collected from the begging of the coreflood (1), middle time (2) and close to the end (3) of the experiments.	

At the top anionic retention ions (sodium) and at the bottom cationic retention ions (bromide).....	60
Figure 4.19—Spent rock images for all experiments conducted with Oil 1. Injection is from left (inlet) to right (outlet). For experiment naming, refer to Table 3.2. .	62
Figure 4.20—Spent rock images for all experiments conducted with Oil 2. Injection is from left (inlet) to right (outlet). For experiment naming, refer to Table 3.2. .	63
Figure 4.21—Residual oil saturation for the average (A) and the comparison of the inlet and outlet (B) of core holder.....	65
Figure 4.22—FTIR spectra for produced oil samples from coreflood tests after water separation.	68
Figure 4.23—FTIR spectra for produced oil asphaltenes from steam and surfactant-steam injection.....	71
Figure 4.24—Dielectric constants values of produced oil (after thermal separation) from steam and surfactant-steam coreflood experiments showing polarity cancellation.....	72
Figure 4.25—Dielectric constants values of produced water from steam and surfactant-steam coreflood experiments showing polarity cancellation.	74
Figure 4.26—Ionic charge of the asphaltenes presented as zeta potential, all values are negative.....	75
Figure 4.27—Surfactant cost to produce one barrel of oil.....	77

LIST OF TABLES

	Page
Table 3.1— Surfactants type and properties.	18
Table 3.2— Summary of the initial and experiment conditions for all coreflood experiments with 60% initial oil and 40% initial water.....	22
Table 3.3— Anions and Cations that can be deducted by IC900 and their standard.	25
Table 4.1— Crude Oil Properties and SARA Fractions, modified with permission from (Alshaikh et al. 2018).	26
Table 4.2— Elemental analysis of crude oil and their asphaltenes.	28
Table 4.3— Key biomarker ratios that are sensitive to crude oil biodegradation and thermal maturity, modified with permission from (Al-Atwah et al. 2018).....	33
Table 4.4— Sulfur biomarker ratio for Oil 1 and Oil 2.	35
Table 4.5— Polarity estimation for crude oils and their SARA fractions.	43
Table 4.6— Summary of the cumulative oil recovery, cumulative water production, the amount of trapped water in oil, maximum oil production rate, and maximum water production rate for all coreflood experiments.	53
Table 4.7— Temperatures at which emulsified water separate from produced oil for each coreflood experiment.	58
Table 4.8— Distilled water ions concentration that used to prepare surfactants solutions.	61
Table 4.9— Summary of the produced oil asphaltenes and residual oil asphaltenes content in 100 g of oil.	67

1. INTRODUCTION

The development of heavy oil resources has become increasingly important to the global energy supply to meet projected increases in oil demand (IEA 2019). There are vast oil resources of heavy oil, oil sand, and bitumen which count for more than 70% of the world's total oil resources (Alboudwarej et al. 2006). Extractions of these viscous oils require thermal enhanced oil recovery techniques like in-situ combustion and steam injection (i.e. steam drive, SAGD, and CSS) (Burger et al. 1985; Hascakir 2017a; Prats 1982). Thermal enhanced oil recovery (EOR) methods offer the most effective ways of extracting these viscous oils because the use of such methods increases the oil's mobility by decreasing their viscosity (Green and Willhite 1998; Hascakir 2017a, 2017b; Hein 2017; Meyer and De Witt 1990; Prats 1982; Sperry et al. 1976). 88% of all thermal EOR methods between 1959 and 2010 were reported to be steam injection which comprised 42% of all EOR methods applied worldwide (Al Adasani and Bai 2011).

In steam injection, an injection well introduces steam to a reservoir where heat is transferred to viscous oils reducing their viscosity and improving their mobility (Green and Willhite 1998; Lake 1989). Hence, when reservoir temperature increases, the amount of residual oil is reduced. In addition, the injected steam distills (distillation process) the oil light fractions and mobilizes them to the steam front introducing miscibility (Lake 1989; Prats 1982). During the steam flood process, there are four distinguished zones: steam zone, condensation zone, oil bank zone, and initial zone (**Figure 1.1**) (Burger et al. 1985; Prats 1982; Willman et al. 1961). Steam has been used extensively as a flooding

fluid in steam injection, cyclic steam injection, and steam-assisted gravity drainage, due to its reliability and easy-to-apply features (Chu 1985; Willman et al. 1961; Wu 1977).

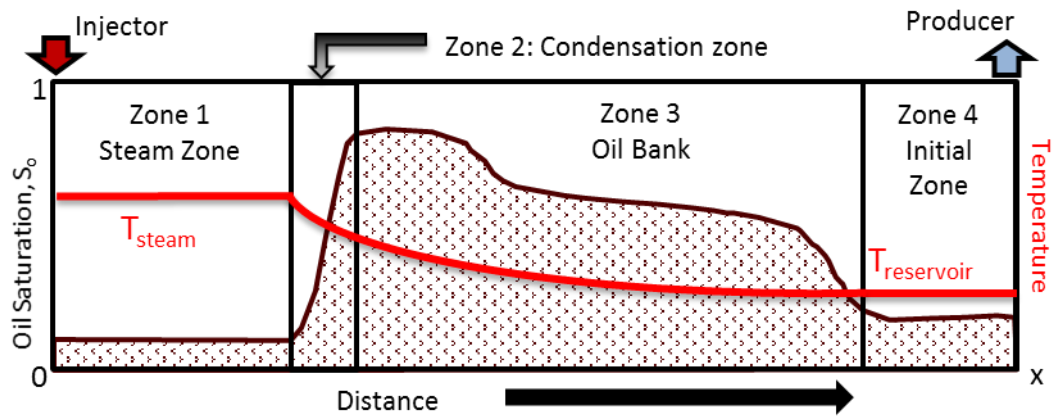


Figure 1.1—Steam injection zones and their temperature profiles, modified from (Prats 1982).

The first use of steam injection was in 1931 when it was tested in 18 ft thick sand at a depth of 380 feet near Woodson, Texas (Prats 1982). After that, there have been many laboratory tests for steam injection (Pirson et al. 1958; Stovall 1934; Walter 1957) but it wasn't implemented into the field until twenty years later when steam soak (i.e. cyclic steam) was tested in Yorba Linda field in California (Burns 1969; Stokes and Doscher 1974). The first real steam drive pilot test was applied in Venezuela (Giusti 1974). The successful results of this pilot test and experimental steam-drive investigation of the Schoonebeek field, Netherlands, resulted in Shell having the first full-field development with steam-drive injection in 1960 (Van Dijk 1968). By 1972, steam flooding had been

extensively employed to recover heavy oil in the USA, Canada, and Venezuela and its advantages have been recognized (Farouq Ali 1974).

Although steam has been successfully applied to enhance the oil recovery, it has many challenges (Burger et al. 1985). Operationally, steam injection suffers from excessive heat losses in surface lines, injection tubing, and overburdened and underburdened rock (Baker 1973; Marx and Langenheim 1959). Other operational challenges of steam injection include steam channeling and gravity override which result in low volumetric sweep efficiency. When steam is injected, it tends to move to the upper part of the reservoir. On the other hand, the condensed water has the tendency to move down due to density difference (Burger et al. 1985; Green and Willhite 1998).

In terms of economic challenge, the steam-to-oil ratio (SOR) is given as the economic limit criteria and this limit fluctuates based on the current oil prices (Sheng 2013; Vogel 1984). The use of natural gas (as an energy source) and freshwater to generate steam increases the cost of the process and harms the environment (Coelho et al. 2017; Deng 2005; Speight 2013). Heating water to generate steam, in general, requires burning of fuel which creates greenhouse gases (GHG); mainly CO₂ but also contains SO₂, NO₂, & CO (Deng 2005; Prats 1982). Besides, treating a large amount of produced water is costly and may lead to the pollution of surface or underground water sources (Ali et al. 2016; Ali and Hascakir 2015, 2017; Deng 2005).

Co-injection of chemical additives has recently been suggested to improve steam injection efficiency by decreasing injected steam amount and environmental footprints of

steam generation and increasing the overall oil recovery (Butler and Mokrys 1993; Mukhametshina et al. 2016). Chemical solvents (e.g. propane, hexane, toluene, and CO₂) and surfactants (e.g. Sodium Dodecyl Sulfate and Cetyl Trimethyl Ammonium Bromide) are the main additives suggested for improving oil displacement via steam (Dixon 1958; Zeidani and Gupta 2012).

Solvent-steam co-injection was proposed by Dixon in 1958, which involved the injection of steam with a solvent being largely in the vapor phase (Dixon 1958). Hernández and Farouq Ali experimentally investigated the process by injecting a slug of solvent followed by steam into a sandpacks core flood (Hernández and Farouq Ali 1972). In 1972, Shell conducted a field pilot test to distill oil's light components by steam injection, which transport to the steam front forming a solvent slug (Volek and Pryor 1972). The first field test of the co-injection of steam and solvent (diesel) was in Venezuela in 1987 (Bracho and Oquendo 1991). Solvent-steam process main mechanisms to enhance heavy crudes are dissolving oil and reducing oil viscosity by heat introduction via steam and oil dilution via solvents (Butler and Mokrys 1993; Coelho et al. 2017; Hascakir 2016; Nasr et al. 2002). While the viscosity reduction makes solvent-steam processes attractive, the toxicity of the solvents chemicals may result in health hazard (Kar and Hascakir 2015; Li et al. 2011; Wang et al. 2014). Moreover, solvent-oil-rock interactions could adversely impact the wettability of the system and reduce the oil recovery (Kar et al. 2015; Kar et al. 2016).

Conversely, wettability can be altered in more favorable ways to recover more oil with the use of surfactants. All surfactants consist of a polar head and nonpolar hydrocarbon tail(s) which make surfactants' amphiphilic compounds, therefore, they are

able to reduce the interfacial tension (IFT) between the aqueous solution and the residual oil (Green and Willhite 1998; Hou and Xu 2016). This reduction in the IFT enables the surfactant flood solution to mobilize trapped oil, to alter rock wettability towards water-wet, and to increase the oil recovery (Green and Willhite 1998). Based on the charges of the polar head of the surfactants, they are classified into four groups: anionic, cationic, nonionic, or zwitterionic (Green and Willhite 1998; Rosen and Kunjappu 2012). The heads of anionic surfactants have a negative charge, while the cationic surfactants have a positive charge. Non-ionic surfactants have no charge in their heads, and if the polar head of the surfactant is charged both with negative and positive ions, the surfactant is called zwitterionic (Green and Willhite 1998; Rosen and Kunjappu 2012).

Surfactants have been used for 80 years to increased oil recovery (Atkinson 1927; Uren and Fahmy 1927). In the 1950s, surfactant chemical injection has become an accepted enhanced oil recovery methodology in many conventional oil applications (Reisberg and Doscher 1956). However, for heavy oil reservoirs, the first use of surfactant as a steam additive was to create foam and enhance macroscopic displacement (Fitch and Minter 1976; Hiraski 1989; Needham 1968). A patent was granted to Needham (1968) that describes the process of plugging high permeable zones diverting steam into less permeable zones. Steam will cause foam as long the temperature is above the boiling point of water and steam is in its gaseous phase. The process is known as the steam-foam process and its main mechanism is to improve the low volumetric sweep efficiency (i.e. macroscopic displacement) caused by steam channeling and gravity overriding during steam injection (Hiraski 1989; Prats 1982). Because steam will condense back to liquid,

the process could include the injection of non-condensable gas along with steam and surfactant solutions to enhance foam-forming (Dilgren et al. 1978). Although steam-foam process has been implemented in the field since 1978 and shown improvement in injection profiles, vertical sweep, and oil recovery, the process was limited to enhance the macroscopic displacement only and failed to consider microscopic or pore-scale displacement (Dilgren et al. 1978; Hiraski 1989; Marsden 1986; Reid and Colonomos 1993).

A number of studies have examined the microscopic displacement enhancement in heavy oil reservoirs by injecting only surfactant, alkali, or their combination without injecting steam (Bryan and Kantzas 2009; Ding et al. 2010; Dong et al. 2009; Fu et al. 2016; Kumar et al. 2012; Mai et al. 2009; Pei et al. 2011; Pei et al. 2013; Pei et al. 2012). The alkali has the ability to generate surfactants *in-situ* by the reaction of converting naphthenic acids in the oil to soap which reduces IFT (Atkinson 1927; Rosen and Kunjappu 2012; Sjoblom 2005). The main mechanisms of this process are emulsification and wettability alteration which enhance the microscopic displacement unlike the steam-foam process (Green and Willhite 1998; Myers 2005). The heavy oil emulsification is achieved by reaching ultralow IFT (i.e., <0.001 dyne/cm) (Hirasaki et al. 2011).

In recent years, there has been an increasing amount of literature on combining steam (thermal EOR) and surfactant (chemical EOR) to enhance heavy crude oil recovery by providing additional oil displacement mechanism with the use of surfactant in addition to reducing oil viscosity using steam injection (Hirasaki et al. 2011; Li et al. 2018; Lu et al. 2017; Srivastava and Castro 2011; Wu et al. 2018; Zeidani and Gupta 2013). These

studies have almost exclusively focused on reducing oil-water IFT and generating oil-in-water emulsions during the surfactant-steam process. Because of the surfactant's polar head and nonpolar hydrocarbon tail, stable emulsion can be formed when surfactants orient themselves between the interface of oil and water (Myers 2005; Rosen and Kunjappu 2012). Nonpolar molecules have a tendency to be positioned primarily in the oil phase, while polar molecules are in the water aqueous phase (Becher 1965; McClements 2016). However, in heavy oil and bitumen, there exist considerable amounts of asphaltenes and resins, which are known as the polar components of crude oils and regarded as natural emulsifiers that produce emulsions (Kokal 2005; Noik et al. 2005). In many thermal-recovery processes, *in-situ* emulsification is always promoted with the presence of asphaltenes at increasing temperature (Chung and Butler 1989; Lu et al. 2017). The presence of polar fractions of crude oils (asphaltenes and resins) and surfactants may promote emulsion formation (Aguilera et al. 2010; Chen and Tao 2005; Friberg et al. 1976; Kokal 2005; McLean and Kilpatrick 1997; Sjoblom 2005). An increase in temperature will decrease oil's viscosity, promoting droplet flocculation and assisting in breaking down emulsions (Jones et al. 1978). Thus, for surfactant-steam injection processes asphaltenes may favor emulsion formation with surfactants.

It is worth to define here emulsion and its formation mechanism to better understand the interaction among water, polar fractions of crude oil, and surfactant. Emulsions are heterogeneous mixtures containing at least one immiscible liquid, intimately dispersed within another in the form of droplets (Becher 1965; Schramm 1992). Three types of emulsions are commonly observed in nature and in engineering application:

oil-in-water (O/W) emulsion in which oil droplets dispersed in water; water-in-oil (W/O) emulsion in which water droplets dispersed in oil; and multiple emulsions (Becher 1965; Schramm 1992). Multiple emulsions have oil droplets dispersed in water droplets that are also dispersed in a continuous oil phase. The characterization of emulsions often includes phase identification, determination of nature and size distribution of the dispersed phase, and stability measurements of the dispersed phase (Schramm 1992).

The phase identification of the oil/water/surfactant systems described by Winsor (i.e., Type II+, II-, and III phase environments) assumed that microemulsion coexists with pure liquid (i.e., pure water or pure oil) at equilibrium (Nelson and Pope 1978; Winsor 1948). This assumption does not hold for crude oil with high asphaltene content (Torrealba and Johns 2018). Heavy crude oils in their structure have a high quantity of asphaltene and resins known to be the polar components of oil, while saturates and aromatics are nonpolar (Akbarzadeh et al. 2007; Al-Atwah et al. 2018; Fan et al. 2002). The interactions of these components with surfactant's polar head or its hydrocarbon nonpolar tails can affect the performance of EOR processes that involve surfactant injection.

In the oil/water/surfactant system, there are intermolecular interactions include electrostatic and van der Waals interactions, see **Figure 1.2** (McClements 2016; Myers 2005). The interaction between surfactants and water is known as ion-dipole or dipole-dipole interaction based on the charge of the head group of surfactants (Kitahara and Konno 1969). The ionic surfactant's head is attractive to the polar water molecules forming ion-dipole interaction while nonionic surfactant's head is attracted to water molecules via

dipole-dipole interaction. Surfactant's hydrocarbon tail, on the other hand, interacts with oil forming van der Waals interaction (Becker 1997).

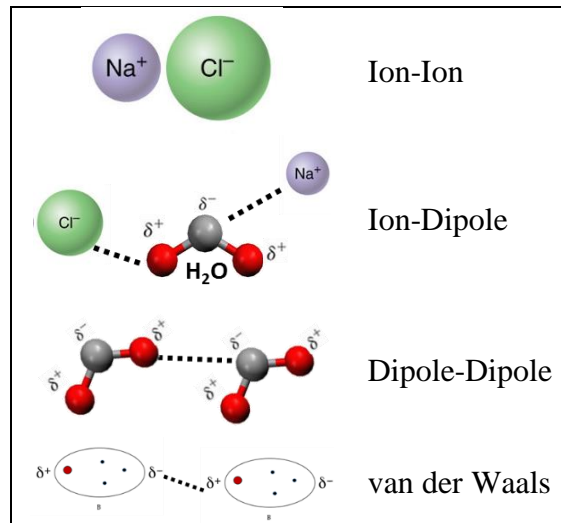


Figure 1.2—Illustration schematic of intermolecular electrostatic interactions and van der Waals between molecules.

Heavy crude oils are rich with polar compounds, as mentioned previously, which makes van der Waals or dipole-dipole interactions possible between these compounds and the polar groups of surfactants. The polar compounds in crude oil are results from functional polar groups containing nitrogen, sulfur, and oxygen (NSO), and inorganic metals (Mullins 2008). These molecules' polarity attributable to an uneven distribution of electrons within each molecule, forming an "electrical dipole" (Becher 1965; McClements 2016; Pauling 1960).

The crude oils can be grouped into four fractions according to their polarization; saturates, aromatics, resins, and asphaltenes (SARA). Saturates are linear, branched, or cyclic alkane chains with no double or triple carbon-carbon bonds, hence, they are nonpolar (Austad et al. 1998; Falls et al. 1994; Hirasaki et al. 2011). Aromatics fraction contains one or more aromatic rings of hydrocarbons with a possible trace of nitrogen, sulfur, and oxygen (NSO), which is known to have little (insignificant) polarity. Resins are a polar fraction of the crude oil, which is soluble in lower molecular weight n-alkanes and contains less amount of metals as compared to asphaltenes. Asphaltenes are the most polar fraction of the crude oil, which is insoluble in lower molecular weight n-alkanes, contains nitrogen, sulfur, and oxygen (NSO) compounds and heavy metals (Akbarzadeh et al. 2007; Fan et al. 2002).

Polarity determination of complex molecules like crude oils is difficult; thus dielectric constant measurements are used to provide information about polarity, which is important due to its impact on dipole-dipole interactions (Hanai et al. 1962; McClements 2016; Punase and Hascakir 2017; Schramm 1992).

In addition to dipole-dipole and ion-dipole interaction, ion-ion and van der Waals interaction may present in the medium depending upon the reservoir system. In heavy oil reservoirs, due to the interaction of heavy components of oil with reservoir rock ion-ion interaction can be observed (Coelho et al. 2017; Kar et al. 2016; Prakoso et al. 2018). It should be noted that ion-ion interaction is the strongest intermolecular interaction among the four intermolecular interactions mentioned above. Even though in heavy oil reservoir, all types of interactions are observed since ion-ion is the strongest one, surfactant

performance may be dominated by the ion-ion interaction. Moreover, since reservoir rocks are negatively charged, the heavy oil components mostly carry the negatively charged reservoir fines and the cationic surfactant head group might be absorbed by the oil fractions rather than water which may even enhance asphaltenes flocculation and consequently precipitation.

The ion-ion electrostatic force of attraction between two oppositely charged particles can generate extremely strong ionic bonds and can be measured by zeta potential (Robertson et al. 1999; Wulfsberg 2000). Zeta potential measurements provide information on the strength of surface charges, and higher values indicate the ion-ion interaction strength (Pan et al. 2012). Zeta potential is defined as the electric potential in the interfacial double layer of a liquid droplet or solid versus a point in the continuous phase far from the interface (Schramm 1992), see **Figure 1.3**. Zeta potential indicates the degree of electrostatic repulsion between similarly charged dispersed colloidal clusters immersed in a continuous dispersing medium. Oppositely charged ions are attracted, and those with similar charge ions are repelled. The importance of zeta potential that it can provide information about the stability of colloidal dispersions (McClements 2016). High absolute values of zeta potential indicate that solid or liquid droplets are electrically stable and have low coagulation or flocculation tendency (Lu and Gao 2010; McClements 2016).

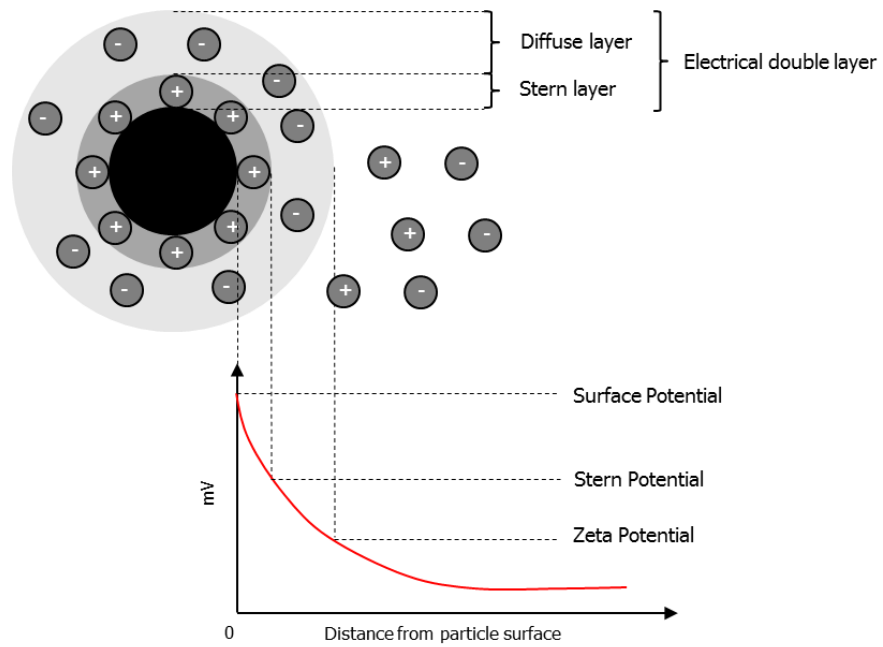


Figure 1.3—Illustration of the electrical double layer around negativity charged solid and zeta potential, modified from (Kaszuba et al. 2010).

2. STATEMENT OF THE PROBLEM

Surfactants literature and experience are in general, built on reservoirs containing light and medium hydrocarbons, which mostly have nonpolar components. The nonpolar tail of the surfactant is designed to stay in the oil phase and surfactant's polar side to stay in the water phase to reduce the forces between oil and water because surfactants place themselves at the interphase of water and oil. For high-viscosity crudes, the situation can be different due to the high-polarity components of crude oils (i.e., resins and asphaltenes) and their impact on the dipole-dipole or ion-dipole interaction among oil, brine, and surfactant phases.

Moreover, these heavy oil fractions carry reservoir rock components that are mainly negatively charged, and the polar head group of surfactants can also be charged, (anionic, cationic, and zwitterionic). Hence, ion-ion interaction as well can affect surfactant flooding performance.

It is not very well documented how dipole-dipole and ion-ion interactions can impact the overall surfactant processes for heavy oil. This study aims to investigate each interaction on heavy oil extraction. In addition, steam is commonly used to enhance heavy oil's mobility, and thus, its impact is studied as well.

3. MATERIALS AND METHODS*

3.1 Materials

In the scope of this dissertation, two crude oil samples from Canada and Mexico were used. Besides, nine surfactants were tested as steam additives, including anionic, cationic, and nonionic surfactants. The next sections will give a characterization of crude oils and surfactants.

3.1.1 Crude Oil Characterization

Oil samples were characterized according to their viscosity by Brookfield viscometer (ASTM D4889-15), and API gravity by Anton Paar densometer (ASTM D4052-16). The crude oil samples are grouped under saturates, aromatics, resins, and asphaltenes (SARA) following the ASTM D2007-11 method based on their solubility in different solvents and adsorption affinity towards the attapulgus clay and silica gel. First, n-pentane solvent is used to separate asphaltenes from other crude oil fractions (i.e., known as deasphalted oil). The deasphalted oil, then, is discharged to a double column glass percolation, in which attapulgus clay is at the top section and silica gel plus clay is at the bottom section. Saturates fraction which is known as a nonpolar fraction of crude

* Part of this chapter is reprinted with permission from: 1) “Extension of Existing Screening Criteria Tables for Thermal Enhanced Oil Recovery Methods through Compositional Analyses of Heavy Oils” by Al-Atwah, I., Alshaikh, M., Sweet, S., Knap, A., and Hascakir, B. presented at the SPE Western Regional Meeting, Garden Grove, California, USA, 22-26 April 2018. Copyright 2018 by Society of Petroleum Engineers. 2) “An Innovative Dielectric Constant Measurement Method to Determine the Ideal Surfactant Candidate to Enhance Heavy Oil Recovery” by Alshaikh, M., Huff, G., and Hascakir, B. presented at the SPE Canada Heavy Oil Technical Conference, Calgary, Alberta, Canada, 13-14 March 2018. Copyright 2018 by Society of Petroleum Engineers. 3) “Anionic Surfactant and Heavy Oil Interaction During Surfactant-Steam Process” by Alshaikh, M., Lee, Y.S., and Hascakir, B. presented at the SPE Western Regional Meeting, San Jose, California, USA, 23-26 April 2019. Copyright 2019 by Society of Petroleum Engineers.

oil is collected at the bottom of the assembly without getting adsorbed to the silica gel or to the clay. On the other hand, aromatics fraction gets adsorbed into attapulsgus clay due to its partial polarity (i.e., contain some heteroatoms). To collect aromatics fractions, the attapulsgus clay in the top section is attached to an extraction assembly and toluene is refluxed. To extract resins, the most polar fraction of the deasphalted oil, the attapulsgus clay in the top section is continuously rinsed with a mixture of acetone and toluene (1:1 volume ratio). The acetone-toluene mixture washes the attapulsgus clay in the top section and extracts the adsorbed resins fraction.

The elemental compositions of crude oils and n-pentane insoluble asphaltenes have been analyzed by Chevron. First, the weight percent of carbon, hydrogen, and nitrogen content by using the standard combustion method and applying the Leco CHN analyzer Carlo Erba model were accomplished. After that, trace elements were deducted using Thermo Intrepid Inductively Coupled Plasma.

In addition to the physical characterization of crude oils, molecular structure and composition analysis were performed on both oils using Agilent Fourier Transform Infrared (FTIR) and 7890B gas chromatograph (GC) equipped with flame ionization detector (FID), respectively. Also, biomarkers analysis in both crude oils were conducted using Agilent 7890B gas chromatograph (GC) interfaced to an Agilent 5977A mass spectrometer detector (GC-MS). Biomarkers have important hydrocarbon groups which are derived from previously living organisms and are used for chemical fingerprinting. Hence, they have an important role to characterize, differentiate, and source identification of environmental forensic studies of oil spills. Because they can be found in crude oils,

rocks, and sediments and carry information about the source and geological conditions. In hydrocarbon exploration and reservoir geochemistry, biomarkers are used to gain information about oil's thermal maturity, source material type, source rock depositional environment, geological age, and oil biodegradation. By the use of the gas chromatography/mass spectrometry (GC/MS), biomarkers can be detected.

The biomarker study was done on both crude oils and their asphaltenes. However, since asphaltenes are solid, hydrous pyrolysis was first used to liquefy asphaltenes. Hydrous pyrolysis was used to liquefy asphaltenes and then use the existing forensic biomarker identification methods to better characterize asphaltenes (Wang et al. 2006). The pyrolysis process is a thermal decomposition of organic material (or organic-rich rocks) at elevated temperatures in the absence of oxygen (Peters et al. 2005). In this work, hydrous pyrolysis (i.e., heating in presence of water) is selected because it is capable of producing saturated hydrocarbons and represent hydrocarbon generation (Lundegard and Senftle 1987). To conduct hydrous pyrolysis, one gram of asphaltenes is placed in a secured stainless steel cylinder (5 cm diameter × 10 cm height) with 30 mL of distilled water. Argon gas was used as an inner gas to maintain non-oxidative environment and pressurize the cylinder at ~200 psi. Then, the cylinder was heated and maintain at 320-350°C using a heating jacket for three days.

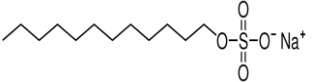
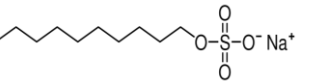
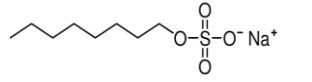
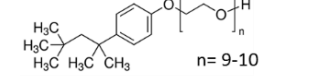
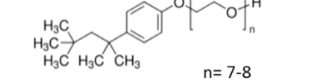
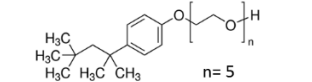
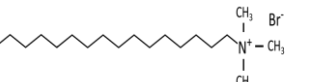
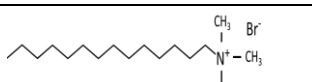
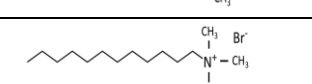
The liquefied asphaltenes is used to identify biomarkers that have heteroatoms and polar functional groups. The identification of these polar biomarkers is performed using GC-MS biomarkers analysis. After collecting the liquefied asphaltenes, it is separated to saturate and aromatic fractions using silica gel. Saturates fraction is eluted using hexane

while aromatics fraction is eluted using dichloromethane. Saturates and aromatics extracts are then concentrated by evaporation under a gentle stream of nitrogen to a final volume of ~10 mL. The samples are transferred to glass vials prior to performing GC-MS run and analysis. The GC-MS is equipped with a DB-1 fused silica 60 m × 0.25 mm × 0.25 μm column with helium as a carrier gas at 1.3 mL/min flow rate. The temperature of the GC-MS oven was programmed at an initial temperature of 35 °C for 2 minutes and increased at a rate of 2 °C/minute to 80°C, then 3 °C/minute from 80°C to 320°C, followed by 15 minutes at 320 °C. The analysis was carried out using 70 eV ionization potentials. Data were acquired in single ion monitoring (SIM) mode with 50 – 100 msec dwell times for ions of interest. Cycle time was approximately 0.7s. Compound ratios were calculated directly from peak areas or peak heights of targeted-biomarkers. The GC-MS analysis involves detecting terpane, and sterane biomarkers, together with the presence of aromatics compounds that contain dibenzothiophene (C₁₂H₈S).

3.1.2 Surfactant Characterization

Anionic surfactants are commonly used in chemical flooding operations (Ma et al. 2013; Mannhardt et al. 1993). In this dissertation, the performances of three anionic surfactants were tested for heavy oil and bitumen recovery and their performance for the first time was compared with three cationic and three nonionic surfactants. The criteria for selecting these surfactants were to have the same molecular structure for the polar head of each surfactant but different nonpolar tail lengths: long, moderate, or short. **Table 3.1** shows the surfactants used in this study with their detailed properties.

Table 3.1— Surfactants type and properties.

No.	Surfactant Name	Abbreviation Used in This Study for Each Surfactant	Chemical Formula	Chemical Structure	Surfactant Type and Hydrocarbon Tail Length	HLB°	MW [#] , g/mole	CMC [±] Value, mM ^Δ
1	Sodium Dodecyl Sulfate	A1	$C_{12}H_{25}SO_4^- Na^+$		Anionic (Long)	40	288	8.39
2	Sodium Decyl Sulphate	A2	$C_{10}H_{21}SO_4^- Na^+$		Anionic (Medium)	41	260	33.2
3	Sodium Octyl Sulfate	A3	$C_8H_{17}SO_4^- Na^+$		Anionic (Short)	41.9	232	130
4	Triton™ X-100	N1	$t\text{-Oct-C}_6\text{H}_4\text{-(OCH}_2\text{CH}_2\text{)}_{10}\text{OH}$		Nonionic (Long)	13.5	625	0.9
5	Triton™ X-114	N2	$(C_2H_4O)_8$ $C_{14}H_{22}O$		Nonionic (Medium)	12.4	537	0.2
6	Triton™ X-45	N3	$t\text{-Oct-C}_6\text{H}_4\text{-(OCH}_2\text{CH}_2\text{)}_5\text{OH}$		Nonionic (Short)	10.4	427	0.1
7	Hexadecyltrimethylammonium Bromide	C1	$C_{19}H_{42}N^+Br^-$		Cationic (Long)	10.3°	2365	0.92
8	Myristyltrimethylammonium Bromide	C2	$C_{17}H_{38}N^+Br^-$		Cationic (Medium)	11.25°	336	5
9	Dodecyltrimethylammonium Bromide	C3	$C_{15}H_{34}N^+Br^-$		Cationic (Short)	12.2°	308	15.6

^Δ Obtained from (Bahri et al. 2006; Egan 1976; Tadros 2006)

[°] HLB: The hydrophilic-lipophilic balance; obtained from (Wang et al. 2008), [#]MW: Molecular weight, [±]CMC: Critical micelles concentration

The molecular structure analysis was performed on these surfactants using Agilent Fourier Transform Infrared (FTIR). In addition to the molecular structure analysis, the bulk polarity of the surfactants solutions was determined via indirectly dielectric constant measurements using vector network analyzer, N9923A FieldFox Handheld at 0.5-4 GHz. CMC concentrations were obtained from (Bahri et al. 2006; Egan 1976; Tadros 2006). The concentrations of the surfactants solutions are varied because their CMC (critical micelles concentration) values which were selected to minimized cost as increasing the concentration beyond the CMC value does not decrease the IFT (Bahri et al. 2006; Egan 1976; Tadros 2006).

Understanding the thermal stability of surfactants is also important at steam temperature. Thus, their thermal stability was measured through thermal gravimetric and differential scanning calorimetry analysis (TGA/DSC) by a NETZSCH STA 449 F3 thermal gravimetric analyzer at 10° K/minute heating rate under air atmosphere with a purge rate of 50 mL/minute and nitrogen serving as a protective gas at a rate of 20 mL/minute (Santacesaria et al. 1991; Zeidani and Gupta 2013; Ziegler and Handy 1981). TGA results provide weight loss behavior of surfactants at varying temperatures while DSC results give an idea about the nature of the chemical reactions (exothermic or endothermic), causing the weight loss (Horowitz and Metzger 1963).

3.2 Methods

Several techniques have been utilized to study the interactions between oil's components and surfactants for surfactant-steam flooding. Details of each experiment, analysis, and test are given below.

3.2.1 Procedure for Tube Tests

Bottle tests were performed to investigate the physical interactions between the surfactants and oil samples. Microemulsion type (i.e., Winsor type I, II, and III) can be determined using this technique (Nelson and Pope 1978; Winsor 1948). In these tests, four grams of oil samples and four grams of surfactant solutions were mixed in test tubes using Bransonic-220 ultrasonic water tub for one hour. Then, the test tubes were left stand vertically for 24 hours allowing separation of phases. Surfactant concentrations were selected to be at the critical micelle concentration level (**Table 3.1**) to reach their minimum IFT values (Green and Willhite 1998).

3.2.2 Procedure for Optical Microscopic Tests

To understand the effectiveness of emulsion formation, the optical microscopic analysis was performed on crude oil and their SARA fractions in the presence of liquid and vapor water. A ProRes CT5 Camera attached to an optical microscope was used (Meiji Techno MT9000). Images were captured after crude oils, and their fractions were subjected to water vapor for ten minutes or liquid water. First, a drop of oil was visualized with a drop of anionic, cationic, and nonionic surfactants solution on a microscope slide, separately. Steam, then, was exposed to the microscope slide for 10 minutes and was

visualized immediately. Similarly, the interaction of surfactants with polar fractions of crude oils (asphaltenes, resins, and asphaltene + resin) under the exposure to steam was visualized. In addition, the impact of the mutual interaction of these polar fractions with nonpolar ones (saturates and aromatic) was also visualized under microscope.

3.2.3 Procedure for Core Flood Tests

Recovery characteristics of two hydrocarbons from Canada and Mexico were investigated by 20 coreflood experiments through steam and surfactant-steam processes. Ottawa sand with 20-40 mesh size with 39.1% porosity was used as a reservoir rock. The pore space was saturated with 60 vol% crude oil and 40 vol% distilled water. The reservoir rock was blended with water and oil by hand and then packed into 20 cm long and 5.36 cm in diameter stainless steel core holder. The inlet of the holder is connected to the steam generator and surfactant container, and the outlet is connected to the backpressure regulator and separator, see **Figure 3.1**.

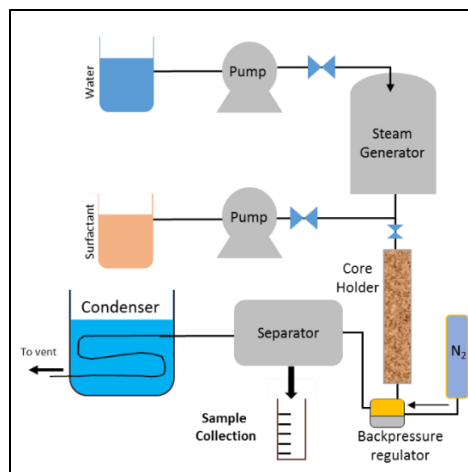


Figure 3.1—Schematic of the experimental setup for steam and surfactant-steam flooding experiments, reprinted with permission from (Alshaikh et al. 2019).

During the experiments, 18 mL/min steam was injected to the core holder with a D-series syringe pump, and 2 mL/min surfactant solution was injected with a Beckman 100A pump. Surfactants solutions were prepared by blending CMC values of surfactants given in **Table 3.1** with distilled water. **Table 3.2** summarizes the initial and experiment conditions for all coreflood experiments.

Table 3.2— Summary of the initial and experiment conditions for all coreflood experiments with 60% initial oil and 40% initial water.

Exp. No.	EOR Type	Crude Oil	Surfactant Name	The surfactant to Steam Injection Rate Ratio, mL/min
1	Steam Injection	Oil-1	NA ^k	0:18
2	SSP [†]	Oil-1	A1 [#]	2:18
3	SSP	Oil-1	A2 ⁺	2:18
4	SSP	Oil-1	A3 [±]	2:18
5	SSP	Oil-1	C1 [‡]	2:18
6	SSP	Oil-1	C2 [‡]	2:18
7	SSP	Oil-1	C3 [‡]	2:18
8	SSP	Oil-1	N1 [×]	2:18
9	SSP	Oil-1	N2 [°]	2:18
10	SSP	Oil-1	N3 [^]	2:18
11	Steam Injection	Oil-2	NA	0:18
12	SSP	Oil-2	A1	2:18
13	SSP	Oil-2	A2	2:18
14	SSP	Oil-2	A3	2:18
15	SSP	Oil-2	C1	2:18
16	SSP	Oil-2	C2	2:18
17	SSP	Oil-2	C3	2:18
18	SSP	Oil-2	N1	2:18
19	SSP	Oil-2	N2	2:18
20	SSP	Oil-2	N3	2:18

[†]SSP: Surfactant-steam Process; ^kNA: Not Applicable

[#]A1: Sodium Dodecyl Sulfate, ⁺A2: Sodium Decyl Sulphate, [±]A3: Sodium Octyl Sulfate

[‡]C1: Hexadecyltrimethylammonium Bromide, [‡]C2: Myristyltrimethylammonium Bromide, [‡]C3: Dodecyltrimethylammonium Bromide

[×]N1: Triton™ X-100, [°]N2: Triton™ X-114, [^]N3: Triton™ X-45

During the coreflood experiments, produced liquids were collected every 20 minutes, and the temperature was monitored continuously with J-type thermocouples connected via cables to a data acquisition system. Produced oil samples were immediately visualized under the Meiji Techno MT9000 optical microscope at 40x magnification to identify and characterize the emulsion types present in produced oil samples. Then, gravity was used to separate the easily separable water from oil. For the emulsified water, evaporation was used to separate water-in-oil emulsion. A Thermolyne furnace was used for evaporation where samples were kept at 60-70 °C for 21 to 42 days during which their weight change was constantly measured. Because it is difficult to separate all water-in-oil emulsion, TGA/DSC was used to determine the water content in the produced oil. Then, several different methods were used to characterize the produced oil samples, which were mostly free from emulsified water.

The molecular structure of the produce crude oils was analyzed using Fourier Transform Infrared (FTIR) Spectroscopy (Agilent, Cary 630) which can provide information about the functional groups present in a sample at varying concentrations (Smith 2011). Moreover, infrared spectra can be used to understand the intermolecular interactions among surfactant, oil, and steam during the surfactant-steam process. As it is mentioned earlier, either ion-ion or dipole-dipole interaction is expected between crude oil and surfactants. To observe dipole-dipole interaction, the dielectric constant measurement was accomplished through vector network analyzer, N9923A FieldFox Handheld at microwave frequency (500 MHz to 4 GHz). To observe ion-ion interaction, zeta potential measurements were achieved on asphaltenes samples from each produced

oil samples by the 90Plus PALS instrument. Asphaltenes are the heaviest fraction of crude oil and may carry reservoir rock in their clusters, while the interaction between reservoir rock and asphaltenes is a physical interaction since the reservoir rocks are in general negatively charged. The physical interaction between rock and asphaltenes, makes the asphaltenes surface charged (Demir et al. 2016; Punase et al. 2017). Hence, zeta potential measurements were only conducted on asphaltenes. For zeta potential measurement, 50 mg of n-pentane separated asphaltenes was dispersed into 15 mL of ethanol using ultrasound tub for 20 minutes (Kar et al. 2015). Then, 1.5 mL volume of this solution was added to 100 mL of 1 mM potassium chloride solution (Kar et al. 2015; Parra-Barraza et al. 2003). Note zeta potential was measured at aqueous solution of 6 ± 1 pH value.

At the end of each experiment, spent rock analyses were achieved through residual oil saturation determination of samples collected at injection and production points using the toluene washing method (Amyx et al. 1960; Kar et al. 2015). The residual oil was further analyzed for asphaltenes content, and spent rock samples were first washed with n-pentane to remove the n-pentane soluble portion of residual oil and then to separate rock from n-pentane insoluble portion of oil; toluene was used (ASTM 2011; Kar et al. 2016). In this study, n-pentane is used to separate asphaltenes and the insoluble portion of crude oil is reported as asphaltenes. It should be noted that as definition asphaltenes are soluble in aromatic solvents and insoluble in n-alkanes (Andersen and Birdi 1991). Thus, after separation of asphaltenes from residual oils, excess toluene and n-pentane were evaporated by heating in the furnace.

Moreover, produced water samples were analyzed by using Thermo Fisher IC900 ion chromatography and through dielectric constant measurements with N9923A FieldFox Handheld. The ion chromatography results are used to analyze surfactant retention for anions and cations during surfactant-steam coreflood. The ion chromatography equipment is a liquid chromatography and capable of deducting seven major anions and six major cations, see **Table 3.3**. The ion chromatography measures ions concentrations of samples by separating ions based on their interaction with a resin. Ions have different types and size which allow for their separation differently. First, the liquid sample is injected and passes through the chromatographic column where the column constituents absorb the ions. After that, the ion extraction liquid (i.e., eluent) is injected into the column, allowing the absorbed ions to separate. Then, the retention time with concentration of the different ions is determined by integrating the spectrum.

Table 3.3— Anions and Cations that can be deducted by IC900 and their standard.

Anions		Cations	
Fluoride	F ⁻	Lithium	Li ⁺
Chlorite	ClO ⁻	Sodium	Na ⁺
Nitrite	NO ₂ ⁻	Ammonium	NH ₄ ⁺
Bromide	Br ⁻	Potassium	K ⁺
Nitrate	NO ₃ ⁻	Magnesium	Mg ⁺²
Phosphate	PO ₄ ⁻³	Calcium	Ca ⁺²
Sulfate	SO ₄ ⁻²		

4. RESULTS AND DISCUSSION*

4.1 Crude Oil Characterization

Table 4.1 gives the characterization of the crude oil samples in terms of physical properties and weight percent of SARA fractions. The crude oil samples exhibit similar physical properties in terms of low °API gravity levels. The viscosity-temperature relation of the two oil samples is given in **Figure 4.1**. Accordingly, Oil 1 was considered a bitumen and Oil 2 is heavy oil, based on their respective viscosities at reservoir temperature (Oil 1's reservoir temperature is 24 °C while for Oil 2 is 70 °C) (Hascakir 2017b; Hein 2017; Meyer and De Witt 1990) and API gravity.

Table 4.1— Crude Oil Properties and SARA Fractions, modified with permission from (Alshaikh et al. 2018).

Property	Crude Oil 1	Standard Error (n = 3)	Crude Oil 2	Standard Error (n = 3)
Viscosity (cP) at 22.3°C	10,100	218	208,500	289
Density (°API) at standard conditions	12.09	0.28	11.56	0.19
SARA Content (wt %)				
Saturates	16.51	0.70	10.14	0.69
Aromatics	37.81	1.95	38.01	1.83
Resins	17.10	1.24	13.09	0.67
Asphaltenes	28.58	0.64	38.76	1.02

* Part of this chapter is reprinted with permission from: 1) “Extension of Existing Screening Criteria Tables for Thermal Enhanced Oil Recovery Methods through Compositional Analyses of Heavy Oils” by Al-Atwah, I., Alshaikh, M., Sweet, S., Knap, A., and Hascakir, B. presented at the SPE Western Regional Meeting, Garden Grove, California, USA, 22-26 April 2018. Copyright 2018 by Society of Petroleum Engineers. 2) “An Innovative Dielectric Constant Measurement Method to Determine the Ideal Surfactant Candidate to Enhance Heavy Oil Recovery” by Alshaikh, M., Huff, G., and Hascakir, B. presented at the SPE Canada Heavy Oil Technical Conference, Calgary, Alberta, Canada, 13-14 March 2018. Copyright 2018 by Society of Petroleum Engineers. 3) “Anionic Surfactant and Heavy Oil Interaction During Surfactant-Steam Process” by Alshaikh, M., Lee, Y.S., and Hascakir, B. presented at the SPE Western Regional Meeting, San Jose, California, USA, 23-26 April 2019. Copyright 2019 by Society of Petroleum Engineers.

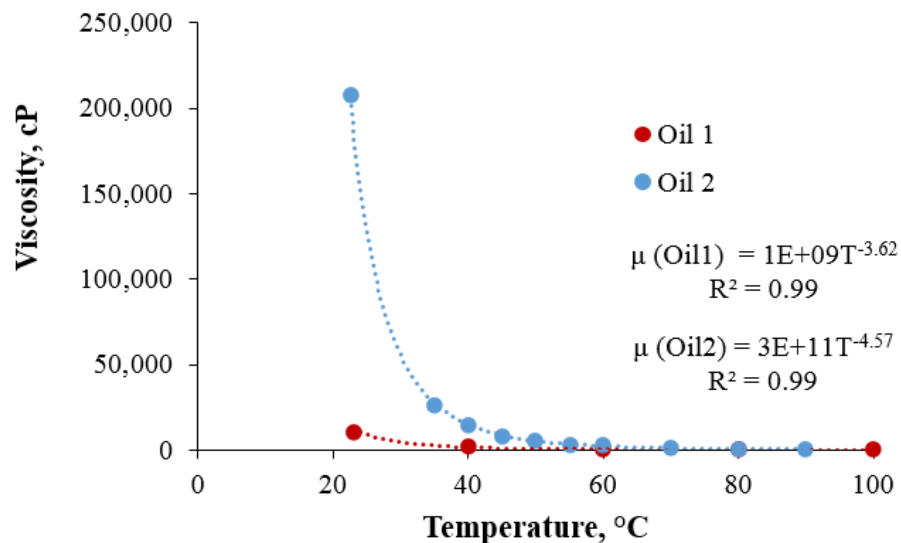


Figure 4.1—Temperature dependence of viscosity for Oil 1 and Oil 2.

In crude oils, while saturates and aromatics represent the nonpolar fractions of crude oil, resins and asphaltenes are known as the polar fractions of crude oil (Crocker and Marchin 1988; Fan and Buckley 2002; Speight 2014). It is observed from the SARA fractions results in **Table 4.1** that Oil 2 has more quantity of polar groups (i.e., resins and asphaltenes) than Oil 1. However, the amount of polar fractions in crude oil does not make Oil 2 more polar than Oil 1. The mutual interaction of these polar groups will determine the magnitude of polarity (Punase and Hascakir 2017).

The elemental analysis of crude oils and their n-pentane separated asphaltenes was performed to investigate heteroatoms and metal content that might be responsible for increasing oil polarity. **Table 4.2** presents the elemental analysis.

Table 4.2— Elemental analysis of crude oil and their asphaltenes.

Sample	Crude Oil 1	Crude Oil 2	Oil 1' Asphaltenes	Oil 2's Asphaltenes
C, wt%	80.9	80.6	80.3	80.4
H, wt%	10.8	10.5	8.19	8.21
N, wt%	≤1.00	≤1.00	1.43	1.38
°O, wt%	2.86	2.53	6.52	1.79
H/C, ratio	0.133	0.130	0.102	0.102
[^]Heteroatoms, wt%	8.3	8.9	11.51	11.39
Trace Elements, ppm				
B	2.68	1.59	6.4	ND
Ca	ND	ND	35.6	ND
Fe	2.49	224	46.1	761
K	5.8	5.2	26	ND
Mg	ND	ND	23.8	ND
Mo	8.9	475	ND	1,460
Na	23.3	8.46	1100	34.1
Ni	68.1	88.4	172	251
P	2.4	2.1	11	ND
S	44,100	52,400	33,800	78,400
Si	ND	45.1	ND	16.2
Sn	1.2	1.4	ND	ND
Ti	2.94	0	0	0
V	172	469	358	1,290
⁺Metals	285	1271	1761.5	3796

ND means non-detectable, signifies that metal concentration is lower than the detection limit (0.01-0.1 µg/L)

°O is calculated from the remaining wt%

[^]Heteroatoms, wt% is the sum of every element (in wt%) except for C and H

⁺Metals is the sum of all metallic elements

The analysis shows the presence of NSO heteroatoms and other inorganic elements at a high percentage (8.3 wt% for Oil 1 and 8.9 wt% for Oil 2) for both crude oils. The observed inorganic metals in crude oils (i.e., Fe, Na, and Ni) might be part of crude oil molecular structure in the form of organometallic compounds, or they might have an inorganic origin and carried by hydrocarbon molecules. Inorganic metals might physically attach to crude oil due to crude oil-reservoir brine and/or crude oil-reservoir rock interaction. These elements might contribute to oil's polarity because of their ions (i.e., Na⁺, K⁺, Ni⁺², and Fe⁺³) and interact with the surfactant's polar head.

Crude oil samples were further characterized for their chemical structure with FTIR and biodegradation analysis. The observed FTIR signatures in **Figure 4.2-A** show that for initial crude oils, the overall spectra are similar, though, the absorbance peaks intensity is altered in several wavenumber regions. For example, in the $\equiv\text{C-H}$ bend region at 740 cm^{-1} , Oil 2 is shown to have a larger peak than Oil 1 (Smith 2011; Stuart 2004) indicating that Oil 2 has more alkynes (unsaturated hydrocarbons) than Oil 1. Peaks at 2853 , 2924 and 2953 cm^{-1} represent CH aliphatic stretches, while peaks at 1376 and 1458 cm^{-1} were due to CH_2 and CH_3 bends (Bellamy 1980; Morrow et al. 2014). The region from 1000 to 600 cm^{-1} is called the fingerprint region, which is typically complex and difficult to interpret, but it is unique for each given compound (Bellamy 1980; Smith 2011). **Figure 4.2-B** shows the spectra of the crude oils' asphaltenes. Peaks at 3000 - 3100 cm^{-1} are because of aromatic C-H stretch and aliphatic C-H stretch are between 2780 and 3000 cm^{-1} . The double bond carbonyl C=O stretch and aromatic C=C stretch are between 1640 - 1800 cm^{-1} and 1620 - 1590 cm^{-1} .

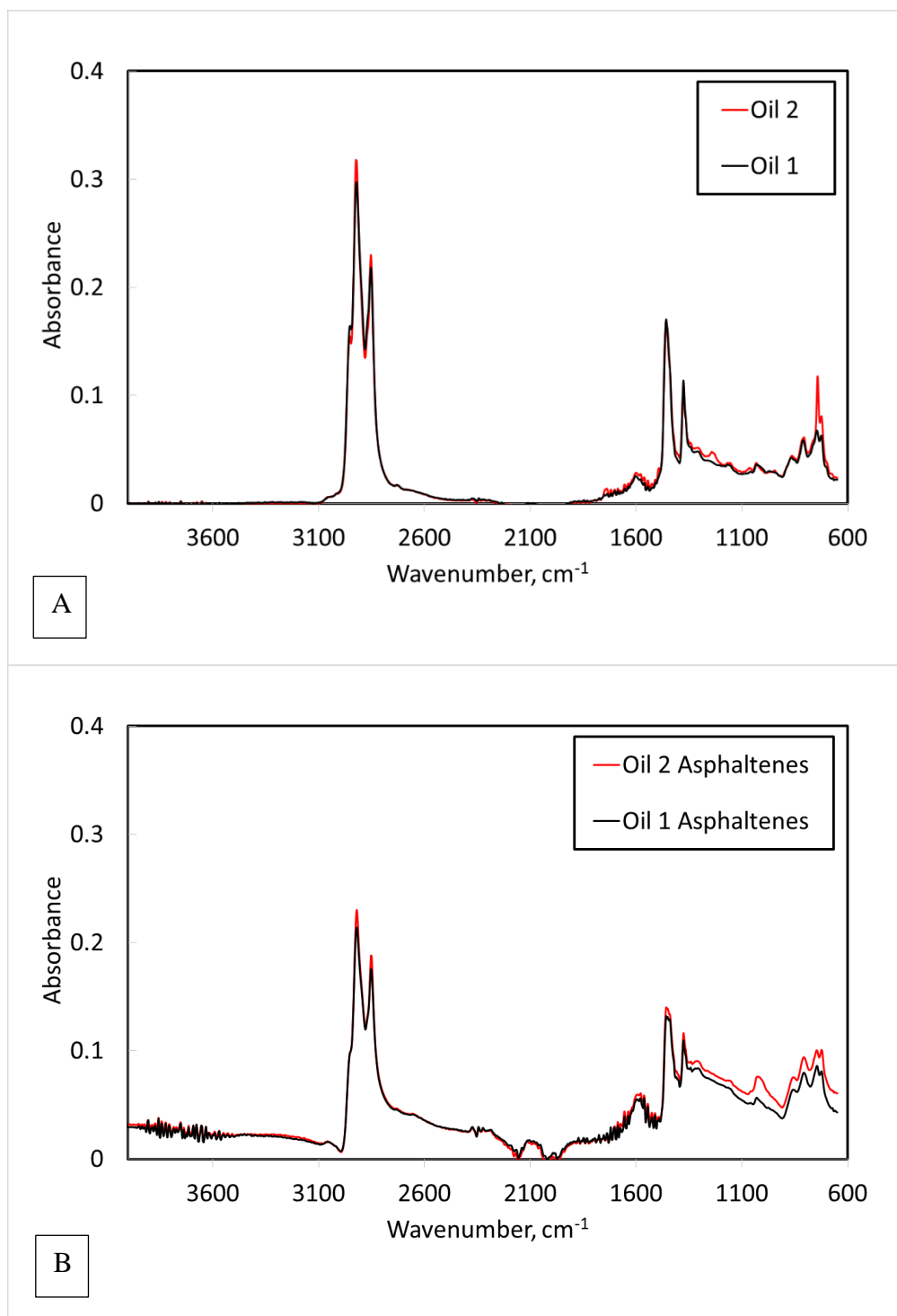


Figure 4.2—FTIR spectra for (A) initial oils and (B) their asphaltenes, modified with permission from (Al-Atwah et al. 2018).

The fingerprint region between 1000 and 600 cm^{-1} might indicate the presence of heteroatoms like sulfur, nitrogen, and oxygen (Coates 2000). A comparison of oil's asphaltenes shows that Oil 2 has a peaks absorption increase in the fingerprint region. Asphaltenes are the heaviest fraction of crude oil and include complex aliphatic hydrocarbon molecules attached to naphthenic rings and aromatic that have heteroatoms like sulfur, nitrogen, oxygen, and metals (Li and Firoozabadi 2010; Speight 2014). The fingerprint region is usually associated with these atoms in addition to aromatic C-H out-of-plane bending (Stuart 2004). Thus, the intensity of the absorption of Oil 2's asphaltenes compared to Oil 1' asphaltenes might indicate that Oil 2's asphaltenes has higher polar groups (i.e., higher polarity). However, the mutual interaction of these polar groups could affect the overall asphaltenes and oil polarity. Note that the small peaks between 2300 and 1800 cm^{-1} are due to diamond ATR crystal and can be ignored (Unur 2013).

While FTIR provides full spectra of crude oil composition, it is very difficult to determine the composition of crude oil through FTIR only; hence, GC-FID is conducted. The observed GC-FID results in **Figure 4.3** show that Oil 1 lacks n-alkanes, unlike Oil 2, which indicates that Oil 1 went through biodegradation (Peters et al. 2005). This finding is also supported by Oil 1's FTIR indicated by lower absorbance in alkanes region 2920 cm^{-1} and 2850 cm^{-1} , see **Figure 4.2-A**. Biodegradation consumes hydrocarbon, thus, making the oil enriched in nitrogen, sulfur, and oxygen (NSO) compounds (Peters et al. 2005). The first hydrocarbons to be consumed are normal, mono- and multi- saturated alkanes, then, light aromatics (e.g., benzene, toluene, and xylenes).

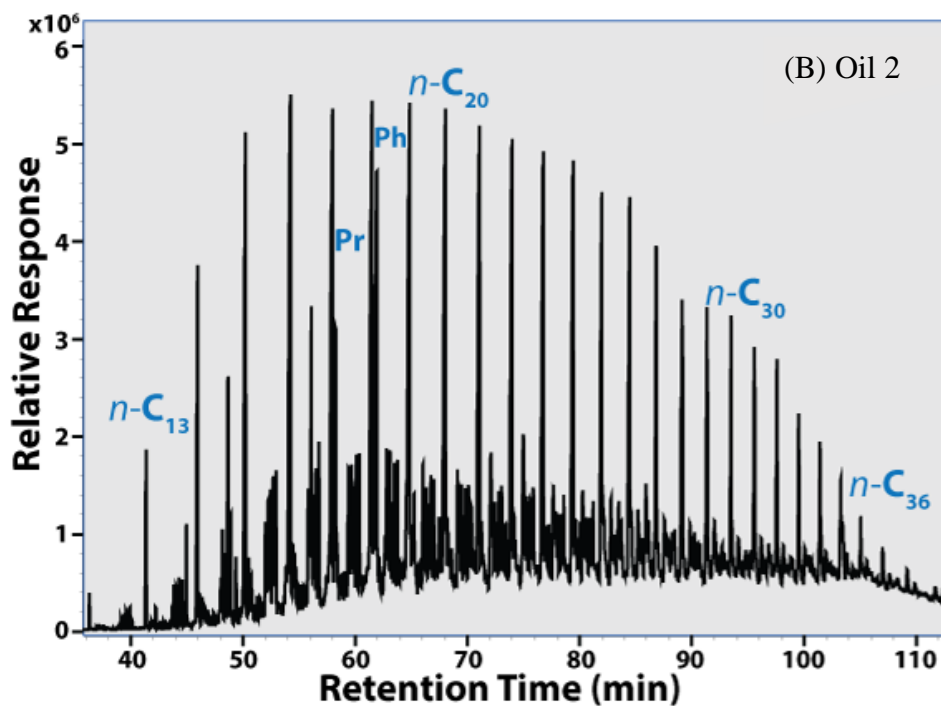
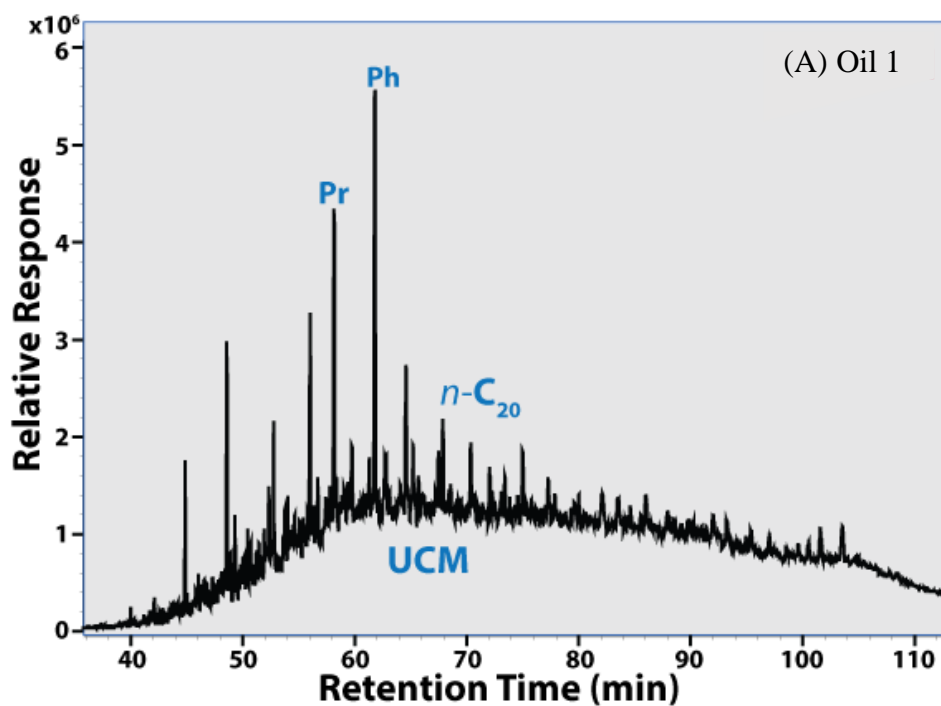


Figure 4.3—GC-FID chromatograms showing overall normal alkane's distribution, Pr: pristane, Ph: phytane, UCM: unresolved complex mixture, reprinted with permission from (Al-Atwah et al. 2018).

In gas chromatography (GC), a hump is visible that consist of bio-resistant compounds that include highly branched and cyclic saturated, aromatic, naphthoaromatic, and polar compounds. This hump is called an unresolved complex mixture (USM), see **Figure 4.3-A**. The USM hump for Oil 1 is shown clearly greater than Oil 2. To determine the biodegrading severity, some key biomarker ratios are used (Peters et al. 2005).

The ratios of specific biomarkers are found to be increasingly used to determine oil biodegradation and thermal maturity, see **Table 4.3** (Peters et al. 2005; Wang et al. 2006). The different compound ratios were calculated directly from peak areas or peak heights of targeted-biomarkers. The distribution of terpane (an unsaturated hydrocarbon obtained from plants) and sterane (saturated polycyclic hydrocarbons which are derived from the sterols of ancient organisms) biomarkers were determined with the presence of aromatics compounds, all detailed calculations are listed in **Appendix A**. Low values of isoprenoids ratio (i.e., pristane/*n*-C17 and phytane/*n*-C18) indicate lower biodegradation (Peters et al. 2005). It is apparent that isoprenoid to *n*-alkane ratios (i.e., pristane and *n*-C17; phytane and *n*-C18) are lower for non-biodegraded oil sample (Oil 2) where there is a relative abundance of *n*-alkanes compared with isoprenoids.

Table 4.3— Key biomarker ratios that are sensitive to crude oil biodegradation and thermal maturity, modified with permission from (Al-Atwah et al. 2018)

Oil Sample#	Pr/ <i>n</i> C17*	Ph/ <i>n</i> C18*	Hopane	Terpane	Sterane	TAS	MAS	Biodegradation Rank
Oil 1	9.68	7.11	0.1	0.12	0.21	0.42	0.36	Moderate
Oil 2	0.31	0.61	0.03	0.07	0.11	0.31	0.41	Non-biodegraded

*Pristane/*n*-C₁₇

*Phytane/ *n*-C₁₈

In **Table 4.3**, the critical biomarker ratios helped determine the biodegradation level of the two crude oils. Based on saturates and aromatics compounds, Oil 2 has a non-biodegraded oil signature and can be characterized by the full preservation of n-alkanes clearly evident in their chromatograms, **Figure 4.3**. On the other hand, Oil 1 is considered moderate biodegradation oil based on the Peters and Moldowan (PM) biodegradation scale (Peters et al. 2005). The moderate biodegradation oil, like Oil 1, is expected to be rich in NSO compounds and heavy metals. The evidence of moderate degradation includes the preservation of diasteranes, while partial degradation of regular sterane biomarkers, such as C27 $\alpha\alpha$ 20R cholestane, C28 $\alpha\alpha$ 20R ergostane and C29 $\alpha\alpha$ 20R stigmastane (Peters et al. 2005). As Terpane, Hopane, and Sterane ratios (formulas are listed in **Appendix A**) increase, the biodegradation of crude oil increases, which makes oil heavier. Note that the biomarker study was conducted on liquefied asphaltenes. This liquid product was then separated into its SARA fractions.

Aromatics fraction, obtained from liquefying asphaltenes, contains sulfur compounds like dibenzothiophenes (DBT) (Schou and Myhr 1988). The results of biomarkers analysis are shown in **Table 4.4** as ratios to normalize the values of the integrated spectra for comparison (the complete list of abbreviations name and chemical formula are in **Appendix A**). Interestingly, these ratios are high for the more mature oil (Oil 1) than Oil 2, which has less maturity. Hence, it is concluded that for more mature and heavily biodegraded oils, high sulfur content is expected in its asphaltenes molecules and, thus, promoting asphaltenes surface charges. Note that in **Table 4.4**, all compounds

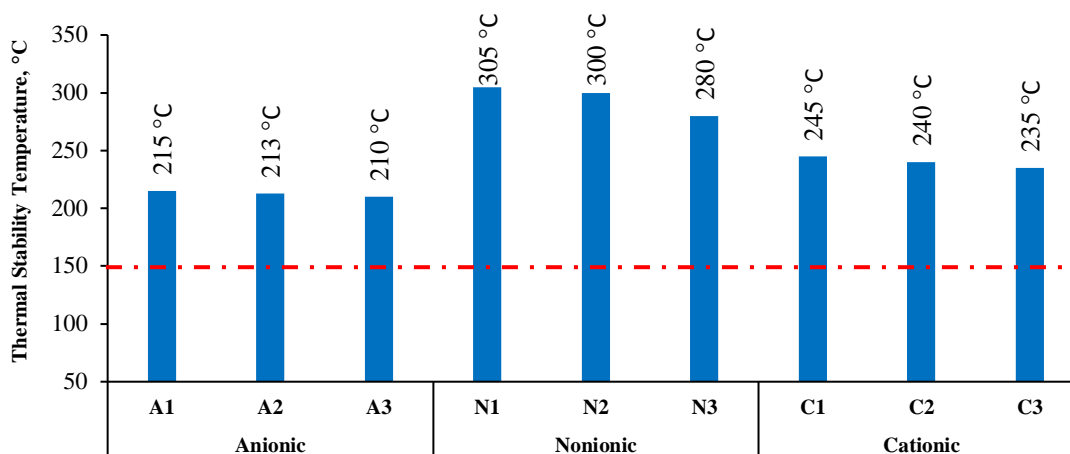
contain dibenzothiophene which has sulfur in their molecular structure (i.e., 4-Methyldibenzothiophene which represents “4MDBT” has dibenzothiophene).

Table 4.4— Sulfur biomarker ratio for Oil 1 and Oil 2.

Biomarker Ratio	Oil 1	Oil 2
4MDBT/DBT	2.43	1.25
23MDBT/DBT	2.21	1.11
1MDBT/DBT	1.74	1.09
4ETDBT/DBT	0.35	0.18
46DMDBT/DBT	2.95	0.74
DMDBT4/DBT	1.04	0.31
DMDBT5/DBT	4.42	1.51
DMDBT6/DBT	3.14	1.00
14DMDBT/DBT	2.26	0.74
DMDBT7/DBT	1.17	0.75
DMDBT8/DBT	0.88	0.40

4.2 Thermal Stability of Surfactants

For surfactants, thermal stability is an essential factor in determining their suitability for surfactant-steam applications. Evaluation of the surfactants via TGA/DSC provided thermal decomposition temperature for each surfactant. After applying 10 °C/minute heating rate in thermal gravimetric analyzer/ differential scanning calorimeter (TGA/DSC), obtained graphs were used to obtain the thermal stability per each surfactant, see **Figure 4.4**. TGA/DSC graphs are provided in **Appendix B** (see **Figures B-1 to B-3**).



A1: Sodium Dodecyl Sulfate, A2: Sodium Decyl Sulphate, A3: Sodium Octyl Sulfate
 C1: Hexadecyltrimethylammonium Bromide, C2: Myristyltrimethylammonium Bromide, C3: Dodecyltrimethylammonium Bromide
 N1: Triton™ X-100, N2: Triton™ X-114, N3: Triton™ X-45

Figure 4.4—TGA results for surfactant solutions indicating the thermal stability temperature of surfactants. The red dashed line represents coreflow experimental temperature. All TGA/DSC curves are provided in Appendix B.

The thermal stability temperature values were obtained at the start point of mass loss. According to these results, all nine surfactants are stable at the experimental temperature used in this thesis (150°C). Increasing the length of the surfactants' hydrocarbon tail appeared to increase thermal stability, which is in agreement with the literature (Taleb et al. 2018); the nonionic surfactants are determined to be the most stable. The FTIR results for these surfactants showed that the polar head group's non-hydrocarbon molecular signature appeared between 1600 and 600 cm^{-1} , see **Figure 4.5**, while the hydrocarbon tail signature was shown between 2819 cm^{-1} and 3000 cm^{-1} (Smith 2011). The observed hydrocarbon tails' signatures are lower for the short surfactants (A3, C3, and N3) and high for the long hydrocarbon tail length surfactants (A1, C1, and N1).

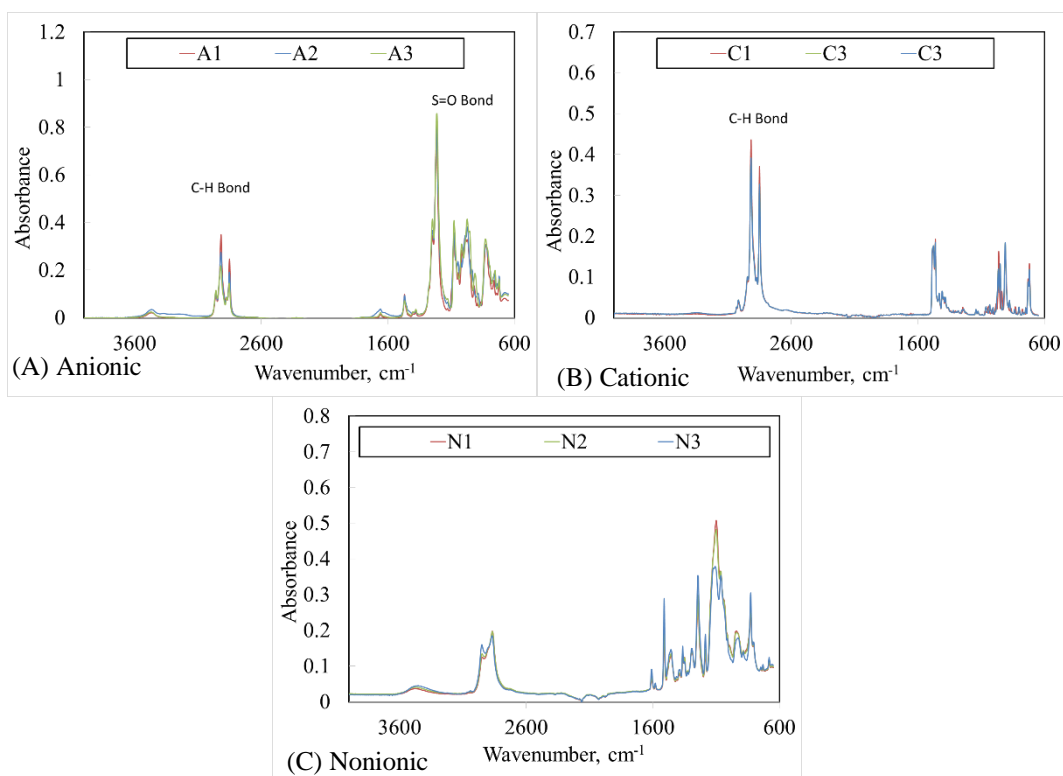
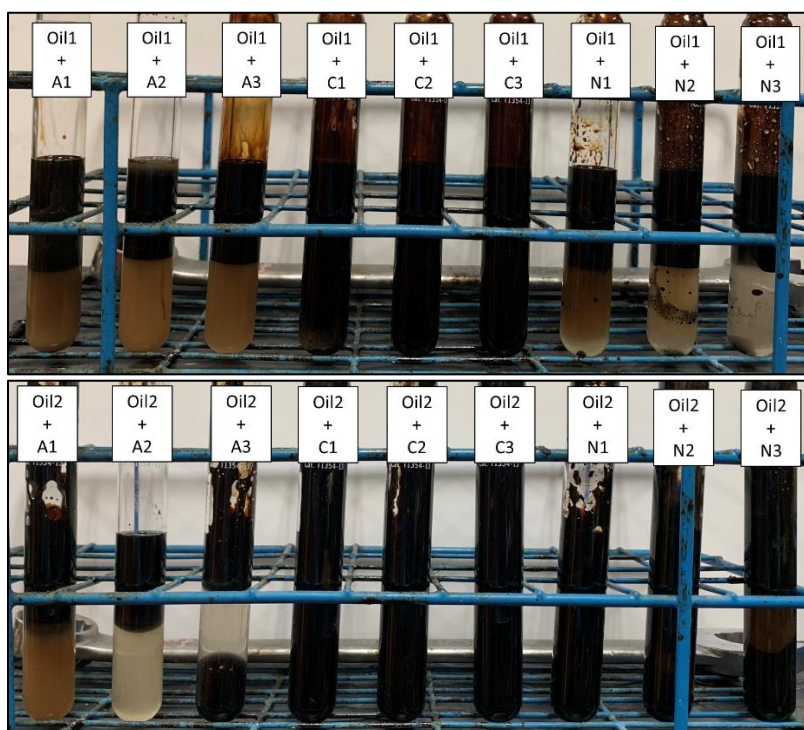


Figure 4.5—Fourier Transform InfraRed (FTIR) spectra of (A) anionic, (B) cationic, and (C) nonionic surfactants, modified with permission from (Alshaikh et al. 2018).

4.3 Bottle Test Results

The effectiveness of surfactants used during a surfactant-steam process is determined not only by the surfactant's thermal stability at steam temperature but also by the surface forces acting at the water-oil interface (Ziegler and Handy 1981). The orientation of surfactants' monomers at the water-oil interface is controlled by the polarity of the oil-water-surfactant system (Rosen et al. 1988). For light/medium crude oils, the polar heads of the surfactant are expected to stay in the polar water phase, and the non-polar hydrocarbon tail of surfactants remain in the oil phase (Green and Willhite 1998).

However, heavy crude oils have a high content of polar functional groups in their structures: namely, resins and asphaltenes (see **Table 4.1**) (Crocker and Marchin 1988; Demirbas 2016). Thus, dipole-dipole and/or ion-dipole interactions can be expected between surfactant heads and resins and/or asphaltenes fractions. To check if such interactions happen among the oils, surfactants, and water, bottle tests were performed, see **Figure 4.6**. Formation of two phases; water continuous phase and that phase, was observed by the end of these tests.



A1: Sodium Dodecyl Sulfate, A2: Sodium Decyl Sulphate, A3: Sodium Octyl Sulfate
 C1: Hexadecyltrimethylammonium Bromide, C2: Myristyltrimethylammonium Bromide, C3: Dodecyltrimethylammonium Bromide
 N1: Triton™ X-100, N2: Triton™ X-114, N3: Triton™ X-45

Figure 4.6—Visualization of bottle test results for oil-surfactant blends for Oil 1 (top) and Oil 2 (bottom).

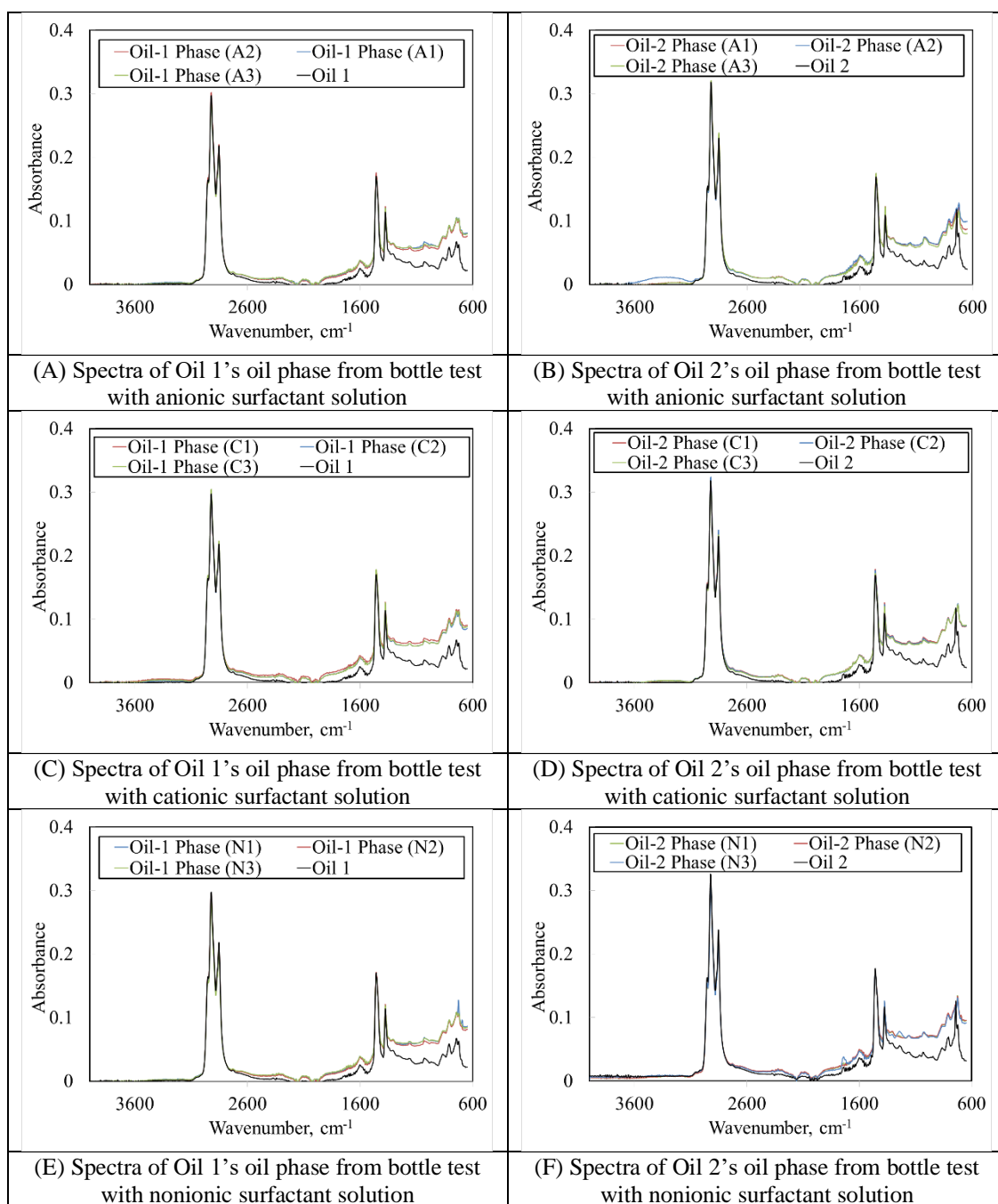


Figure 4.7—FTIR spectra of oil phase after mixing surfactant solution, modified with permission from (Alshaikh et al. 2019).

Water and oil phases from bottle tests were first examined with FTIR. The FTIR results of the separated oil phase are presented in **Figure 4.7** and **Figure 4.8** for the water phase. Comparison between the initial oil samples' FTIR and the FTIR of the separated oil phases from the bottle tests show higher peaks at the fingerprint regions ($1000\text{-}600\text{ cm}^{-1}$). This increase in the molecular signature might indicate that the interaction of heteroatoms from the surfactant solutions.

FTIR results of the water phases, obtain from bottle tests, in **Figure 4.8** show oil signature in addition to water signature (i.e., peaks at 2850 , 2920 , and 2950 cm^{-1}). For the spectra of water phases for Oil 1, O-H stretch peak at 3280 cm^{-1} and O-H bend at 1630 cm^{-1} are lower, see **Figure 4.8-C** (Smith 2011; Stuart 2004). At the same time, oil's molecular signatures become stronger with the surfactant tail length increase (i.e., peaks at 2853 , 2924 and 2953 cm^{-1} and peaks at 1376 and 1458 cm^{-1}). It appears that oil-in-water emulsions are deductible mostly for Oil 1 with cationic and nonionic surfactant, see **Figure 4.8-C and E**. For Oil 2 water phases' FTIR, only water signature is showing at 3280 cm^{-1} and 1630 cm^{-1} and no significant oil-in-water emulsions were deducted, see **Figure 4.8-B, D, and F**. This difference in emulsion formation is because of the different electrostatic interactions between crude oils and each type of the surfactant.

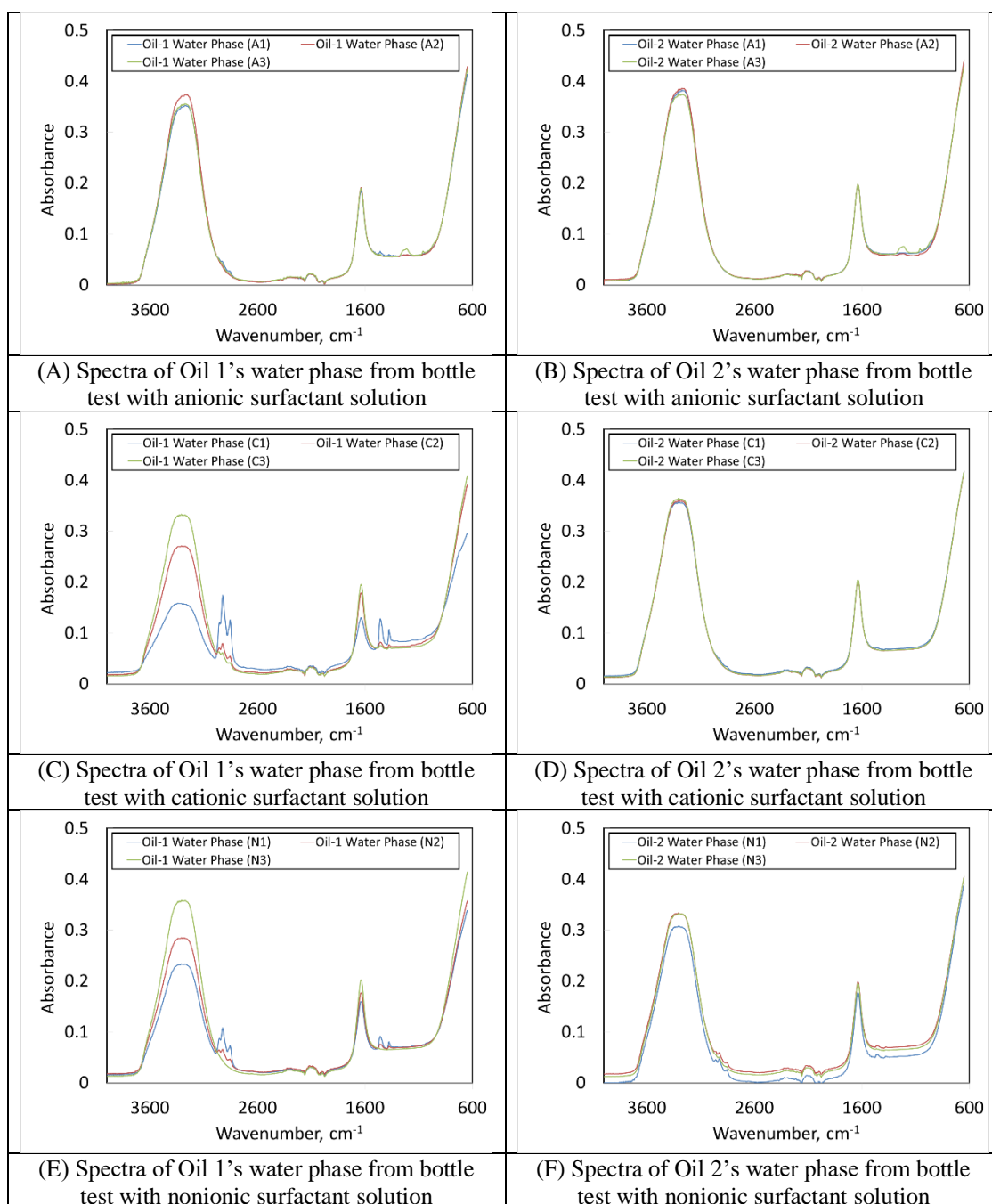


Figure 4.8—FTIR spectra of water phase after mixing surfactant solution with crude oils (bottle test) showing water and oil signatures, modified with permission from (Alshaikh et al. 2019).

Dipole-dipole interaction is one of the electrostatic interactions between the crude oil and surfactants and to understand its effect, measurements of the dielectric constant were performed on the separated phases obtained through the bottle test. **Figure 4.9** shows the results of the dielectric constant measurement for the two phases.

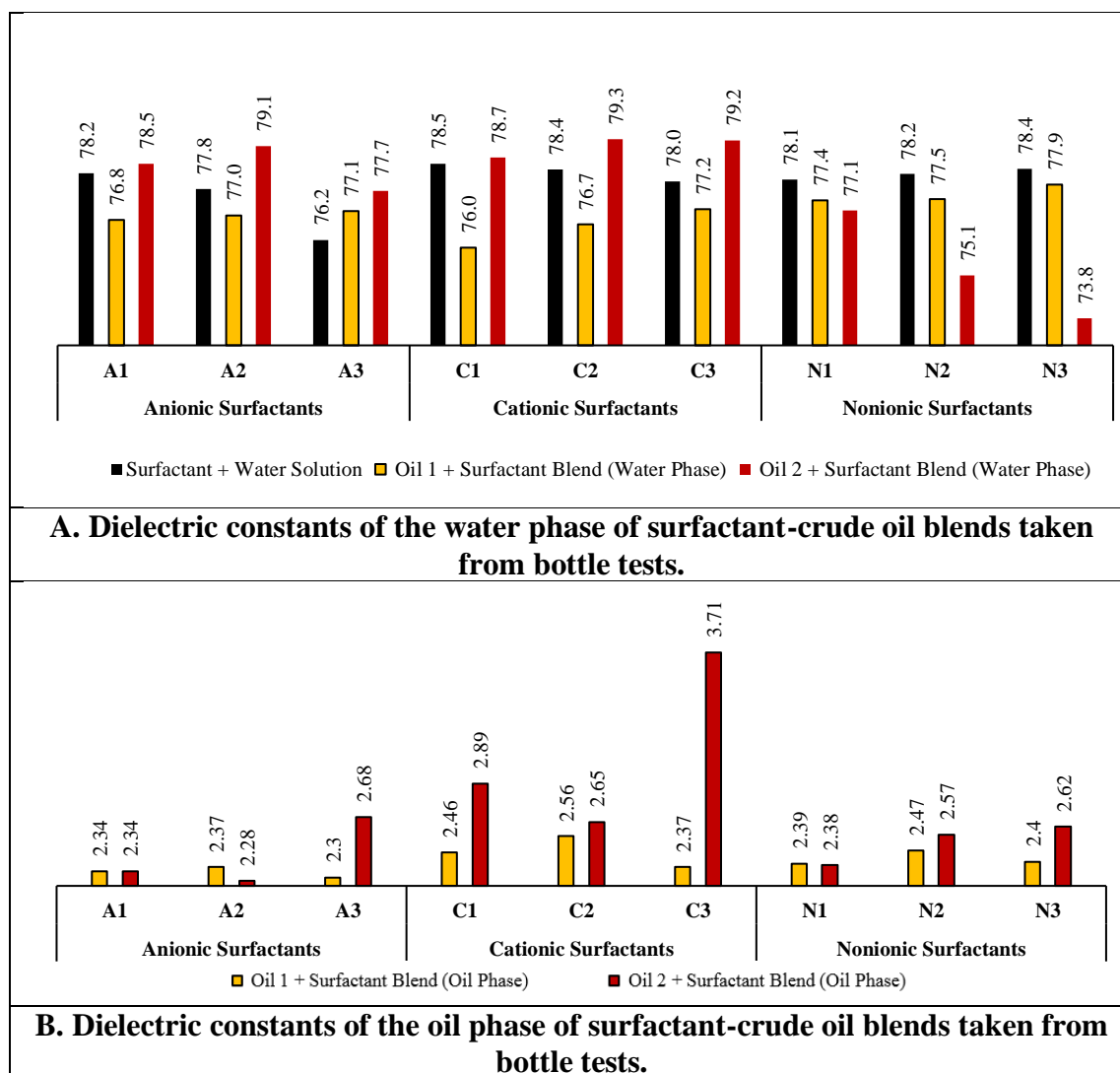


Figure 4.9—Dielectric constants of water phase (A) and oil phase (B) of surfactant-crude oil blends taken from bottle tests.

The dielectric constant (ϵ) is a function of frequency and in this study microwave frequency in the range of 500 MHz and 4 GHz was used to understand the dipolar effect. The results of the water phase, in general, show high dielectric constant values (i.e., high dipole-dipole interaction) that are close to the dielectric constant of water ($\epsilon = 80$). To better understand the contribution of initial oils and their SARA fractions, indirect polarity measurements of water and oil phases obtained through bottle tests. The dielectric constant measurements were carried out on the water and oil samples collected from bottle tests and results were compared to initial oil samples dielectric constant, see **Table 4.5**.

Table 4.5— Polarity estimation for crude oils and their SARA fractions.

Fractions	Crude Oil 1	Crude Oil 2
Crude Oil	2.89	2.51
Saturates	2.42	2.39
Aromatics	3.45	3.34
Resins	4.22	3.33
Asphaltenes	4.90	3.40

Note that Oil 1's polar components have high dielectric constant and thus higher polarity than Oil 2. This indicates that Oil 1 has more polar components than Oil 1, and these polar components involved in dipole-dipole interaction with water causing polarity cancellation (Punase and Hascakir 2017) and overall lower dielectric constant of Oil 1's water phase. Due to polarity cancellation, the dielectric constant values reported for water

phase in **Figure 4.9-A** is lower than water and for oil phase in **Figure 4.9-B** the values are lower than oil or/and their main polar fractions (namely asphaltenes and resins).

Having the oil phase's dielectric constant value be lower than the initial oil's dielectric constant indicates that there were dipole-dipole interactions between the oil's polar functional group, leading to polarity cancellation and reducing the overall polarity of the oil phase. However, the high dielectric constant value of the oil phase may indicate the presence of water droplets as O/W emulsion which have a much higher polarity. The dielectric constant values of the oil phase from mixing cationic surfactants solutions gave the highest values for both crude oils. This indicates higher polarity because of water droplets that exist as emulsions in the oil. On the other hand, mixing anionic surfactants with crude oils gave the lowest dielectric constants for their oil phase while the nonionic surfactants gave moderate values of oil phase's dielectric constants, see **Figure 4.9**.

4.4 Visualization of Water-Surfactant-Oil Interactions Under Optical Microscopy

To visualize the polar-polar interaction and how cancellation occurs among polar and non-polar groups of crude oils as they interact with water and surfactants, optical microscopy analyses were carried out. Crude oil samples and their SARA fractions were subjected to steam for 10 minutes or liquid water in the presence or absence of surfactant solutions. The crude oil samples and their polar fractions were visualized under an optical microscope before and after steam and surfactant-steam exposure. Their interactions were visualized simultaneously under an optical microscope.

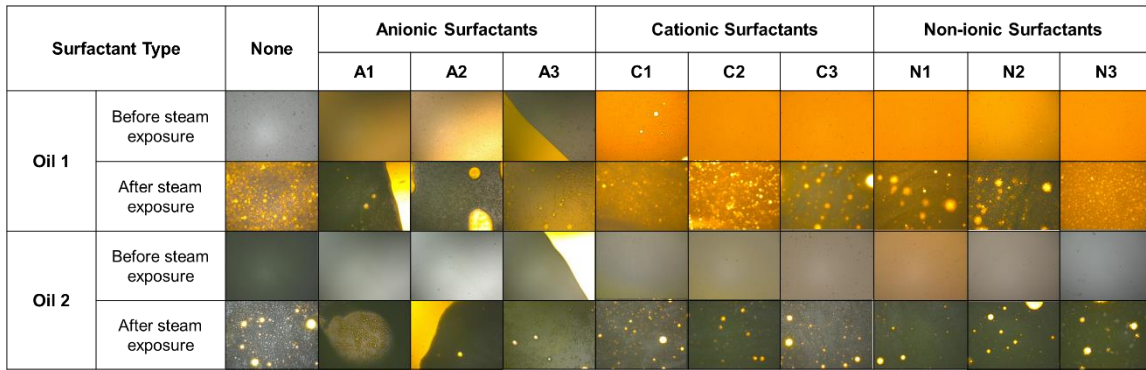


Figure 4.10—Surfactant-crude oil interaction before and after steam exposure at 100x magnification; oil samples were exposed to steam at 150°C for 10 minutes at atmospheric pressure, modified with permission from (Alshaikh et al. 2018).

Images obtained from the optical microscopic of the crude oil samples interaction with a drop from nine different surfactant solutions before and after steam exposure are given in **Figure 4.10**. These images show a clear trend for cationic and nonionic surfactants improving emulsion formation significantly for both oils. Moreover, the addition of surfactants helped to enhance emulsion formation after steam exposure (i.e., enhanced electrostatic interaction between oil, surfactants, and steam), as shown in the before and after images appearing in **Figure 4.10**. The droplet size of the emulsion was observed to be smaller after the addition of a surfactant, the presence of which increased emulsion stability. The main aim of the surfactant enhanced oil recovery processes is to form stable emulsions that have a small droplet size. Hence, it was observed for Oil 1 that the anionic surfactants provide more emulsions that were smaller and better distributed. Optical microscopy analyses were extended over the SARA fractions allowing for an examination of steam and surfactant interaction with the oil's polar components. First, resins and asphaltenes interaction with steam were studied. After that, the mutual

interaction of oil polar fractions (resins and asphaltenes) were investigated with and without steam exposure. The nonpolar fraction (saturates and aromatics), then, added to study their effects as well.

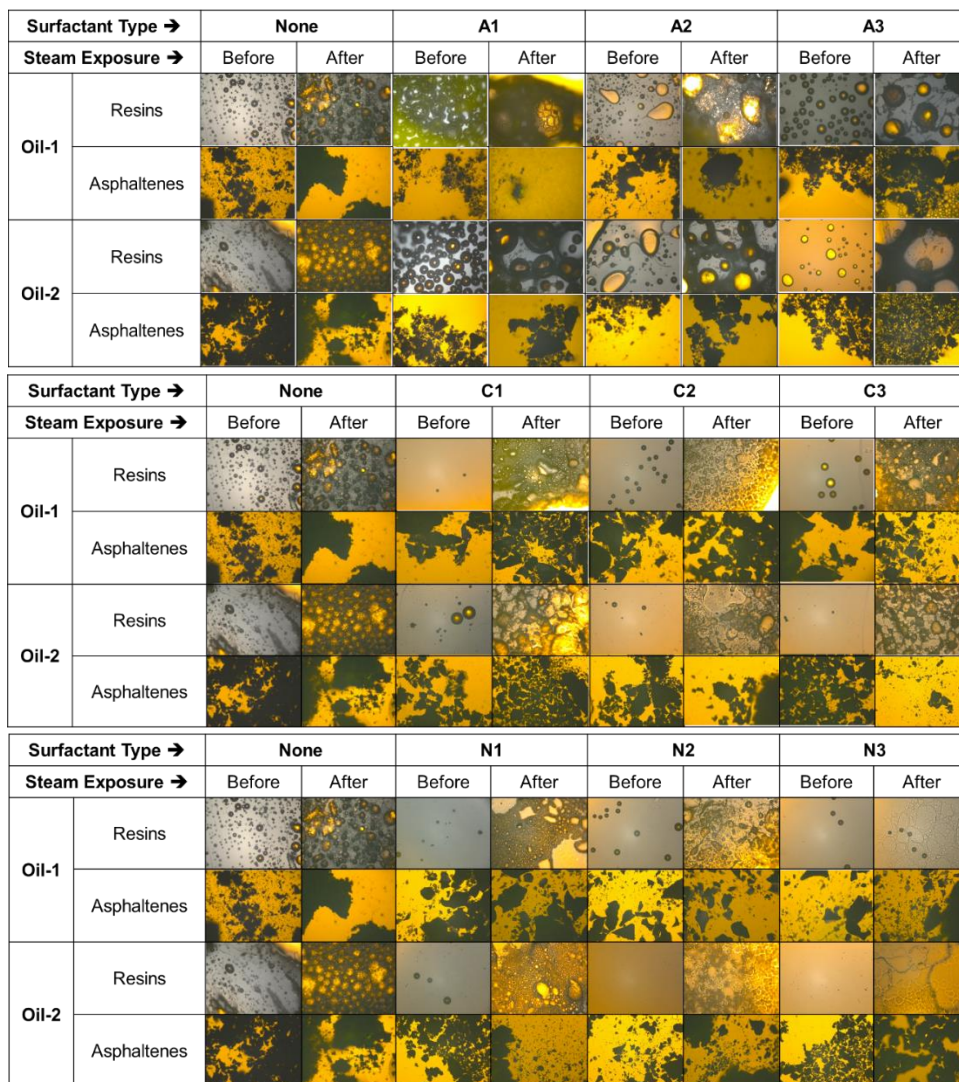


Figure 4.11—Anionic (top), cationic (middle), and nonionic (bottom) surfactant-resin fraction of crude oil and surfactant-asphaltene fraction of crude oil interactions before and after steam exposure at 100x magnification; oil samples were exposed to steam at 150°C for 10 minutes at atmospheric pressure, modified with permission from (Alshaikh et al. 2018).

As shown in **Figure 4.11**, resin fractions, as compared to asphaltene fractions, were mainly responsible for emulsion formation. The magnitude of the emulsion formed within the resins varied with the type of surfactant and emulsion formation in some cases is enhanced after the exposure to steam. Interestingly, almost no emulsion formation was observed when the asphaltenes interacted with surfactant solutions alone which means that no electrostatic or dipole-dipole interaction is taking place. Although asphaltenes have been reported to be the most polar fraction in crude oil (Akbarzadeh et al. 2007; Fan et al. 2002), electrostatic interactions were not visible (see **Figure 4.11**) between the asphaltenes and water or asphaltenes and surfactants. Therefore, microscopic analyses were conducted to better understand emulsion formation when asphaltenes mutually interact with other oil fractions. First, the mutual interactions of asphaltenes with resins and then the role of aromatics and finally the role of saturates were investigated in emulsion formation with each surfactant in the presence of liquid or vapor water. **Figure 4.12** shows the results of these analyses for anionic surfactants, **Figure 4.13** for cationic surfactants, and **Figure 4.14** for non-ionic surfactants. It should be noted that the blends of SARA in microscopic analyses prepared by considering the ratios of each fraction present in the initial crude oil (see, **Table 4.1**) and CMC value of surfactants (see, **Table 3.1**).

Surfactant Type →		None		A1		A2		A3	
Steam Exposure →		Before	After	Before	After	Before	After	Before	After
Oil-1	Resins + Asphaltenes								
Oil-2	Resins + Asphaltenes								
Oil-1	Resins+ Asphaltene+ Aromatics								
Oil-2	Resins+ Asphaltene+ Aromatics								
Oil-1	All Fractions								
Oil-2	All Fractions								

Figure 4.12—Anionic surfactant-[resins+asphaltenes+aromatics+saturates fraction of crude oil] interaction before and after steam exposure at 100x magnification; oil samples were exposed to steam at 150°C for 10 minutes at atmospheric pressure, modified with permission from (Alshaikh et al. 2018).

Surfactant Type →		None		C1		C2		C3	
Steam Exposure →		Before	After	Before	After	Before	After	Before	After
Oil-1	Resins + Asphaltenes								
Oil-2	Resins + Asphaltenes								
Oil-1	Resins+ Asphaltene+ Aromatics								
Oil-2	Resins+ Asphaltene+ Aromatics								
Oil-1	All Fractions								
Oil-2	All Fractions								

Figure 4.13—Cationic surfactant-[resins+asphaltenes+aromatics+saturates fraction of crude oil] interaction before and after steam exposure at 100x magnification; oil samples were exposed to steam at 150°C for 10 minutes at atmospheric pressure.

Surfactant Type →		None		N1		N2		N3	
Steam Exposure →		Before	After	Before	After	Before	After	Before	After
Oil-1	Resins + Asphaltenes								
Oil-2	Resins + Asphaltenes								
Oil-1	Resins+ Asphaltene+ Aromatics								
Oil-2	Resins+ Asphaltene+ Aromatics								
Oil-1	All Fractions								
Oil-2	All Fractions								

Figure 4.14—Nonionic surfactant-[resins+asphaltenes+aromatics+saturates fraction of crude oil] interaction before and after steam exposure at 100x magnification; oil samples were exposed to steam at 150°C for 10 minutes at atmospheric pressure.

It has been observed that for both crude oil types and all surfactant blends, the mutual interaction between resins and asphaltenes generally reduces the formation of emulsions. It appears that resins and asphaltenes interacted with each other but did not interact with the water/steam and/or surfactants. The addition of aromatics fraction to asphaltenes and resins blend generated emulsions (mainly for Oil 1) for the water and anionic surfactants, see after steam exposure images in **Figure 4.12**. As saturates fraction added to the blends (all fractions in **Figure 4.12**, **Figure 4.13**, and **Figure 4.14**), emulsion formation was observed in almost all cases. The asphaltenes oil fraction is known to be soluble in aromatics and insoluble in saturates (Andersen and Birdi 1991; Prakoso et al. 2017; Speight 2014). Hence, in the case of [resins+asphaltenes+aromatics], the asphaltenes fraction was more soluble because both resins and aromatics have solvating

capacity of asphaltenes. Asphaltenes solubility may create polar and nonpolar sides for surfactants to interact with and form emulsions. Adding saturates fraction, however, caused asphaltenes instability and participation that makes the resins' sides more available to interact with the surfactants.

The results indicate that the emulsion formation is controlled mainly by asphaltenes by inhibiting its formation. Thus, if the emulsion formation wants to be advanced with the use of surfactants in heavy oil reservoirs, asphaltenes precipitants might be used to reduce the interaction of resins with asphaltenes. To such a degree, as the resins fraction is freed, they will interact more with surfactants and form emulsion much more effectively. This finding is also confirmed by additional microscopic images showing in **Figure 4.15**. Resins fraction was added to aromatics and then to saturates fraction and exposed to steam. The images show emulsions in all cases after steam exposure. Resins and aromatics fractions are the main fractions contributing to emulsion formation. This interaction is being deteriorated in the presence of asphaltenes for both oils and for all surfactants. Emulsion size is bigger in Oil 1 but their sizes are getting smaller with the addition of saturates. Thus, emulsion stabilization is maintained by saturates fraction. (note that smaller the emulsion size creates more stable emulsion).

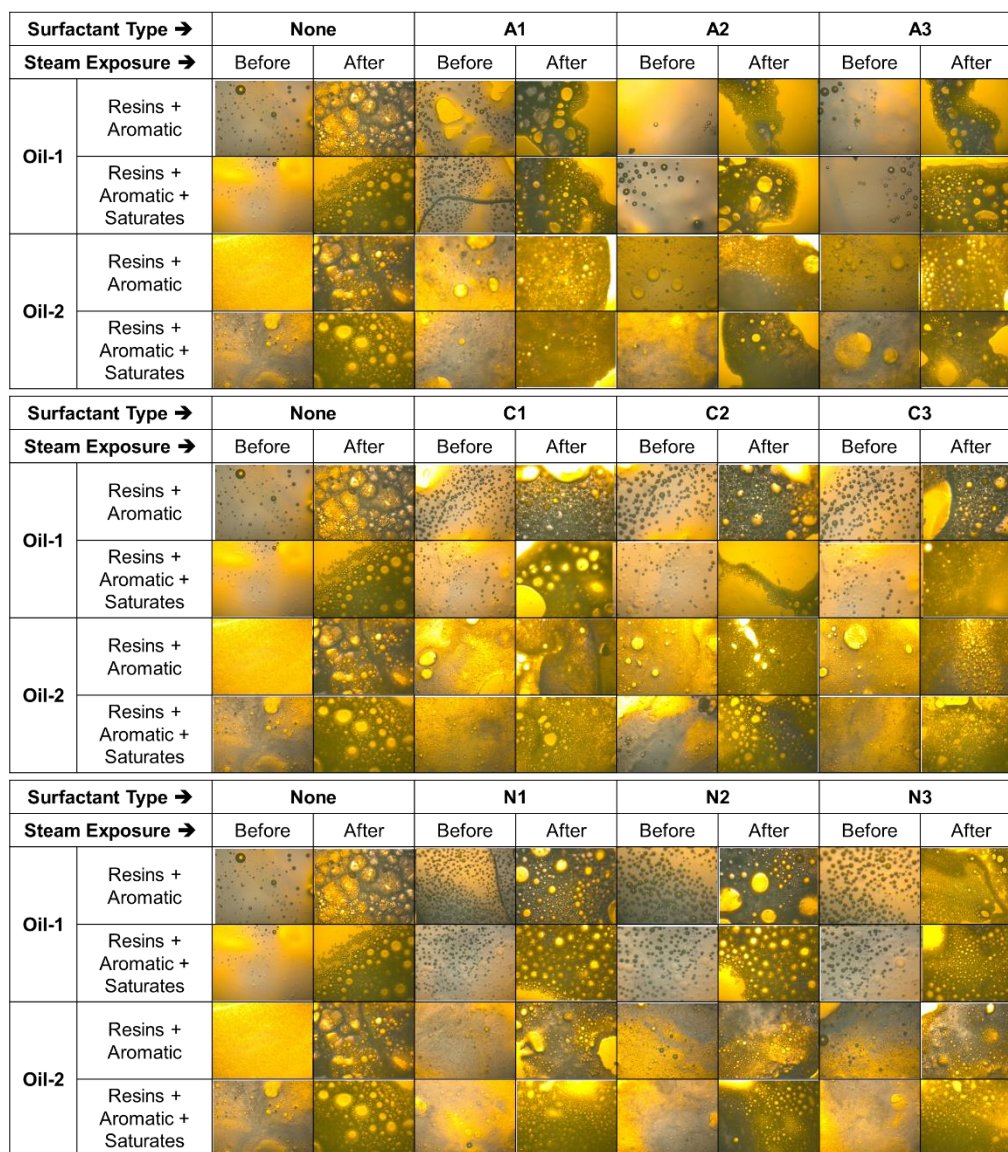


Figure 4.15— Anionic (top), cationic (middle), and nonionic (bottom) surfactant-[resins+aromatics+saturates fraction of crude oil] interaction before and after steam exposure at 100x magnification; oil samples were exposed to steam at 150°C for 10 minutes at atmospheric pressure.

4.5 Coreflood Experiments Results

The best method to evaluate and analyze the performance of the surfactant-steam process is by conducting coreflood laboratory experiments that provide an assessment for the process success. This method is particularly useful in studying the possible interactions that take place using detailed analysis of produced liquids and spent rock.

20 coreflood experiments were conducted, **Table 4.6** shows the steam and surfactant-steam coreflood experiments results for Oil 1 and Oil 2 in terms of cumulative oil recovery weight percent. The cumulative oil recoveries with time are reported in **Appendix C** for each coreflood experiment along with oil and water production rates. In addition, the recorded temperature profiles at the center of the core sample throughout the experiment are reported **Appendix D**. Note that for all coreflood experiments, temperature profiles are similar and in the range of 120-140 °C.

Table 4.6—Summary of the cumulative oil recovery, cumulative water production, the amount of trapped water in oil, maximum oil production rate, and maximum water production rate for all coreflood experiments.

Oil Type	Exp. No.	Surfactant Type	Surfactant Name	Total Experiment Time, min	Cumulative Oil Recovery, wt%	Cumulative Water Production, g	Water Trapped in Oil, wt%	Maximum Oil rate, g/hr	Time at Maximum Oil rate, min	Maximum Water rate, g/hr	Time at Maximum water rate, min
Oil 1	E1	Steam	-	175	57.77	1579.5	19.33	143	8	814	13
	E2	Steam + Anionic	A1	166	65.94	1903.8	14.83	331	9	1229	22
	E3		A2	210	62.86	1975.5	8.04	222	8	1173	23
	E4		A3	183	62.61	2270.2	0.03	208	10	1216	25
	E5	Steam + Cationic	C1	192	59.65	2193.2	6.66	294	8	1245	20
	E6		C2	185	67.46	2131.5	0.47	302	9	1097	24
	E7		C3	216	61.70	2274.5	0.24	269	9	1268	23
	E8	Steam + Nonionic	N1	210	58.64	2463.6	13.52	343	6	1395	23
	E9		N2	221	61.39	2243.1	6.04	311	8	1201	19
	E10		N3	211	58.50	2573.8	0	300	8	1211	20
	E11	Steam	-	219	49.73	1697.0	16.67	305	6	1212	21
	E12	Steam + Anionic	A1	240	52.68	3525.4	19.03	241	9	1141	21
	E13		A2	154	57.94	2149.2	17.19	227	11	1155	23
	E14		A3	216	63.77	2077.0	0.32	297	9	1229	23
	E15	Steam + Cationic	C1	209	56.17	2332.8	10.48	147	9	1143	21
	E16		C2	180	56.47	1956.6	6.51	227	9	1312	22
	E17		C3	275	66.28	2480.4	0.81	280	10	1187	24
	E18	Steam + Nonionic	N1	249	57.96	2516.4	5.59	230	8	1197	20
	E19		N2	214	61.70	2779.6	7.21	272	9	1175	23
	E20		N3	190	59.90	2196.2	0.7	225	10	1218	24

Table 4.6 summarizes the cumulative oil recovery, cumulative water recovery, trapped water content, maximum oil rate, and maximum water rate for all coreflood experiments. The cumulative oil recovery results of steam and surfactant-steam injection show that surfactant additives were successful to increase oil recovery for both crude oils. The cumulative oil production of the Oil 2 steam injection experiment was considerably lower compared to Oil 1's steam injection experiment (E1 and E11). In **Figure 4.16**, the observed performance of the surfactant additives varied for both crude oils. While the ionic surfactant with the longest tail length performed better for Oil 1 (i.e., higher oil recovery), it performed poorly for Oil 2.

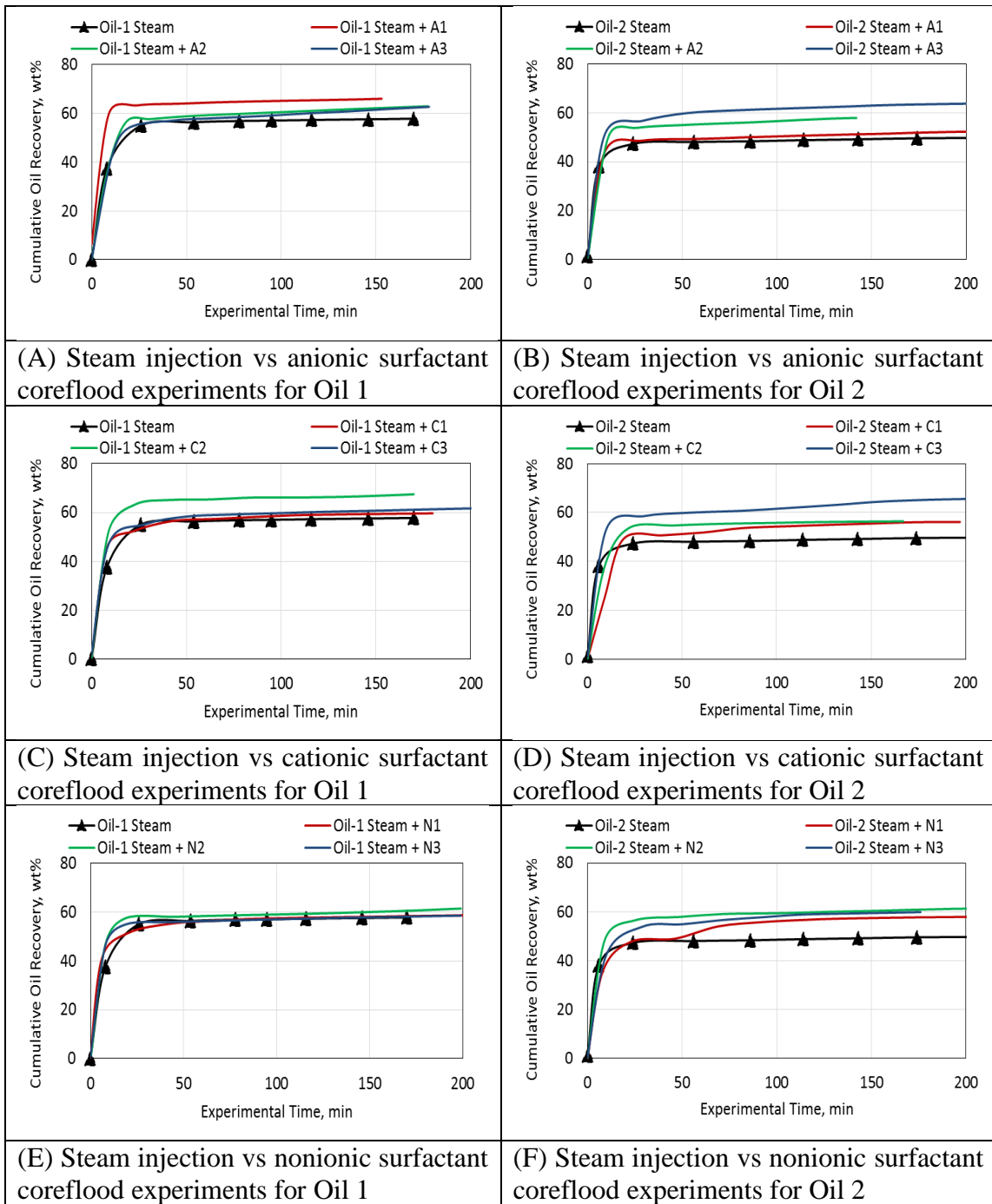


Figure 4.16—Cumulative oil recovery from steam and surfactant-steam coreflood results.

Note that most of oil is recovered in the first 25 minutes and very small recovery is obtained afterward. By examining the cumulative oil recovery plots with time, the surfactants with the longest and medium hydrocarbon tail length performed better for Oil 1 while the shortest and medium hydrocarbon tail length surfactants outperformed the longest tail length surfactant for Oil 2. In **Appendix C**, the oil recovery rates for crude oils' surfactant-steam coreflood experiments show a similar trend and **Table 4.6** summarizes these results.

The steam coreflood for Oil 2 (E11) gives the greatest oil recovery rate, however, it resulted in the lowest cumulative oil recovery. In addition, the produced oil from the steam injection coreflood experiment has high water content trapped in oil in the form of water-in-oil emulsions. On the other hand, the results of the E20 experiment with N3 cationic surfactant-steam injection show very low water content in produced oil and the cumulative oil recovery is high. Separation of produced water-in-oil emulsions is difficult, and to assess the difficulty, TGA/DSC and conventional furnace were used along with analyzing produced oil's quality.

4.5.1 Characterization of emulsion in Produced Oil Samples

The heat has been often used to break the water-in-oil emulsion (Becker 1997). Heat introduction to emulsion causes water droplets to collide and an increase in viscosity difference between oil and water enhancing separation (Schramm 1992). In this study, heat has been used to separate water trapped in oil in the form of emulsions in two ways; first, for the easily separable water, produced oil samples were heated by conventional oven at a slow heating rate. Then, TGA/DSC experiments were applied at 10 °C/min

heating rate to determine the amount of water in severe emulsion form. **Figure 4.17** reports weight loss of each sample in time spent in the conventional oven at 60-70 °C.

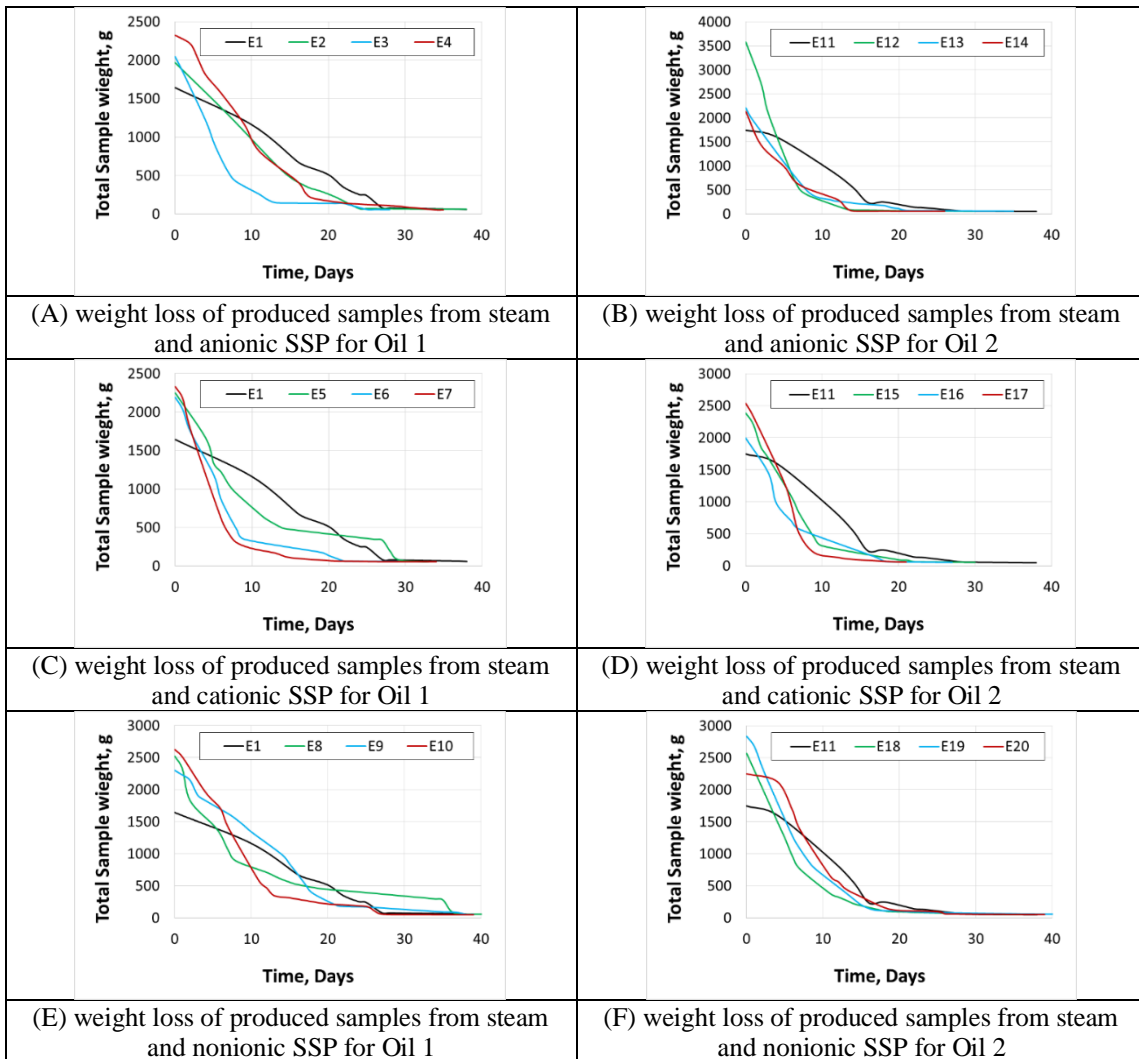


Figure 4.17—Produced oil samples weight loss with time spent on the oven at 60°-70° C showing the difficulty of separating water-in-oil emulsions.

Most of the free water is separated within the first 10 days; then, water separation becomes more difficult because water is now in the oil as emulsions. The weight loss due

to water evaporation in the oven becomes a very slow process. Hence, TGA/DSC was used to determine the amount of water trapped in oil in the form of water-in-oil emulsions. Produced oil samples were subjected to TGA/DSC analysis at 10 °C/min heating rate under air injection until reaching 200 °C. The temperature value at which the water content is lost is used to define the difficulty of the emulsion removal process. The higher the temperature means emulsions separation was difficult. The summary of the results summary is given in **Table 4.7** and all TGA/DSC plots are in **Appendix E**.

Table 4.7— Temperatures at which emulsified water separate from produced oil for each coreflood experiment.

Flood Type	Surfactant Name and Hydrocarbon Tail Length	Exp. No.	Water evaporation Temperature, °C	Exp. No.	Water evaporation Temperature, °C
Steam Injection	-	E1	124	E11	120
Anionic Surfactant- Steam Injection	A1: SDS	E2	130	E12	135
	A2: SDeS	E3	130	E13	135
	A3: SOS	E4	110	E14	120
Cationic Surfactant- Steam Injection	C1: CTAB	E5	135	E15	120
	C2: MTAB	E6	118	E16	115
	C3: DTAB	E7	118	E17	115
Nonionic Surfactant- Steam Injection	N1: X-100	E8	121	E18	120
	N2: X-114	E9	123	E19	120
	N3: X-45	E10	110	E20	110

A1: Sodium Dodecyl Sulfate, A2: Sodium Decyl Sulphate, A3: Sodium Octyl Sulfate

C1: Hexadecyltrimethylammonium Bromide, C2: Myristyltrimethylammonium Bromide, C3: Dodecyltrimethylammonium Bromide

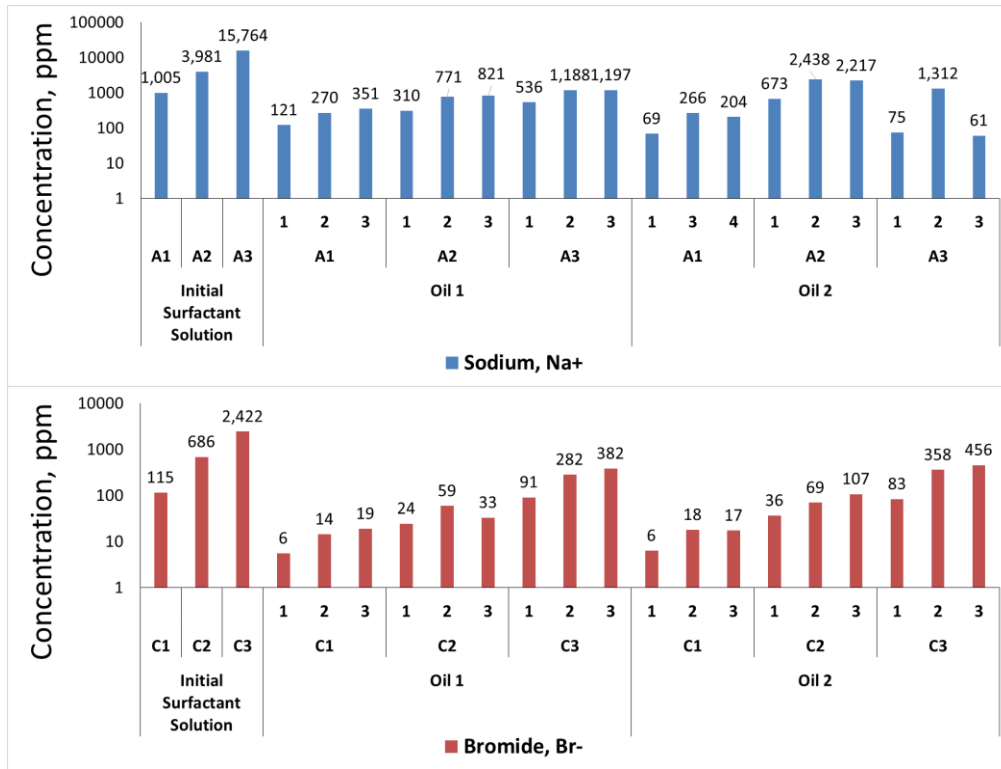
N1: Triton™ X-100, N2: Triton™ X-114, N3: Triton™ X-45

Results in **Table 4.7** indicate that when nonionic surfactants used as an additive for surfactant-steam injection, the emulsion separation was easier. Note that these nonionic surfactants have the highest thermal stability in **Figure 4.4**. Overall, TGA/DSC

results show that water-in-oil emulsion for Oil 1 is harder to separate than Oil 2. During steam injection, emulsion formation is expected due to crude oil natural emulsifying agents (Kokal 2005; Schramm 1992; Schramm and Smith 1985).

4.5.2 Produced Water Analysis

In the coreflood experiments, anionic surfactants with sodium sulfate head and cationic surfactants with nitrogen bromide head were used. Analyzing sodium and bromide ions will give information about surfactant retention. Hence, three produced water samples from the coreflood tests were collected; one at the beginning of the flood, middle, and near the end of the flood experiments. The samples were filtered and run through ion chromatography to determine the yielded bromide or sodium ions concentration. The results are given in **Figure 4.18** including the initial concentration of surfactants solutions.



A1: Sodium Dodecyl Sulfate, A2: Sodium Decyl Sulphate, A3: Sodium Octyl Sulfate
 C1: Hexadecyltrimethylammonium Bromide, C2: Myristyltrimethylammonium Bromide, C3: Dodecyltrimethylammonium Bromide

Figure 4.18—Ions concentration of produced water showing surfactants retention for three produced water samples that are collected from the begging of the coreflood (1), middle time (2) and close to the end (3) of the experiments. At the top anionic retention ions (sodium) and at the bottom cationic retention ions (bromide).

The results indicate that there is at least 10% surfactant retention, and the retention of anionic surfactants is higher than cationic surfactants. In our coreflood experiments, sand was used as reservoir rock which contains a large amount of negatively charged silica. Hence, it is concluded that the electrostatic repulsion between the negatively charged surfactants and sand prevents anionic surfactant adsorption, unlike the cationic surfactants. For nonionic surfactants, there are no specific ions that can be traced to the

surfactants like sodium ions (Na⁺) in anionic surfactants or bromide ions (Br⁻) for cationic surfactants.

The used distilled water to prepare surfactant solutions has been also tested for its ion content. The results in **Table 4.8** show that distilled water has low ion concentrations, in particular, sodium and bromide ions are very low (~0.05 ppm) which makes distilled water interactions minimized. The measured concentrations of produce water samples where in the distilled water range, thus, they were not reported.

Table 4.8—Distilled water ions concentration that used to prepare surfactants solutions.

Anions	Concentration, ppm	Cations	Concentration, ppm
Floride	0.06	Lithium	0.01
Chlorite	0.08	Sodium	0.05
Nitrite	0.06	Ammonium	0.03
Bromide	0.05	Potassium	0.035
Nitrate	0.04	Magnesium	0.09
Phosphate	0	Calcium	0.19
Sulfate	0		

4.5.3 Residual Oil Analysis and Spent Rock Inspection

Figure 4.19 and **Figure 4.20**, provide an overview of spent rock images at the end of the coreflood experiments for Oil 1 and Oil 2, respectively.

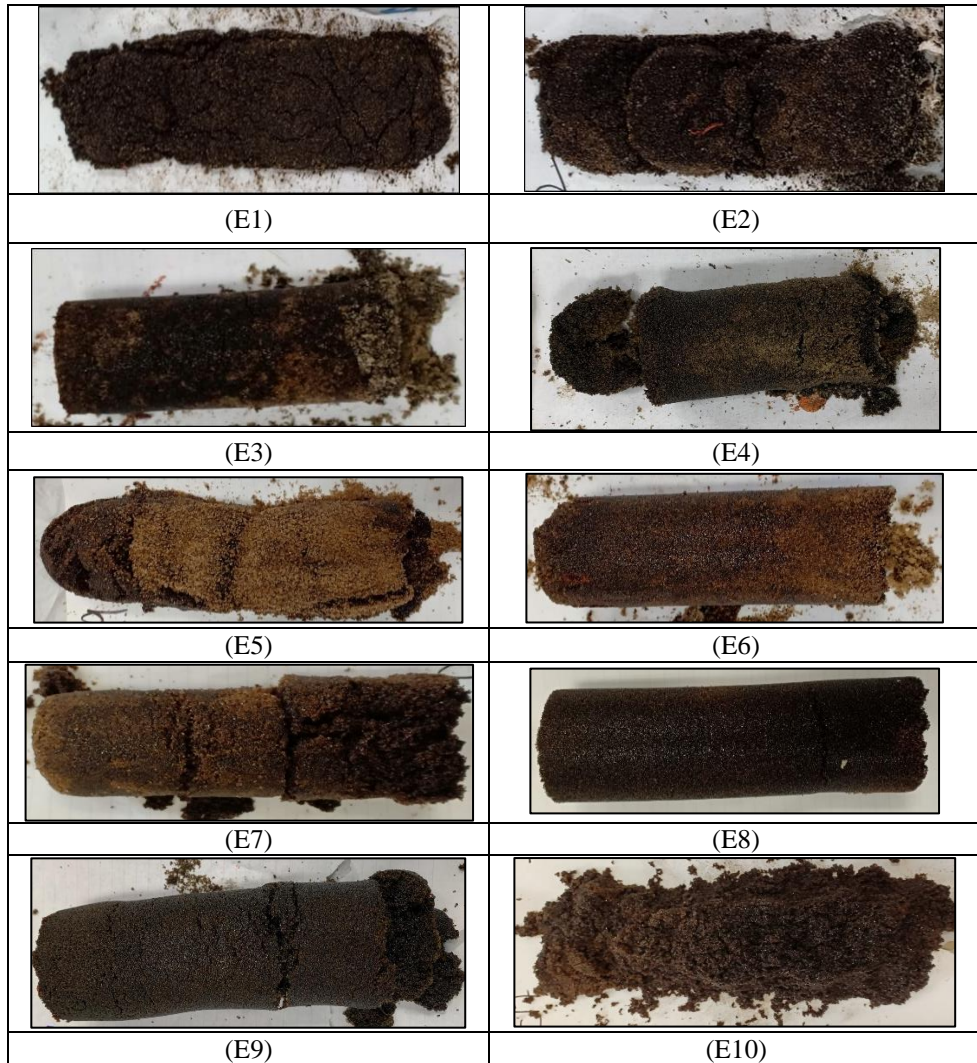


Figure 4.19—Spent rock images for all experiments conducted with Oil 1. Injection is from left (inlet) to right (outlet). For experiment naming, refer to Table 3.2.



Figure 4.20—Spent rock images for all experiments conducted with Oil 2. Injection is from left (inlet) to right (outlet). For experiment naming, refer to Table 3.2.

For both crude oils, the images show that steam injection experiments yielded the darkest spent rock color compared to surfactant-steam injection spent rock images which is consistent with residual oil saturation results (i.e., the darker the color indicate that more oil is left behind). For Oil 1, spent rock's lightest color was observed for surfactant-steam experiments of the three cationic surfactants (E5, E6, and E7) followed by the nonionic surfactants coreflood experiments (E8, E9, and E10). These results suggest that cationic surfactants may be best suited to displace Oil 1. This finding is also supported by the

cumulative oil recovery values. Another observation that could be mistakenly made is about the consolidation of the spent rock. All of the spent rock are consolidated after the coreflood experiments, although some spent rock appears to be unconsolidated because the spent rocks were taken out from the core holder immediately.

For Oil 2, what stands out in **Figure 4.20** is the surfactant-steam experiments of nonionic surfactants have the lightest spent rock's color in comparison with other surfactant-steam injection experiments, see E18, E19, and E20 spent rock's images. The anionic surfactant-steam experiments are the second in terms of spent rock's light color, especially experiment E14 with the shortest hydrocarbon surfactant's tail. The most surprising aspect of the E12 image is the lighter color on the right side (the outlet) of the spent rock. As surfactant and steam being injected, it is expected that most of the oil will be displaced from near the inlet to accumulate before being produced at the outlet. The light color near the outlet indicates that the displacement might not be uniform and the crude oil is left behind trapped without having steam or surfactant displacement. The steam and surfactants bypassed the trapped oil and produced most of the oil near the outlet.

Spent rocks are used to obtain information about the residual oil and residual oil's asphaltenes. The average residual oil saturations, along with the inlet and outlet residual oil saturations for all coreflood experiments, are presented in **Figure 4.21** (sample calculation is in **Appendix F**). Overall, these results indicate that residual oil saturation for surfactant-steam injection is lower than steam injection alone for both crude oils. Oil 2 has more oil remains than Oil 1 after steam injection as discussed previously. The

residual oil saturations near the inlet and the outlet show the sweep direction indicated by the low saturation values near the inlet.

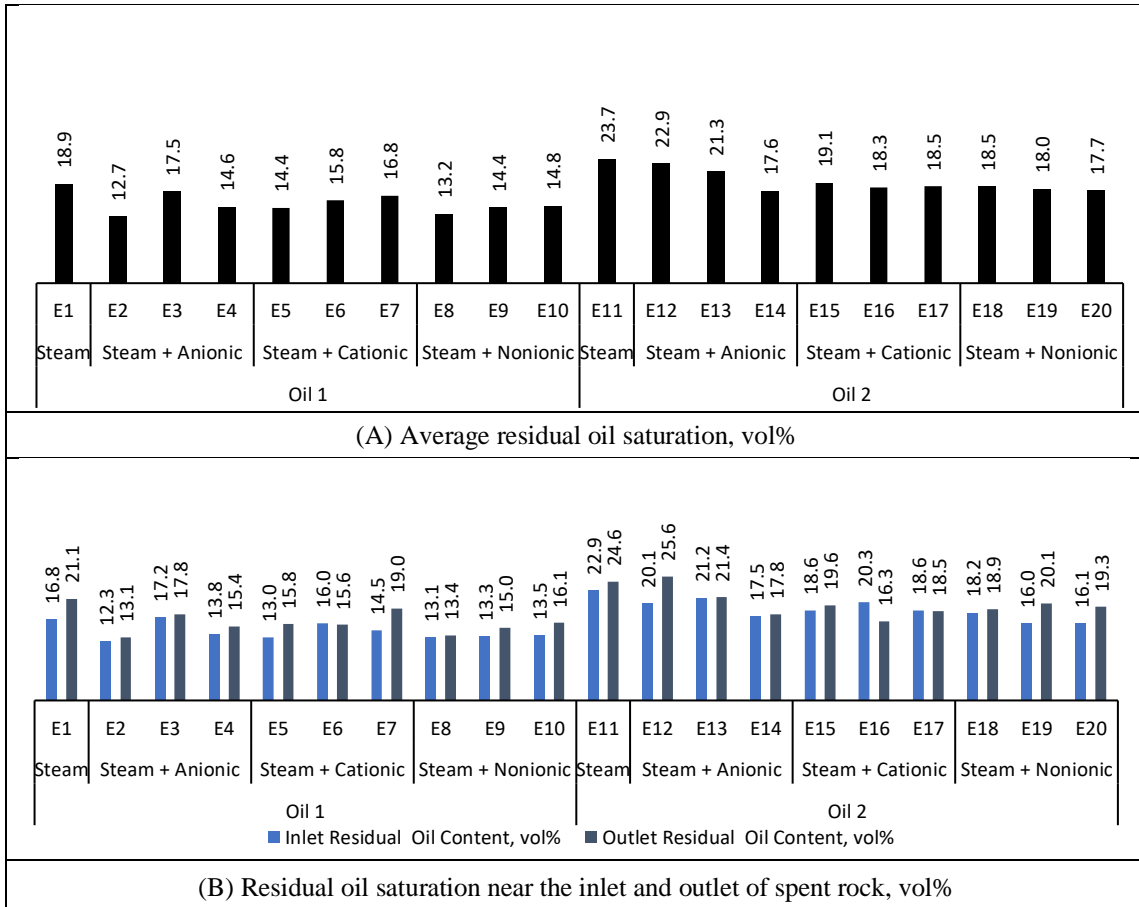


Figure 4.21—Residual oil saturation for the average (A) and the comparison of the inlet and outlet (B) of core holder.

4.6 Analysis of Residual and Produced Oil's Asphaltenes

Asphaltenes are the most polar fraction of the crude oil because of the attached heteroatoms and heavy crude oils have large quantities (Crocker and Marchin 1988). Its precipitation might cause severe formation damage in oil reservoirs reducing oil

production and makes transportation and processing difficult (Becker 1997). During the surfactant-steam process, asphaltene charged surfaces are expected to interact with surfactant's charged polar head. Hence, asphaltene content of produced and residual oil during surfactant-steam coreflood experiments are determined.

Table 4.9 presents the residual oil asphaltene and produced oil asphaltene from steam and surfactant-steam coreflood experiments of 100 g oil. Note that the initial oil asphaltene are 28.6 wt% for Oil 1 and 38.8 wt% for Oil 2. The results show produced oils have fewer asphaltene than initial oils after steam injection for both oils (11.0 g for Oil 1 and 16.51 g for Oil 2). Data from this table show that for almost all surfactant-steam experiments, the produced oil asphaltene content is higher than produced oil asphaltene from the steam injection (see, E2-E10 vs. E1 and E12-E20 vs. E11). The anionic surfactant-steam injection with A2 is the only exception (E13). Interestingly, as the surfactant hydrocarbon head gets shorter, the content of asphaltene in the produced oil becomes much higher than the asphaltene content in the residual oil (see, E4, E7, and E10).

Overall, the results of residual and produce oil's asphaltene show that as the asphaltene in the produced oil increase, the asphaltene content in residual oil decrease when compared to initial oil asphaltene. For example, the residual oil's asphaltene content for E1 has decreased by 17.58 g compared to initial oil asphaltene (28.6 gram). Together these results provide important insights into the interaction between asphaltene and different types of surfactants. The results indicate that asphaltene, which are the most polar component of crude oil, can affect the efficiency of the surfactant-steam process by

interacting with surfactants' polar heads. Hence, produced oil and produced oil's asphaltenes were analyzed using the FTIR spectrum.

Table 4.9— Summary of the produced oil asphaltenes and residual oil asphaltenes content in 100 g of oil.

Oil Type	Exp. No.	Surfactant Type	Surfactant Name	Initial Oil's Asphaltenes, g	Produced Oil's Asphaltenes, g	Residual Oil's Asphaltenes, g
Oil 1	E1	Steam	-	28.58	11.00	17.58
	E2	Steam + Anionic	A1	28.58	16.88	11.70
	E3		A2	28.58	18.60	9.98
	E4		A3	28.58	22.35	6.23
	E5	Steam + Cationic	C1	28.58	19.68	8.90
	E6		C2	28.58	17.88	10.70
	E7		C3	28.58	19.25	9.33
	E8	Steam + Nonionic	N1	28.58	16.30	12.28
	E9		N2	28.58	17.88	10.70
	E10		N3	28.58	22.70	5.88
Oil 2	E11	Steam	-	38.76	16.51	22.25
	E12	Steam + Anionic	A1	38.76	17.33	21.43
	E13		A2	38.76	15.70	23.06
	E14		A3	38.76	29.21	9.55
	E15	Steam + Cationic	C1	38.76	23.82	14.94
	E16		C2	38.76	25.98	12.78
	E17		C3	38.76	26.45	12.31
	E18	Steam + Nonionic	N1	38.76	27.47	11.29
	E19		N2	38.76	25.68	13.08
	E20		N3	38.76	24.26	14.50

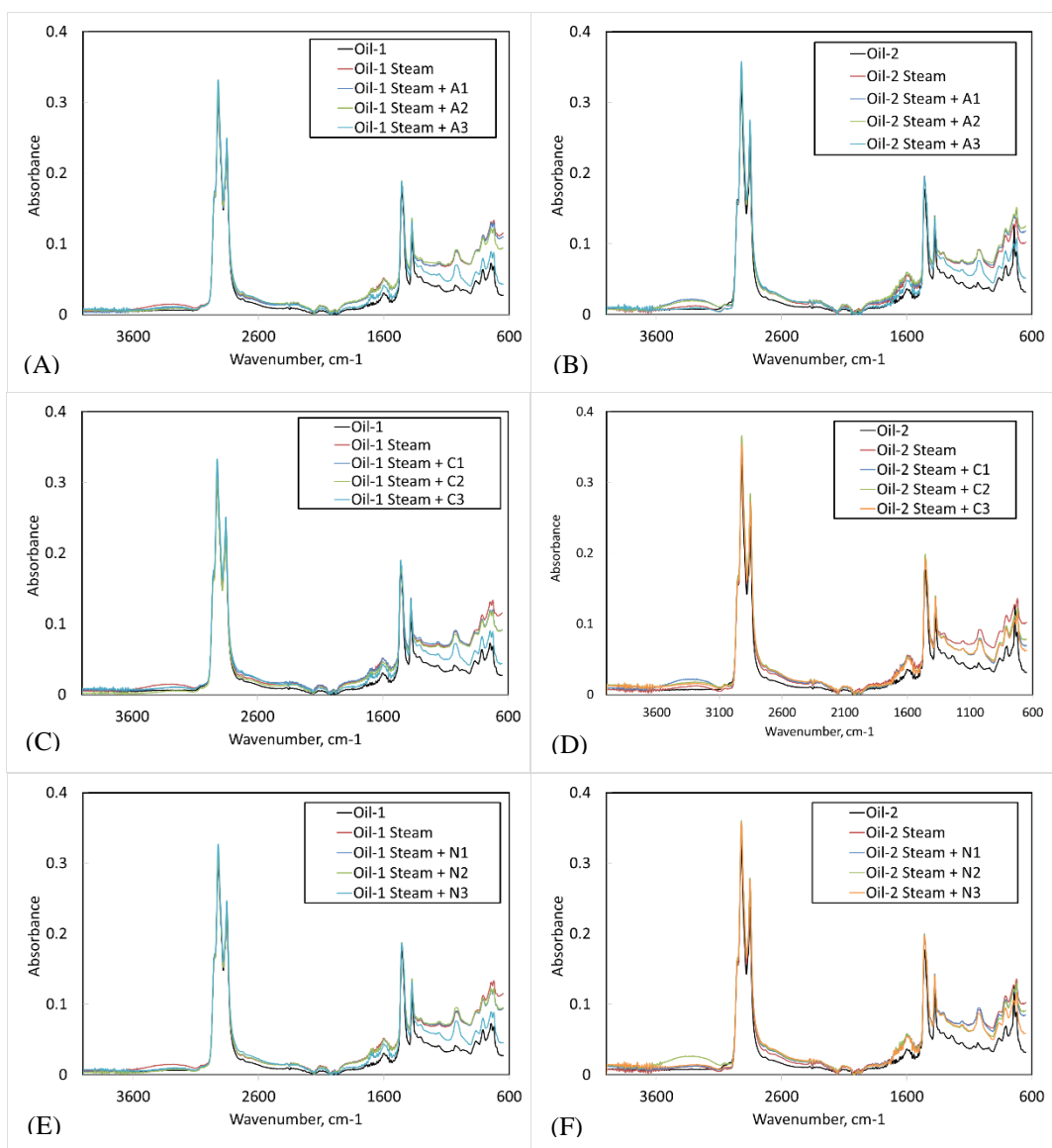


Figure 4.22—FTIR spectra for produced oil samples from coreflood tests after water separation.

The FTIR of the produced oils from steam and surfactant-steam coreflood experiments are presented in **Figure 4.22**. The observed FTIR spectra show identical peaks in the aliphatic bond regions ($2955\text{--}2851\text{ cm}^{-1}$) but taller peaks in the region between

1700 cm^{-1} and 600 cm^{-1} compared to initial oil (Smith 2011; Stuart 2004). In general, the spectra are similar with some intensity differences. For example, in the aromatic C=C bond region around 1590 cm^{-1} , produced oil's spectrums from steam and surfactant-steam coreflood experiments show higher peaks (Smith 2011; Stuart 2004). There is a significant increase at 1025 cm^{-1} which indicates the presence of S=O stretching in all asphaltenes samples that separated from produced oils of steam and surfactant-steam coreflood. This means that during steam flooding there was an interaction between oxygen and sulfur that exist in the crude oil. In addition, the fingerprint region has a significant increase compared to the initial oil's spectra. However, the fingerprint region increase in general may actually indicate the presence of water.

The FTIR signature of distilled water is characterized by O-H stretch peak at 3280 cm^{-1} and O-H bend at 1630 cm^{-1} (Stuart 2004). The presence of water in produced oils is supported by the estimated produced oil's water content, see **Table 4.6**. For example, the water content of the produced oil from the surfactant-steam coreflood experiment "E7: Oil 1 Steam + C3" is 0.3% and the FTIR result show low peaks in 1700-600 cm^{-1} region, see **Figure 4.22-B**. On the other hand, the produced oil sample from "E5: Oil 1 Steam + C1" coreflood experiment which has a water content value of 6.7%, has much higher peaks at 1700-600 cm^{-1} region, see **Figure 4.22-B**.

FTIR spectra of the produced oil asphaltenes were also examined, see **Figure 4.23**. It has been observed that for produced oil's asphaltenes, only fingerprint regions gave different FTRIR signatures. Note that during the vibration, a change in the molecules dipole moment occurs which is reflected in strong adsorption for permanently polarized

molecules (Stuart 2004). Hence, intense adsorption of a sample means that the sample has higher dipole moment (i.e., higher polarity). The different in asphaltenes adsorption indicates that during steam and surfactant-steam experiments, there was an interaction between the charged asphaltenes and steam, surfactant and/or reservoir rock. Interestingly, in comparison with initial oil asphaltenes, there is an increase between 980 cm^{-1} and 1050 cm^{-1} for both oils. These peaks are suspected to be related to silicon compounds existed in reservoir rock (Smith 2011; Stuart 2004). It seems that Oil 2 interacted in a different way than Oil 1 when observing the intensity in the aliphatic bond regions ($2955\text{-}2851\text{ cm}^{-1}$) and around 1000 cm^{-1} . In surfactant-steam flood for heavy oils, the charged polar head group of surfactants may interact with the charged polar functional groups (e.g., nitrogen, sulfur, and oxygen) attached to crude oils rather than the water itself.

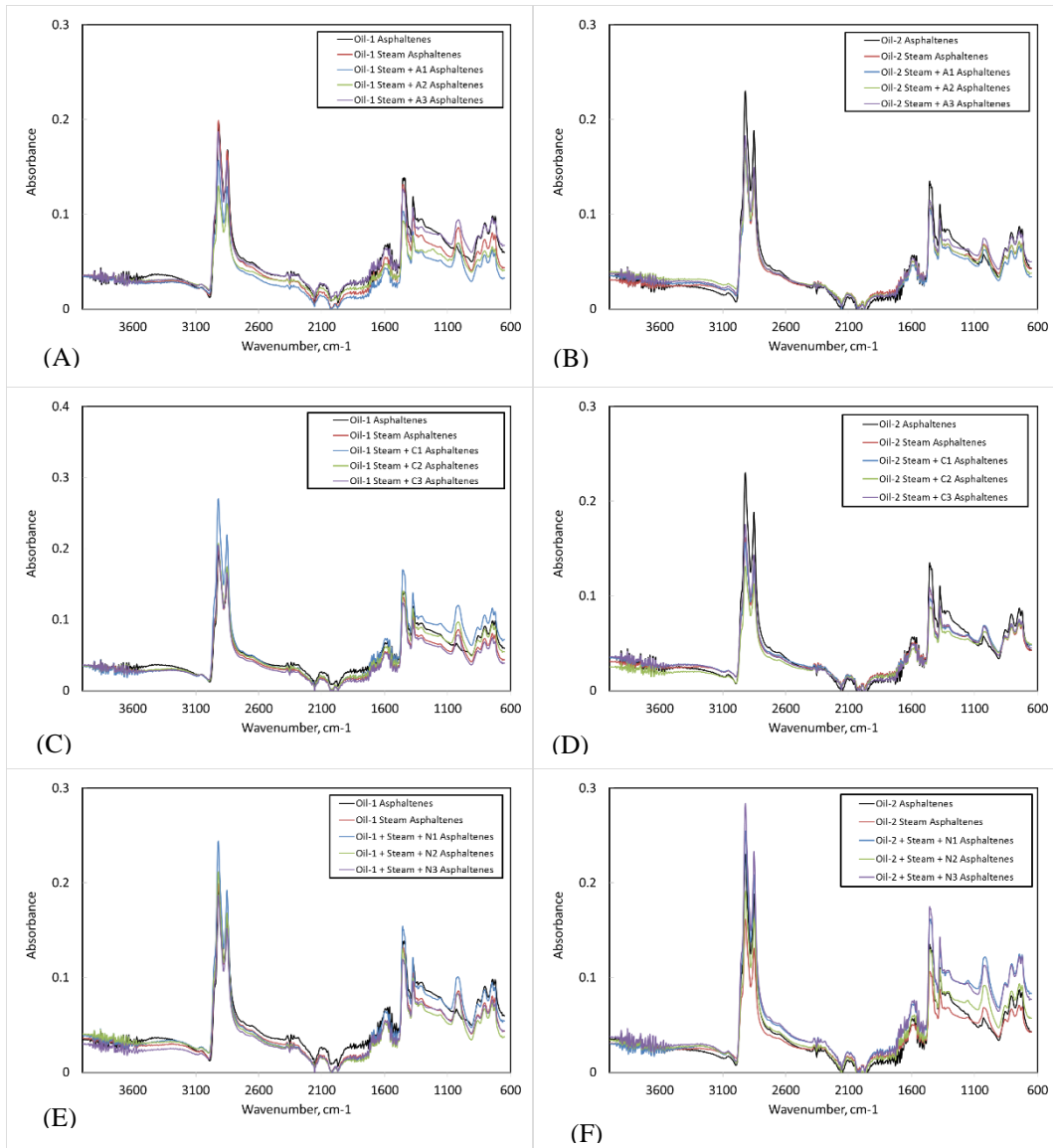


Figure 4.23—FTIR spectra for produced oil asphaltenes from steam and surfactant-steam injection.

4.6.1 Dielectric Constant Measurements (Dipole-Dipole Interaction)

Dielectric constant indirectly indicates the role of dipole-dipole interaction in steam and surfactant-steam processes, see **Figure 4.24**.

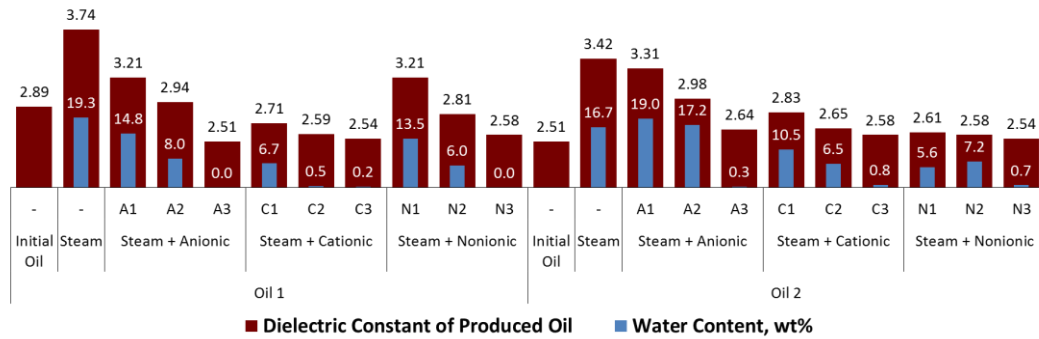


Figure 4.24—Dielectric constants values of produced oil (after thermal separation) from steam and surfactant-steam coreflood experiments showing polarity cancellation.

In a system, the overall polarity can be estimated by the summation of each component's polarity (Lowry 1927). However, polar-polar interaction of two different polar molecules may cancel out each other. Lower summation rule may not apply in some systems (Punase and Hascakir 2017). This rule is given with equation (1) below for a two-component system (oil and water).

$$\epsilon_{emulsion} = \epsilon_{oil} * v_{oil} + \epsilon_{water} * v_{water} \quad (1)$$

where, $\epsilon_{mixture}$: is the calculated mixture dielectric constant, ϵ_{oil} : measured dielectric constant of oil sample, v_{oil} : volume fraction of oil in the mixture, ϵ_{water} : measured dielectric constant of water (80), v_{water} : volume fraction of surfactant in the mixture.

The results in **Figure 4.24** do not show agreement with Lowry summation rule. For example, using the Lowry mixing rule equation (1) the produced oil dielectric constant of A1 surfactant-steam coreflood should be 17.8 according to Lowry's law. Thus, for the

system given in **Figure 4.24**, components interaction is different and more complicated than the interaction given with Lowry's equation.

In addition, it is observed that the polarity of the produced oils at low water content shows dielectric constants values that are less than the initial oil value, see **Figure 4.24**. For example, produced Oil 1 with A3 surfactant-steam experiment has a dielectric constant value of 2.59, which is lower than the initial oil's dielectric constant of 2.89. This is another indication of polarity cancellation (Punase and Hascakir 2017). Likewise, there is polarity cancellation indicated by the low dielectric constant values of produced Oil 1 from surfactant-steam experiments with C3 and N3 surfactants. Note that Oil 1 is moderately biodegraded, and it is expected to be enriched with heteroatoms that give higher dielectric constant. For Oil 2, and even this oil has high asphaltenes content, it is non-biodegraded, and its polar components polarity are lower than Oil 1 as indicated by their dielectric constant values. The produced oil from surfactant-steam coreflood of Oil 2 has fewer changes than Oil 1's produced oil dielectric constant.

Produced water's dielectric constants results are, generally, high and very close to the water dielectric constant of 80, **Figure 4.25**. The emulsion produced with water (O/W emulsion) may be the main reason for the decrease in polarity.

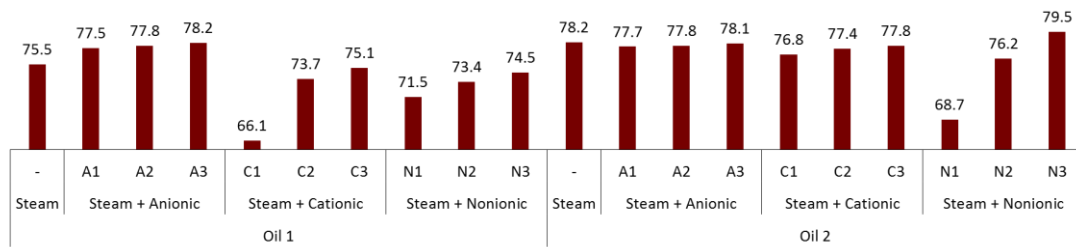


Figure 4.25—Dielectric constants values of produced water from steam and surfactant-steam coreflood experiments showing polarity cancellation.

The dielectric constants result overall provided only information on dipole-dipole interaction, and there might be an interaction that is stronger and could not be detected using dielectric constant measurements on the range of 0.5-4 GHz. Thus, we want to examine the ion-dipole or ion-ion interaction that might be occurring and because asphaltenes is the heaviest crude oil fraction contains most heteroatoms functional groups that can cause electrical charges promoting ion interaction, it was under test.

4.6.2 Zeta Potential Measurements

Previous studies showed that because of asphaltenes electrical charges, interactions of asphaltenes with reservoirs fines might occur (Prakoso et al. 2018; Qiao et al. 2017; Rodriguez-Navarro et al. 2000). Hence, the interaction between the charged surfaces of asphaltenes with surfactants charged head might be inevitable. To check this claim, ion-dipole and ion-ion interactions were indirectly determined through zeta potential measurements.

To measure asphaltenes' electrical surface charges, zeta potential measurements were conducted for all produced oil's asphaltenes from steam and surfactant-steam coreflood experiments, and the results are presented in **Figure 4.26**.

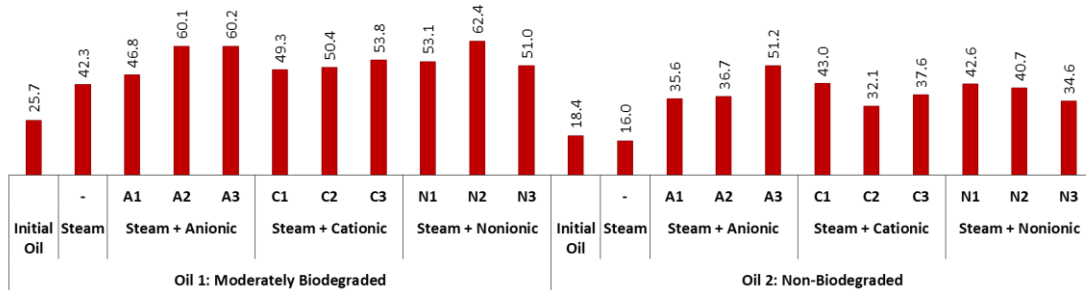


Figure 4.26—Ionic charge of the asphaltenes presented as zeta potential, all values are negative.

Overall, the results show that Oil 1's asphaltenes have a high absolute value of zeta potential when compared to Oil 2's asphaltenes which indicate higher stability of Oil 1's asphaltenes. In addition, the ionic content of the surfactant head seems like interacting with the charges attached to asphaltenes surface, indicated by the increase of zeta potential absolute values when comparing initial oil's asphaltenes and produced oil's asphaltenes from surfactant-steam experiments. The change of produced oil's asphaltenes charges to higher zeta potential values is an indication of solid stability and fewer asphaltenes precipitation. Interestingly, Oil 1 performed better under steam and surfactant-steam experiments as discussed previously. For both crude oils, the data shows that oil recovery is high when zeta potential values of produced oil's asphaltenes are high. For example, produced oil's asphaltenes from coreflood experiments E2-E10 have zeta potential values

46.8 mV to 62.4 mV which correspond to low residual oil values of 12.7 vol% to 16.8 vol% (i.e., higher oil production), see **Figure 4.21** and **Figure 4.26**. On the other hand, the steam coreflood (E1) with high residual oil saturation of 18.9 vol% has the lowest zeta potential value of 42.3 mV for its produced oil's asphaltenes. It was, also, observed that for Oil 2 there was a significant increase in oil recovery when applying surfactant-steam process unlike Oil 1. At the same time, there was a significant change in zeta potential values of produced asphaltenes (from 16 mV to 32.1-51.2 mV).

It appears that co-injecting surfactants with steam enhanced asphaltenes stability via ion-ion interaction evidenced by the high zeta potential values of produced asphaltenes, **Figure 4.26**. Thus, the asphaltenes precipitation is expected to be reduced (Hunter 1981). In oil reservoirs, asphaltenes could be destabilized and precipitate due to temperature, pressure, and crude oil composition changes (Leontaritis et al. 1994; Zhang and Chen 2018). This precipitation can cause severe formation damage and wettability alteration of the reservoir's rock to oil-wet, which can reduce oil production significantly (Kokal and Sayegh 1995; Leontaritis 1989; Zhang and Chen 2018). Another possible explanation for the increased oil recovery of surfactant-steam coreflood experiments is that the formation damage was reduced by having surfactants interacting and stabilizing crude oil's asphaltenes. For Oil 1's steam coreflood experiment (E1), the formation damage was less severe than Oil 2 (E11) which can be seen by the low zeta potential value of produce asphaltenes from Oil 2 steam coreflood experiment in comparison with Oil 1's steam injection produce asphaltenes (42.3 mV vs 16.0 mV). Note that Oil 2 has more asphaltenes content than Oil 1, **Table 4.1**. Hence, Oil 1's steam coreflood experiment was

more successful than Oil 2. In addition, surfactants co-injection with steam enhanced the asphaltenes stability for Oil 1 and Oil 2, reducing formation damage caused by asphaltenes precipitation; however, the significant increase in production was more noticeable in Oil 2 due to less formation damage severability of Oil 1’s steam injection coreflood when compared to Oil 2.

4.6.3 Economic Analysis

An economic analysis was conducted to study the feasibility of using surfactants as additives. **Figure 4.27** shows a comparison of surfactant cost to produce one crude oil barrel. Detail calculation sample and surfactants’ cost references are presented in **Appendix G**. The data shows that nonionic surfactants are the most economical surfactant additives to use. It cost less than \$4 to produce one barrel of oil using nonionic surfactants as steam additives. This is due to the low cost of these surfactants and their low CMC values compared to anionic and cationic surfactants.

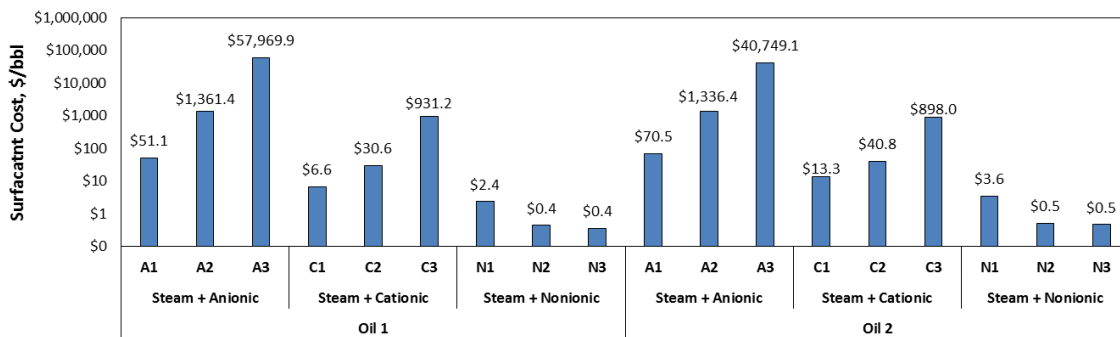


Figure 4.27—Surfactant cost to produce one barrel of oil.

5. CONCLUSION AND FUTURE WORK

5.1 Conclusions

In surfactant-steam flooding for heavy oils, the polar head groups of surfactants may interact with the polar functional groups in crude oil, rather than the water itself forming dipole-dipole or ion-dipole interaction. This interaction can be strong and reach ionic level interaction because of the oil reservoir's rock charges carried by crude oil. This study investigated whether the polar fractions of heavy crude oil interact with the polar heads of surfactants rather than their non-polar tails during surfactant-steam process by evaluating dipole-dipole, and ion-ion interactions.

A new technique for indirectly quantifying dipole-dipole interactions in order to identify the best surfactant candidates for increasing oil recovery was developed. This new technique uses dielectric constant measurements to determine the polarity within the emulsion layer of surfactant solution-oil blends.

Steam and surfactant-steam laboratory coreflood experiments for two heavy crude oils were conducted to study the process efficiency and the electrostatic interactions have taken place. Based on the coreflood experimental results of steam and surfactant-steam injection, the injection of surfactants improves the oil recovery compared to steam injection alone. The presence of chemical surfactants increases oil production, significantly, due to emulsion promotion caused by lowering oil-water interfacial tension.

Analyses conducted in this study suggests that during the steam and surfactant-steam injection for heavy oil reservoir, dipole-dipole, ion-dipole, and ion-ion interaction exist. Heavy crude oil has a considerable amount of resins and asphaltenes which are

regards as the oil's polar component proven by their high dielectric constant values. The results indicate that charged surfactant head is interacting with the oil charged polar component 'asphaltenes' via dipole-dipole and ion-ion interaction. The dielectric constant measurement shows the dipole-dipole interaction while zeta potential proved the existing of ion-ion interaction. The polar interaction can cause polarity cancellation for the crude oils. Surfactant-steam processes helped to stabilize the heavy crude oil's asphaltenes reducing formation damage.

In addition, economic analysis was performed. The results show the feasibility to use nonionic surfactants as steam additives at low cost.

5.2 Future Work

The current study highlights the importance of emulsion formation and its role in enhancing oil recovery from heavy oil reservoirs. The study was limited to 1D coreflood experiments in which the macroscopic displacement efficiency was not apprehended. In spite of its limitation, the study certainly adds to our understanding the importance of polar oil component interaction with chemical surfactants in microscopic efficiency. This would be a fruitful area for further work. A natural progression of this work is to analyze 3D coreflood tests and investigate the macroscopic efficiency enhancement if surfactants are used as additives in steam injection.

Further experimental investigations are needed to investigate the effect of mixing surfactants and alkali as steam additives. The alkali is known to have the ability to

generate surfactants in-situ by the reaction of converting naphthenic acids in the oil to soap — using alkali as steam additive is promising to reduce implementation cost.

Also, a greater focus on interfacial tension measurements at high temperatures (steam temperature) could produce interesting findings that account more for understanding of emulsions formation. Most current surfactants studies on light oils indicate the critical role of low IFT between oil and surfactant solutions in oil emulsification and enhancing production. Hence, a further study could assess the effects of IFT for heavy crude oils at steam temperature.

REFERENCES

- Aguilera, B., Delgado, J., and Cardenas, A. 2010. Water-in-Oil Emulsions Stabilized by Asphaltenes Obtained from Venezuelan Crude Oils. *Journal of Dispersion Science and Technology* **31** (3): 359-363. <https://doi.org/10.1080/01932690903196144>
- Akbarzadeh, K., Hammami, A., Kharrat, A., Zhang, D., Allenson, S., Creek, J., Kabir, S., Jamaluddin, A., Marshall, A.G., and Rodgers, R.P. 2007. Asphaltenes—Problematic but Rich in Potential. *Schlumberger Oilfield Review* **19** (2): 22-43.
- Al-Atwah, I., Alshaikh, M., Sweet, S., Knap, A., and Hascakir, B. 2018. Extension of Existing Screening Criteria Tables for Thermal Enhanced Oil Recovery Methods through Compositional Analyses of Heavy Oils. Paper presented at the SPE Western Regional Meeting, Garden Grove, California, USA, 22-26 April. SPE-190026-MS. <https://doi.org/10.2118/190026-MS>.
- Al Adasani, A. and Bai, B. 2011. Analysis of Eor Projects and Updated Screening Criteria. *Journal of Petroleum Science and Engineering* **79** (1-2): 10-24. <https://doi.org/10.1016/j.petrol.2011.07.005>
- Alboudwarej, H., Felix, J., Taylor, S., Badry, R., Bremner, C., Brough, B., Skeates, C., Baker, A., Palmer, D., and Anchorage, K. 2006. Highlighting Heavy Oil. *Schlumberger Oilfield Review* **18** (2): 34-53.
- Ali, M., Banerjee, S., and Hascakir, B. 2016. Produced Water Management for Thermal Enhanced Oil Recovery. Paper presented at the SPE Heavy Oil Conference and Exhibition, Kuwait City, Kuwait, 6-8 December 2016. SPE-184139-MS. <https://doi.org/10.2118/184139-MS>.
- Ali, M. and Hascakir, B. 2015. A Critical Review of Emerging Challenges for the Oil Field Waters in the United States. Paper presented at the SPE E&P Health, Safety, Security and Environmental Conference-Americas, Denver, Colorado, USA, 16-18 March. SPE-173529-MS. <https://doi.org/10.2118/173529-MS>.
- Ali, M. and Hascakir, B. 2017. Water/Rock Interaction for Eagle Ford, Marcellus, Green River, and Barnett Shale Samples and Implications for Hydraulic-Fracturing-Fluid Engineering. *SPE Journal* **22** (01): 162-171. SPE-177304-PA. <https://doi.org/10.2118/177304-PA>
- Alshaikh, M., Huff, G., and Hascakir, B. 2018. An Innovative Dielectric Constant Measurement Method to Determine the Ideal Surfactant Candidate to Enhance Heavy Oil Recovery. Paper presented at the SPE Canada Heavy Oil Technical Conference, Calgary, Alberta, Canada, 13-14 March. SPE-189752-MS. <https://doi.org/10.2118/189752-MS>.

- Alshaikh, M., Lee, Y.S., and Hascakir, B. 2019. Anionic Surfactant and Heavy Oil Interaction During Surfactant-Steam Process. Paper presented at the SPE Western Regional Meeting, San Jose, California, USA, 23-26 April. SPE-195254-MS. <https://doi.org/10.2118/195254-MS>.
- Amyx, J., Bass, D., and Whiting, R.L. 1960. *Petroleum Reservoir Engineering: Physical Properties*, First edition. New York: McGraw-Hill, Inc.
- Andersen, S.I. and Birdi, K.S. 1991. Aggregation of Asphaltenes as Determined by Calorimetry. *Journal of Colloid and Interface Science* **142** (2): 497-502. [https://doi.org/10.1016/0021-9797\(91\)90079-N](https://doi.org/10.1016/0021-9797(91)90079-N)
- ASTM International. (2011). ASTM D2007-11, "Standard Test Method for Characteristic Groups in Rubber Extender and Processing Oils and Other Petroleum-Derived Oils by the Clay–Gel Absorption Chromatographic Method". West Conshohocken, PA, <https://doi.org/10.1520/D2007-11>
- Atkinson, H. 1927. Recovery of Petroleum from Oil-Bearing Sands. USA Patent No. 1651311A.
- Austad, T., Matre, B., Milner, J., Saevareid, A., and Øyno, L. 1998. Chemical Flooding of Oil Reservoirs 8. Spontaneous Oil Expulsion from Oil-and Water-Wet Low Permeable Chalk Material by Imbibition of Aqueous Surfactant Solutions. *Colloids and Surfaces A: Physicochemical and Engineering Aspects* **137** (1): 117-129. [https://doi.org/10.1016/S0927-7757\(97\)00378-6](https://doi.org/10.1016/S0927-7757(97)00378-6)
- Bahri, M.A., Hoebeke, M., Grammenos, A., Delanaye, L., Vandewalle, N., and Seret, A. 2006. Investigation of Sds, Dtab and Ctab Micelle Microviscosities by Electron Spin Resonance. *Colloids and Surfaces A: Physicochemical and Engineering Aspects* **290** (1-3): 206-212. <https://doi.org/10.1016/j.colsurfa.2006.05.021>
- Baker, P. 1973. Effect of Pressure and Rate on Steam Zone Development in Steamflooding. *Society of Petroleum Engineers Journal* **13** (05): 274-284. SPE-4141-PA. <https://doi.org/10.2118/4141-PA>
- Becher, P. 1965. *Emulsions: Theory and Practice*, Second edition. USA: Reinhold Publishing Corporation.
- Becker, J. 1997. *Crude Oil Waxes, Emulsions, and Asphaltenes*, First edition. Tulsa, OK: Pennwell Books.
- Bellamy, L. 1980. *The Infrared Spectra of Complex Molecules*, Second edition. London: Springer.

- Bracho, L. and Oquendo, O. 1991. Steam-Solvent Injection, Well Lsj-4057, Tia Juana Field, Western Venezuela. Paper presented at the SPE International Thermal Operations Symposium, Bakersfield, California, 7-8 February. SPE-21530-MS. <https://doi.org/10.2118/21530-MS>.
- Bryan, J. and Kantzas, A. 2009. Potential for Alkali-Surfactant Flooding in Heavy Oil Reservoirs through Oil-in-Water Emulsification. *Journal of Canadian Petroleum Technology* **48** (02): 37-46. PETSOC-09-02-37. <https://doi.org/10.2118/09-02-37>
- Burger, J., Sourieau, P., and Combarous, M. 1985. *Thermal Methods of Oil Recovery*, First edition. Houston, USA: Gulf Publishing Company.
- Burns, J. 1969. A Review of Steam Soak Operations in California. *Journal of Petroleum Technology* **21** (01). SPE-2117-PA. <https://doi.org/10.2118/2117-PA>
- Butler, R.M. and Mokrys, I.J. 1993. Recovery of Heavy Oils Using Vapourized Hydrocarbon Solvents: Further Development of the Vapex Process. *Journal of Canadian Petroleum Technology* **32** (06): 56-62. PETSOC-93-06-06. <https://doi.org/10.2118/93-06-06>
- Chemical, O. Sodium Decyl Sulphate Surfactant <https://www.oakwoodchemical.com>. Accessed 9-23-2019.
- Chen, G. and Tao, D. 2005. An Experimental Study of Stability of Oil–Water Emulsion. *Fuel processing technology* **86** (5): 499-508. <https://doi.org/10.1016/j.fuproc.2004.03.010>
- Chu, C. 1985. State-of-the-Art Review of Steamflood Field Projects. *Journal of Petroleum Technology* **37** (10): 1887-1902. SPE-11733-PA. <https://doi.org/10.2118/11733-PA>
- Chung, K.H. and Butler, A. 1989. In Situ Emulsification by the Condensation of Steam in Contact with Bitumen. *Journal of Canadian Petroleum Technology* **28** (01). PETSOC-89-01-04. <https://doi.org/10.2118/89-01-04>
- Coates, J. 2000. Interpretation of Infrared Spectra, a Practical Approach. *Encyclopedia of analytical chemistry*. <https://doi.org/10.1002/9780470027318.a5606>
- Coelho, R., Ovalles, C., Benson, I.P., and Hascakir, B. 2017. Effect of Clay Presence and Solvent Dose on Hybrid Solvent-Steam Performance. *Journal of Petroleum Science and Engineering* **150**: 203-207. <https://doi.org/10.1016/j.petrol.2016.12.006>

- Crocker, M. and Marchin, L. 1988. Wettability and Adsorption Characteristics of Crude-Oil Asphaltene and Polar Fractions. *Journal of Petroleum Technology* **40** (04): 470-474. SPE-14885-PA. <https://doi.org/10.2118/14885-PA>
- Demir, A.B., Bilgesu, I.H., and Hascakir, B. 2016. The Effect of Brine Concentration on Asphaltene Stability. Paper presented at the SPE Annual Technical Conference and Exhibition, Dubai, UAE, 26-28 September. <https://doi.org/10.2118/181706-MS>.
- Demirbas, A. 2016. Deposition and Flocculation of Asphaltenes from Crude Oils. *Petroleum Science and Technology* **34** (1): 6-11. <https://doi.org/10.1080/10916466.2015.1115875>
- Deng, X. 2005. Recovery Performance and Economics of Steam/Propane Hybrid Process. Paper presented at the SPE International Thermal Operations and Heavy Oil Symposium, Calgary, Alberta, Canada 1-3 November. <https://doi.org/10.2118/97760-MS>.
- Dilgren, R.E., Hirasaki, G.J., Hill, H.J., and Whitten, D.G. 1978. Steam-Channel-Expanding Steam Foam Drive. USA Patent No. 4086964A.
- Ding, B., Zhang, G., Ge, J., and Liu, X. 2010. Research on Mechanisms of Alkaline Flooding for Heavy Oil. *Energy & Fuels* **24** (12): 6346-6352. <https://doi.org/10.1021/ef100849u>
- Dixon, H.O. 1958. Recovering Oils from Formations. USA Patent No. 2,862,558.
- Dong, M., Ma, S., and Liu, Q. 2009. Enhanced Heavy Oil Recovery through Interfacial Instability: A Study of Chemical Flooding for Brintnell Heavy Oil. *Fuel* **88** (6): 1049-1056. <https://doi.org/10.1016/j.fuel.2008.11.014>
- Egan, R.W. 1976. Hydrophile-Lipophile Balance and Critical Micelle Concentration as Key Factors Influencing Surfactant Disruption of Mitochondrial Membranes. *Journal of Biological Chemistry* **251** (14): 4442-4447. <https://doi.org/10.1074/jbc.M505924200>
- Falls, A.H., Thigpen, D., Nelson, R.C., Ciaston, J., Lawson, J., Good, P., Ueber, R., and Shahin, G. 1994. Field Test of Cosurfactant-Enhanced Alkaline Flooding. *SPE Reservoir Engineering* **9** (03): 217-223. SPE-24117-PA. <https://doi.org/10.2118/24117-PA>
- Fan, T. and Buckley, J.S. 2002. Rapid and Accurate Sara Analysis of Medium Gravity Crude Oils. *Energy & Fuels* **16** (6): 1571-1575. <https://doi.org/10.1021/ef0201228>

- Fan, T., Wang, J., and Buckley, J.S. 2002. Evaluating Crude Oils by Sara Analysis. Paper presented at the SPE/DOE Improved Oil Recovery Symposium, Tulsa, Oklahoma, USA, 13-17 April. SPE-75228-MS. <https://doi.org/10.2118/75228-MS>.
- Farouq Ali, S. 1974. Current Status of Steam Injection as a Heavy Oil Recovery Method. *Journal of Canadian Petroleum Technology* **13** (01). PETSOC-74-01-06. <https://doi.org/10.2118/74-01-06>
- Fitch, J.P. and Minter, R.B. 1976. Chemical Diversion of Heat Will Improve Thermal Oil Recovery. Paper presented at the SPE Annual Fall Technical Conference and Exhibition, New Orleans, Louisiana, 3-6 October. <https://doi.org/10.2118/6172-MS>.
- Friberg, S., Jansson, P.O., and Cederberg, E. 1976. Surfactant Association Structure and Emulsion Stability. *Journal of Colloid and Interface Science* **55** (3): 614-623. [https://doi.org/10.1016/0021-9797\(76\)90072-2](https://doi.org/10.1016/0021-9797(76)90072-2)
- Fu, L., Zhang, G., Ge, J., Liao, K., Pei, H., Jiang, P., and Li, X. 2016. Study on Organic Alkali-Surfactant-Polymer Flooding for Enhanced Ordinary Heavy Oil Recovery. *Colloids and Surfaces A: Physicochemical and Engineering Aspects* **508**: 230-239. <https://doi.org/10.1016/j.colsurfa.2016.08.042>
- Giusti, L. 1974. Csv Makes Steam Soak Work in Venezuela Field.[Description of New Steam Injection Method]. *Oil Gas J.* **72** (44).
- Green, D.W. and Willhite, P.G. 1998. *Enhanced Oil Recovery*, First Edition. Richardson, TX: Henry L. Doherty Memorial Fund of AIME
- Hanai, T., Koizumi, N., and Goto, R. 1962. Dielectric Constants of Emulsions. *Institute for Chemical Research* **40** (4): 240-271.
- Hascakir, B. 2016. How to Select the Right Solvent for Solvent-Aided Steam Injection Processes. *Journal of Petroleum Science and Engineering* **146**: 746-751.
- Hascakir, B. 2017a. Introduction to Thermal Enhanced Oil Recovery (Eor) Special Issue. *Journal of Petroleum Science and Engineering* **154**: 438-441. <https://doi.org/10.1016/j.petrol.2017.05.026>
- Hascakir, B. 2017b. A New Approach to Determine Asphaltenes Stability. Paper presented at the SPE Annual Technical Conference and Exhibition, San Antonio, Texas, USA, 9-11 October 2017. SPE-187278-MS. <https://doi.org/10.2118/187278-MS>.
- Hein, F.J. 2017. Geology of Bitumen and Heavy Oil: An Overview. *Journal of Petroleum Science and Engineering* **154**: 551-563.

- Hernández, O.E. and Farouq Ali, S. 1972. Oil Recovery from Athabasca Tar Sand by Miscible-Thermal Methods. Paper presented at the Annual Technical Meeting, Calgary, Alberta, May 16 - 19. PETSOC-7249. <https://doi.org/10.2118/7249>.
- Hirasaki, G., Miller, C.A., and Puerto, M. 2011. Recent Advances in Surfactant Eor. *SPE Journal* **16** (04). SPE-115386-PA. <https://doi.org/10.2118/115386-PA>
- Hiraski, G.J. 1989. The Steam-Foam Process. *Journal of Petroleum Technology* **41** (05): 449-456. SPE-19505-PA. <https://doi.org/10.2118/19505-PA>
- Horowitz, H.H. and Metzger, G. 1963. A New Analysis of Thermogravimetric Traces. *Analytical Chemistry* **35** (10): 1464-1468.
- Hou, W. and Xu, J. 2016. Surfactant-Free Microemulsions. *Current Opinion in Colloid & Interface Science* **25**: 67-74. <https://doi.org/10.1016/j.cocis.2016.06.013>
- Hunter, R.J. 1981. *Zeta Potential in Colloid Science: Principles and Applications*, First edition. New York, USA: Academic press.
- Jones, T., Neustadter, E., and Whittingham, K. 1978. Water-in-Crude Oil Emulsion Stability and Emulsion Destabilization by Chemical Demulsifiers. *Journal of Canadian Petroleum Technology* **17** (02). PETSOC-78-02-08. <https://doi.org/10.2118/78-02-08>
- Kar, T. and Hascakir, B. 2015. The Role of Resins, Asphaltenes, and Water in Water–Oil Emulsion Breaking with Microwave Heating. *Energy & Fuels* **29** (6): 3684-3690. <https://doi.org/10.1021/acs.energyfuels.5b00662>
- Kar, T., Mukhametshina, A., Unal, Y., and Hascakir, B. 2015. The Effect of Clay Type on Steam-Assisted-Gravity-Drainage Performance. *Journal of Canadian Petroleum Technology* **54** (06): 412-423. <https://doi.org/10.2118/173795-PA>
- Kar, T., Ovalles, C., Rogel, E., Vien, J., and Hascakir, B. 2016. The Residual Oil Saturation Determination for Steam Assisted Gravity Drainage (Sagd) and Solvent-Sagd. *Fuel* **172**: 187-195. <https://doi.org/10.1016/j.fuel.2016.01.029>
- Kaszuba, M., Corbett, J., Watson, F.M., and Jones, A. 2010. High-Concentration Zeta Potential Measurements Using Light-Scattering Techniques. *Philosophical Transactions of the Royal Society A: Mathematical, Physical and Engineering Sciences* **368** (1927): 4439-4451.
- Kitahara, A. and Kon-no, K. 1969. Mechanism of Solubilization of Water by Oil-Soluble Surfactant Solutions II. Cationic Surfactants. *Journal of Colloid and Interface Science* **29** (1): 1-5. [https://doi.org/10.1016/0021-9797\(69\)90339-7](https://doi.org/10.1016/0021-9797(69)90339-7)

- Kokal, S.L. 2005. Crude Oil Emulsions: A State-of-the-Art Review. *SPE Production & facilities* **20** (01): 5-13. SPE-77497-PA. <https://doi.org/10.2118/77497-PA>
- Kokal, S.L. and Sayegh, S.G. 1995. Asphaltenes: The Cholesterol of Petroleum. Paper presented at the Middle East Oil Show, Bahrain, 11-14 March. SPE-29787-MS. <https://doi.org/10.2118/29787-MS>.
- Kumar, R., Dao, E., and Mohanty, K. 2012. Heavy-Oil Recovery by in-Situ Emulsion Formation. *SPE Journal* **17** (02): 326-334. SPE-129914-PA. <https://doi.org/10.2118/129914-PA>
- Lake, L.W. 1989. *Enhanced Oil Recovery*, First edition. USA: Prentice Hall, Inc.
- Leontaritis, K. 1989. Asphaltene Deposition: A Comprehensive Description of Problem Manifestations and Modeling Approaches. Paper presented at the SPE production operations symposium, Oklahoma City, Oklahoma, 13-14 March. SPE-18892-MS. <https://doi.org/10.2118/18892-MS>.
- Leontaritis, K., Amaefule, J., and Charles, R. 1994. A Systematic Approach for the Prevention and Treatment of Formation Damage Caused by Asphaltene Deposition. *SPE Production & Facilities* **9** (03): 157-164.
- Li, X., Shi, L., Li, H., Liu, P., Luo, J., and Yuan, Z. 2018. Experimental Study on Viscosity Reducers for Sagd in Developing Extra-Heavy Oil Reservoirs. *Journal of Petroleum Science and Engineering* **166**: 25-32. <https://doi.org/10.1016/j.petrol.2018.03.022>
- Li, X., Sun, W., Wu, G., He, L., Li, H., and Sui, H. 2011. Ionic Liquid Enhanced Solvent Extraction for Bitumen Recovery from Oil Sands. *Energy & Fuels* **25** (11): 5224-5231. <https://doi.org/10.1021/ef2010942>
- Li, Z. and Firoozabadi, A. 2010. Modeling Asphaltene Precipitation by N-Alkanes from Heavy Oils and Bitumens Using Cubic-Plus-Association Equation of State. *Energy & fuels* **24** (2): 1106-1113. <https://doi.org/10.1021/ef9009857>
- Lowry, H.H. 1927. The Significance of the Dielectric Constant of a Mixture. *Journal of the Franklin Institute* **203** (3): 413-439. [https://doi.org/10.1016/S0016-0032\(27\)91179-X](https://doi.org/10.1016/S0016-0032(27)91179-X)
- Lu, C., Liu, H., Zhao, W., Lu, K., Liu, Y., Tian, J., and Tan, X. 2017. Experimental Investigation of in-Situ Emulsion Formation to Improve Viscous-Oil Recovery in Steam-Injection Process Assisted by Viscosity Reducer. *SPE Journal* **22** (01): 130-137. SPE-181759-PA. <https://doi.org/10.2118/181759-PA>

- Lu, G.W. and Gao, P. 2010. Emulsions and Microemulsions for Topical and Transdermal Drug Delivery. In *Handbook of Non-Invasive Drug Delivery Systems*, USA: Elsevier.
- Lundegard, P.D. and Senftle, J.T. 1987. Hydrous Pyrolysis: A Tool for the Study of Organic Acid Synthesis. *Applied Geochemistry* **2** (5): 605-612. [https://doi.org/10.1016/0883-2927\(87\)90012-6](https://doi.org/10.1016/0883-2927(87)90012-6)
- Ma, K., Cui, L., Dong, Y., Wang, T., Da, C., Hirasaki, G.J., and Biswal, S.L. 2013. Adsorption of Cationic and Anionic Surfactants on Natural and Synthetic Carbonate Materials. *Journal of colloid and interface science* **408**: 164-172. <https://doi.org/10.1016/j.jcis.2013.07.006>
- Mai, A., Bryan, J., Goodarzi, N., and Kantzas, A. 2009. Insights into Non-Thermal Recovery of Heavy Oil. *Journal of Canadian Petroleum Technology* **48** (03): 27-35. PETSOC-09-03-27. <https://doi.org/10.2118/09-03-27>
- Mannhardt, K., Schramm, L., and Novosad, J. 1993. Effect of Rock Type and Brine Composition on Adsorption of Two Foam-Forming Surfactants. *SPE Advanced Technology Series* **1** (01): 212-218. SPE-20463-PA. <https://doi.org/10.2118/20463-PA>
- Marsden, S. 1986. Foams in Porous Media. *U. S. Department of Energy*. <https://doi.org/10.2172/5866567>
- Marx, J.W. and Langenheim, R.H. 1959. Reservoir Heating by Hot Fluid Injection. *Transactions of the AIME* **216**: 312-215. SPE-1266-G.
- McClements, D.J. 2016. *Food Emulsions: Principles, Practices, and Techniques*, Third edition. USA: CRC press.
- McLean, J.D. and Kilpatrick, P.K. 1997. Effects of Asphaltene Aggregation in Model Heptane-Toluene Mixtures on Stability of Water-in-Oil Emulsions. *Journal of Colloid and Interface Science* **196** (1): 23-34. <https://doi.org/10.1006/jcis.1997.5177>
- Meyer, R.F. and De Witt, W. 1990. *Definition and World Resources of Natural Bitumens*, First edition. Denver, CO: US Government Printing Office.
- Monthly Oil Market Report. International Energy Agency. <http://www.oilmarketreport.org>. Accessed 01/10/2019.
- Mukhametshina, A., Kar, T., and Hascakir, B. 2016. Asphaltene Precipitation During Bitumen Extraction with Expanding-Solvent Steam-Assisted Gravity Drainage:

- Effects on Pore-Scale Displacement. *SPE Journal* **21** (02): 380-392. SPE-170013-PA. <https://doi.org/10.2118/170013-PA>
- Mullins, O.C. 2008. Review of the Molecular Structure and Aggregation of Asphaltenes and Petroleomics. *Spe Journal* **13** (01): 48-57. SPE-95801-PA. <https://doi.org/10.2118/95801-PA>
- Myers, D. 2005. *Surfactant Science and Technology*, Third edition. John Wiley & Sons.
- Nasr, T., Beaulieu, G., Golbeck, H., and Heck, G. 2002. Novel Expanding Solvent-Sagd Process “Es-Sagd”. Paper presented at the Canadian International Petroleum Conference, Calgary, Alberta 11-13 June. PETSOC-2002-072-EA. <https://doi.org/10.2118/2002-072-EA>.
- Needham, R.B. 1968. Plugging High Permeability Earth Strata. USA Patent No. 3412793A.
- Nelson, R.C. and Pope, G.A. 1978. Phase Relationships in Chemical Flooding. SPE-6773-PA. <https://doi.org/10.2118/6773-PA>
- Noik, C., Dalmazzone, C.S., Goulay, C., and Glenat, P. 2005. Characterisation and Emulsion Behaviour of Athabasca Extra Heavy Oil Produced by Sagd. Paper presented at the SPE International Thermal Operations and Heavy Oil Symposium, Calgary, Alberta, Canada, 1-3 November. SPE-97748-MS. <https://doi.org/10.2118/97748-MS>.
- Pan, H., Marsh, J.N., Christenson, E.T., Soman, N.R., Ivashyna, O., Lanza, G.M., Schlesinger, P.H., and Wickline, S.A. 2012. Postformulation Peptide Drug Loading of Nanostructures. In *Methods in Enzymology*: Elsevier. 508.
- Parra-Barraza, H., Hernández-Montiel, D., Lizardi, J., Hernández, J., Urbina, R.H., and Valdez, M.A. 2003. The Zeta Potential and Surface Properties of Asphaltenes Obtained with Different Crude Oil/N-Heptane Proportions. *Fuel* **82** (8): 869.
- Pauling, L. 1960. *The Nature of the Chemical Bond*, Third edition. Ithaca, New York: Cornell university press.
- Pei, H., Zhang, G., Ge, J., Jin, L., and Liu, X. 2011. Analysis of Microscopic Displacement Mechanisms of Alkaline Flooding for Enhanced Heavy-Oil Recovery. *Energy & Fuels* **25** (10): 4423-4429. <https://doi.org/10.1021/ef200605a>
- Pei, H., Zhang, G., Ge, J., Jin, L., and Ma, C. 2013. Potential of Alkaline Flooding to Enhance Heavy Oil Recovery through Water-in-Oil Emulsification. *Fuel* **104**: 284-293. <https://doi.org/10.1016/j.fuel.2012.08.024>

- Pei, H., Zhang, G., Ge, J., Tang, M., and Zheng, Y. 2012. Comparative Effectiveness of Alkaline Flooding and Alkaline–Surfactant Flooding for Improved Heavy-Oil Recovery. *Energy & Fuels* **26** (5): 2911-2919. <https://doi.org/10.1021/ef300206u>
- Peters, K.E., Walter, C., and Moldowan, M. 2005. *The Biomarker Guide, Volume 2–Biomarkers and Isotopes in Petroleum Exploration and Earth History*: Cambridge University Press, UK.
- Pirson, S., Wong, T., and Ramsey, P. 1958. A Novel Method of Recovering Heavy Viscous Crude Oils and Tar by Combined in Situ Thermal Treatment and Gravity Drainage. Paper presented at the The secondary Recovery Symposium, Wichita Falls, 5-6 May. SPE-1077-G.
- Prakoso, A., Punase, A., Rogel, E., Ovalles, C., and Hascakir, B. 2018. Effect of Asphaltene Characteristics on Its Solubility and Overall Stability. *Energy & Fuels* **32** (6): 6482-6487. <https://doi.org/10.1021/acs.energyfuels.8b00324>
- Prakoso, A.A., Punase, A.D., and Hascakir, B. 2017. A Mechanistic Understanding of Asphaltenes Precipitation from Varying-Saturate-Concentration Perspectives. *SPE Production & Operations* **32** (01): 86-98. SPE-177280-PA. <https://doi.org/10.2118/177280-PA>
- Prats, M. 1982. *Thermal Recovery*, First edition. Dallas, TX: H.L. Doherty Memorial Fund of AIME.
- Punase, A. and Hascakir, B. 2017. Stability Determination of Asphaltenes through Dielectric Constant Measurements of Polar Oil Fractions. *Energy & Fuels* **31** (1): 65-72. <https://doi.org/10.1021/acs.energyfuels.6b01045>
- Punase, A., Hascakir, B., Demir, A., and Bilgesu, H. 2017. Inorganic Content of Asphaltenes Impacts Asphaltenes Stability. Paper presented at the SPE Latin America and Caribbean Petroleum Engineering Conference, Buenos Aires, Argentina, 17-19 May. <https://doi.org/10.2118/185543-MS>.
- Qiao, P., Harbottle, D., Tchoukov, P., Masliyah, J., Sjoblom, J., Liu, Q., and Xu, Z. 2017. Fractionation of Asphaltenes in Understanding Their Role in Petroleum Emulsion Stability and Fouling. *Energy & Fuels* **31** (4): 3330-3337. <https://doi.org/10.1021/acs.energyfuels.6b02401>
- Reid, T. and Colonos, P. 1993. Supporting Technology for Enhanced Oil Recovery: Eor Thermal Processes. *Seventh Amendment and Extension to Annex 4*. <https://www.doi.org/10.2172/574305>
- Reisberg, J. and Doscher, T.M. 1956. Interfacial Phenomena in Crude Oil-Water Systems. *Producers monthly* **21** (1): 43-50.

- Robertson, G.P., Sollins, P., Ellis, B.G., and Lajtha, K. 1999. Exchangeable Ions, Ph, and Cation Exchange Capacity. In *Standard Soil Methods for Long-Term Ecological Research*, New York: Oxford University Press.
- Rodriguez-Navarro, C., Doehne, E., and Sebastian, E. 2000. How Does Sodium Sulfate Crystallize? Implications for the Decay and Testing of Building Materials. *Cement and concrete research* **30** (10): 1527-1534. [https://doi.org/10.1016/S0008-8846\(00\)00381-1](https://doi.org/10.1016/S0008-8846(00)00381-1)
- Rosen, M.J. and Kunjappu, J.T. 2012. *Surfactants and Interfacial Phenomena*, Fourth edition. Hoboken, New Jersey: John Wiley & Sons.
- Rosen, M.J., Zhu, Z.H., Gu, B., and Murphy, D.S. 1988. Relationship of Structure to Properties of Surfactants. 14. Some N-Alkyl-2-Pyrrolidones at Various Interfaces. *Langmuir* **4** (6): 1273-1277.
- Santacesaria, E., Gelosa, D., Di Serio, M., and Tesser, R. 1991. Thermal Stability of Nonionic Polyoxyalkylene Surfactants. *Journal of applied polymer science* **42** (7): 2053-2061. <https://doi.org/10.1002/app.1991.070420733>
- Schou, L. and Myhr, M. 1988. Sulfur Aromatic Compounds as Maturity Parameters. In *Organic Geochemistry in Petroleum Exploration*: Elsevier.
- Schramm, L.L. 1992. *Fundamentals and Applications in the Petroleum Industry*, Washington, DC: American Chemical Society.
- Schramm, L.L. and Smith, R.G. 1985. The Influence of Natural Surfactants on Interfacial Charges in the Hot-Water Process for Recovering Bitumen from the Athabasca Oil Sands. *Colloids and surfaces* **14** (1): 67-85. [https://doi.org/10.1016/0166-6622\(85\)80042-1](https://doi.org/10.1016/0166-6622(85)80042-1)
- Sheng, J. 2013. *Enhanced Oil Recovery Field Case Studies*, First edition. USA: Gulf Professional Publishing.
- Sigma-Aldrich. Surfactants. <https://www.sigmaaldrich.com>. Accessed 9-23-2019.
- Sjoblom, J. 2005. *Emulsions and Emulsion Stability: Surfactant Science Series*, 2nd Edition. Boca Raton: CRC Press.
- Smith, B.C. 2011. *Fundamentals of Fourier Transform Infrared Spectroscopy*, USA: CRC press.
- Speight, J.G. 2013. *Enhanced Recovery Methods for Heavy Oil and Tar Sands*, First edition. Houston, TX: Gulf Publishing Company.

- Speight, J.G. 2014. *The Chemistry and Technology of Petroleum*, 5th edition. Boca Raton, FL: CRC Press.
- Sperry, J.S., Krajicek, R.W., and South Jr, D.P. 1976. Thermal Injection Process for Recovery of Heavy Viscous Petroleum. USA Patent No. 3948323A.
- Srivastava, P. and Castro, L.U. 2011. Successful Field Application of Surfactant Additives to Enhance Thermal Recovery of Heavy Oil. Paper presented at the SPE Middle East Oil and Gas Show and Conference, Manama, Bahrain, 25-28 September. SPE-140180-MS. <https://doi.org/10.2118/140180-MS>.
- Stokes, D. and Doscher, T. 1974. Shell Makes a Success of Steam Flood at Yorba Linda. *Oil Gas J.* **72** (35).
- Stovall, S. 1934. Recovery of Oil from Depleted Sands by Means of Dry Steam. *Oil Weekly* **73**: 17-24.
- Stuart, B. 2004. *Infrared Spectroscopy: Fundamental and Applications*, First edition. UK: John Wiley & Sons Ltd.
- Tadros, T.F. 2006. *Applied Surfactants: Principles and Applications*, First edition. Mörlenbach, Germany: John Wiley & Sons.
- Taleb, K., Pillin, I., Grohens, Y., and Saidi-Besbes, S. 2018. Gemini Surfactant Modified Clays: Effect of Surfactant Loading and Spacer Length. *Applied Clay Science* **161**: 48-56. <https://doi.org/10.1016/j.clay.2018.03.015>
- Torrealba, V.A. and Johns, R.T. 2018. Partition-Coefficient Relations for Improved Equation-of-State Description of Microemulsion-Phase Behavior. *SPE Journal*.
- Unur, E. 2013. Functional Nanoporous Carbons from Hydrothermally Treated Biomass for Environmental Purification. *Microporous and Mesoporous Materials* **168**: 92-101. <https://doi.org/10.1016/j.micromeso.2012.09.027>
- Uren, L.C. and Fahmy, E. 1927. Factors Influencing the Recovery of Petroleum from Unconsolidated Sands by Waterflooding. *Transactions of the AIME* **77** (01): 318-335. SPE-927318-G. <https://doi.org/10.2118/927318-G>
- Van Dijk, C. 1968. Steam-Drive Project in the Schoonebeek Field, the Netherlands. *Journal of Petroleum Technology* **20** (03). SPE-1917-PA. <https://doi.org/10.2118/1917-PA>
- Vogel, J. 1984. Simplified Heat Calculations for Steamfloods. *Journal of petroleum technology* **36** (07): 1,127-121,136. SPE-11219-PA. <https://doi.org/10.2118/11219-PA>

- Volek, C. and Pryor, J. 1972. Steam Distillation Drive-Brea Field, California. *Journal of Petroleum Technology* **24** (08): 899-906. SPE-3441-PA. <https://doi.org/10.2118/3441-PA>
- Walter, H. 1957. Application of Heat for Recovery of Oil: Field Test Results and Possibility of Profitable Operation. *Journal of Petroleum Technology* **9** (02): 16-22. SPE-712-G. <https://doi.org/10.2118/712-G>
- Wang, T., Zhang, C., Zhao, R., Zhu, C., Yang, C., and Liu, C. 2014. Solvent Extraction of Bitumen from Oil Sands. *Energy & Fuels* **28** (4): 2297-2304. <https://doi.org/10.1021/ef402101s>
- Wang, Z., Stout, S.A., and Fingas, M. 2006. Forensic Fingerprinting of Biomarkers for Oil Spill Characterization and Source Identification. *Environmental Forensics* **7** (2): 105-146. <https://doi.org/10.1080/15275920600667104>
- Wang, Z., Xu, J.-H., Zhang, W., Zhuang, B., and Qi, H. 2008. Cloud Point of Nonionic Surfactant Triton X-45 in Aqueous Solution. *Colloids and Surfaces B: Biointerfaces* **61** (1): 118-122. <https://doi.org/10.1016/j.colsurfb.2007.07.013>
- Willman, B.T., Valleroy, V.V., Runberg, G.W., Cornelius, A.J., and Powers, L.W. 1961. Laboratory Studies of Oil Recovery by Steam Injection. SPE-1537-G-PA. <https://doi.org/10.2118/1537-G-PA>
- Winsor, P. 1948. Hydrotropy, Solubilisation and Related Emulsification Processes. *Transactions of the Faraday Society* **44**: 376-398.
- Wu, C.H. 1977. A Critical Review of Steamflood Mechanisms. Paper presented at the SPE California Regional Meeting, Bakersfield, California, 13-15 April. SPE-6550-MS. <https://doi.org/10.2118/6550-MS>.
- Wu, Z., Huiqing, L., Wang, X., and Zhang, Z. 2018. Emulsification and Improved Oil Recovery with Viscosity Reducer During Steam Injection Process for Heavy Oil. *Journal of industrial and engineering chemistry* **61**: 348-355. <https://doi.org/10.1016/j.jiec.2017.12.033>
- Wulfsberg, G. 2000. *Inorganic Chemistry*, First edition. Sausalito, California: University Science Books.
- Zeidani, K. and Gupta, S. 2012. Hydrocarbon Recovery from Bituminous Sands with Injection of Surfactant Vapour. USA Patent No. 20130081808A1.
- Zeidani, K. and Gupta, S.C. 2013. Surfactant-Steam Process: An Innovative Enhanced Heavy Oil Recovery Method for Thermal Applications. Paper presented at the SPE

Heavy Oil Conference-Canada, Calgary, Alberta, Canada 11-13 June.
<https://doi.org/10.2118/165545-MS>.

Zhang, J. and Chen, Z. 2018. Formation Damage by Thermal Methods Applied to Heavy Oil Reservoirs. In *Formation Damage During Improved Oil Recovery, USA*: Elsevier.

Ziegler, V.M. and Handy, L.L. 1981. Effect of Temperature on Surfactant Adsorption in Porous Media. *Society of Petroleum Engineers Journal* **21** (02): 218-228. SPE-8264-PA. <https://doi.org/10.2118/8264-PA>

APPENDIX A

THE DIAGNOSTIC RATIOS OF BIOMARKERS

Table A.1— Biomarker identified in this study with their full name, and chemical formula.

Biomarker Abbreviation	Biomarker Full Name	Chemical Formula
DBT	Dibenzothiophene	C ₁₂ H ₈ S
4MDBT	4-Methyl dibenzothiophene	C ₁₃ H ₁₀ S
23MDBT	2 & 3 Methyl dibenzothiophene	C ₁₃ H ₁₀ S
1MDBT	1 Methyl dibenzothiophene	C ₁₃ H ₁₀ S
4ETDBT	4 Eethyl dibenzothiophene	C ₁₄ H ₁₂ S
46DMDBT	4,6 Dimethyl dibenzothiophene	C ₁₄ H ₁₂ S
DMDBT4	Dimethyl dibenzothiophene 4	C ₁₄ H ₁₂ S
DMDBT5	Dimethyl dibenzothiophene 5	C ₁₄ H ₁₂ S
DMDBT6	Dimethyl dibenzothiophene 6	C ₁₄ H ₁₂ S
14DMDBT	1,4 Dimethyl dibenzothiophene	C ₁₄ H ₁₂ S
DMDBT7	Dimethyl dibenzothiophene 7	C ₁₄ H ₁₂ S
DMDBT8	Dimethyl dibenzothiophene 8	C ₁₄ H ₁₂ S

The diagnostic ratios include Terpane, Hopane, Sterane, TAS, and MAS ratios. The following equations have been used to obtain the ratios using the integrated peak areas from GC-MS spectrums (Peters et al. 2005).

$$\text{Hopane Ratio (25norHop/Hop)} = \frac{\text{C}_{29} \text{ 17}\alpha \text{ 25-norhopane}}{\text{C}_{30} \text{ 17}\alpha} \quad (1)$$

$$\text{Terpane Ratio (C}_{24}\text{Tet/Hop)} = \frac{\text{C}_{24} \text{ tetracyclic terpane}}{\text{C}_{30} \text{ 17}\alpha} \quad (2)$$

$$\text{Sterane Ratio} \left(\frac{\text{Diaster}}{\text{Diaster+ster}} \right) = \frac{\text{C}_{27} \beta \alpha \text{ 20S+20R diacholestane}}{\text{C}_{27} \beta \alpha \text{ 20S+20R diacholestane} + \text{C}_{27} \alpha \alpha \text{ 20S+20R} \& \beta \beta \text{ 20S+20R cholestane}} \quad (3)$$

$$\text{TriAromatic Steroid Ratio (TAS)} = \frac{(\text{C}_{20}+\text{C}_{21}) \text{ triaromatic steroid}}{\text{C}_{20}+\text{C}_{21}+\text{C}_{26}+\text{C}_{27}+ \text{C}_{28}} \quad (4)$$

$$\text{MonoAromatic Steroid Ratio (MAS)} = \frac{(C_{21}+C_{22})\text{monoaromatic steroid}}{C_{21}+C_{22}+C_{27}+C_{28}+C_{29}} \quad (5)$$

APPENDIX B

TGA AND DSC CURVES FOR SURFACTANTS' THERMAL STABILITY

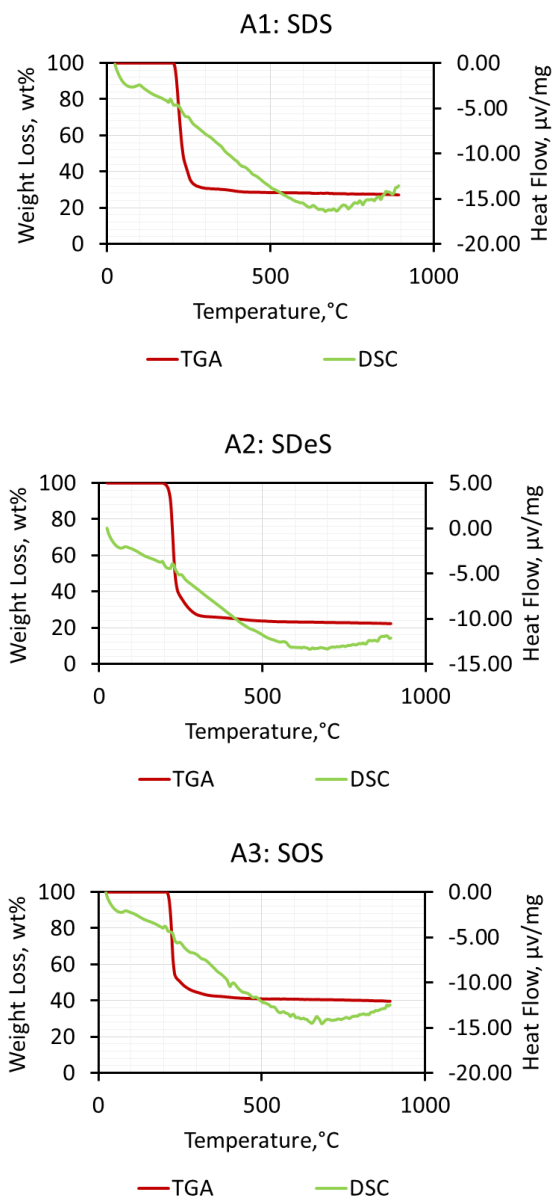


Fig. B.1 - Determination of surfactants' thermal stability at varying temperatures under air atmosphere at a purge rate of 50 mL/minute and nitrogen as protective gas at a rate of 20 mL/minute at $10^\circ \text{K}/\text{minute}$ for anionic surfactants with TGA/DSC.

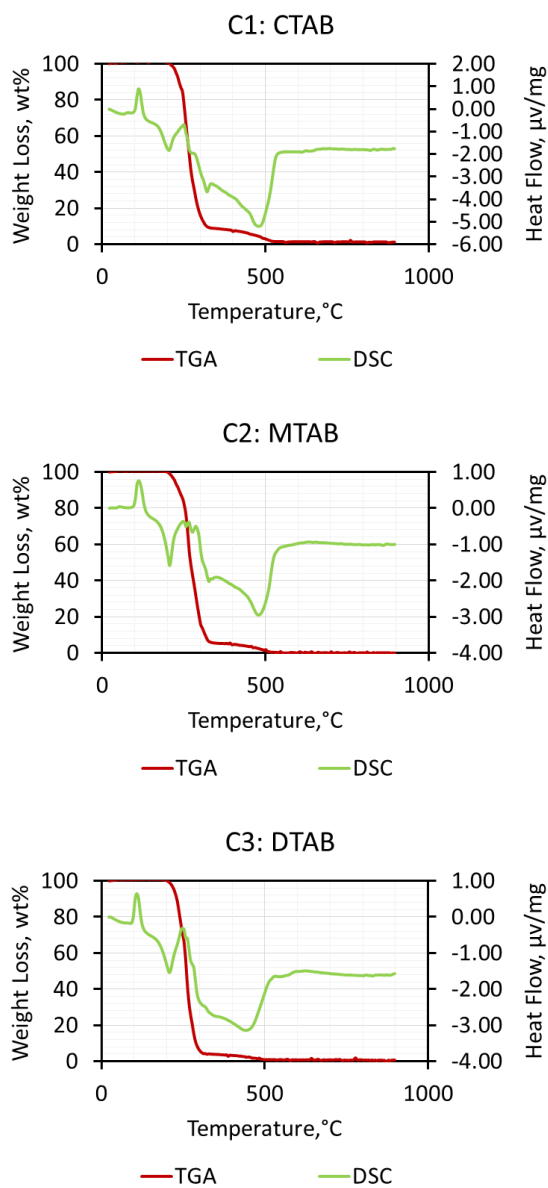


Fig. B.2- Determination of surfactants' thermal stability at varying temperatures under air atmosphere at a purge rate of 50 mL/minute and nitrogen as protective gas at a rate of 20 mL/minute at 10° K/minute for cationic surfactants with TGA/DSC.

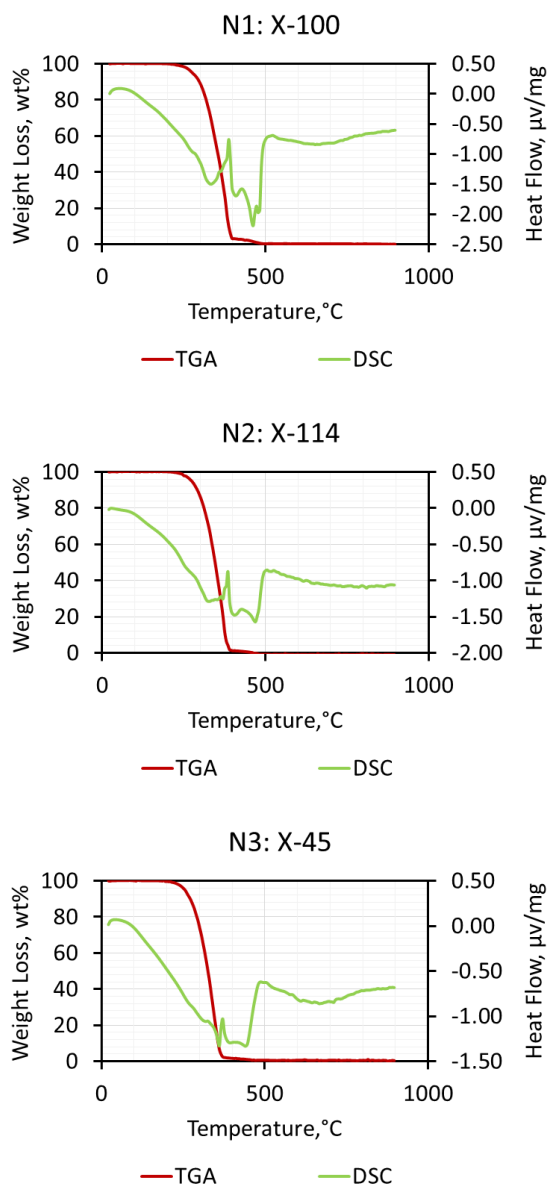
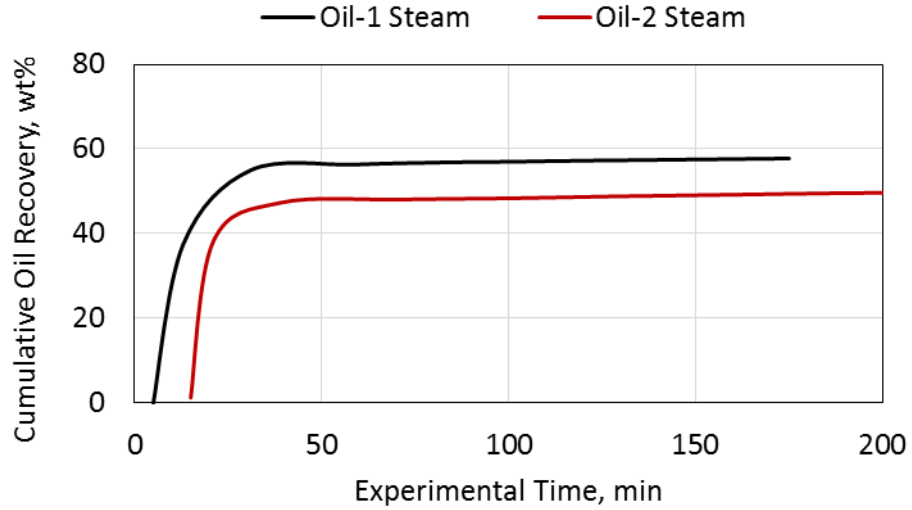


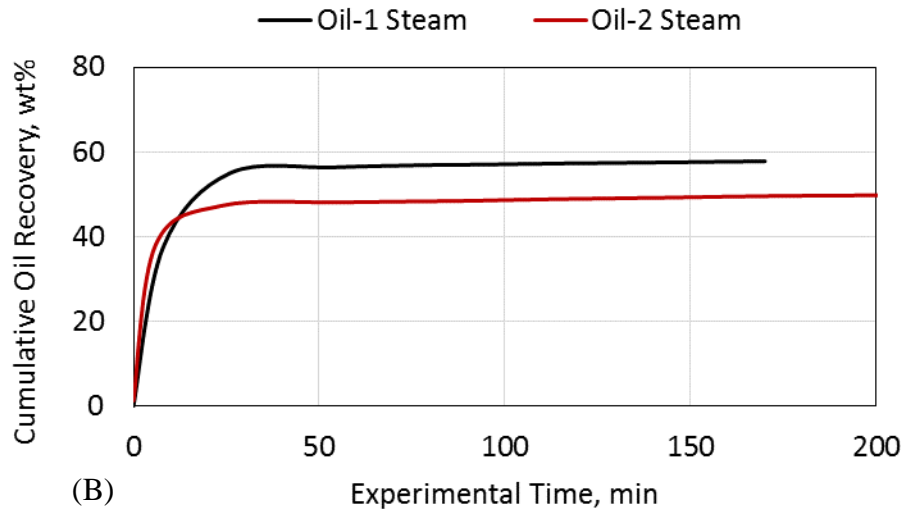
Fig. B.3 - Determination of surfactants' thermal stability at varying temperatures under air atmosphere at a purge rate of 50 mL/minute and nitrogen as protective gas at a rate of 20 mL/minute at 10° K/minute for nonionic surfactants with TGA/DSC.

APPENDIX C

CUMULATIVE OIL PRODUCTION GRAPHS

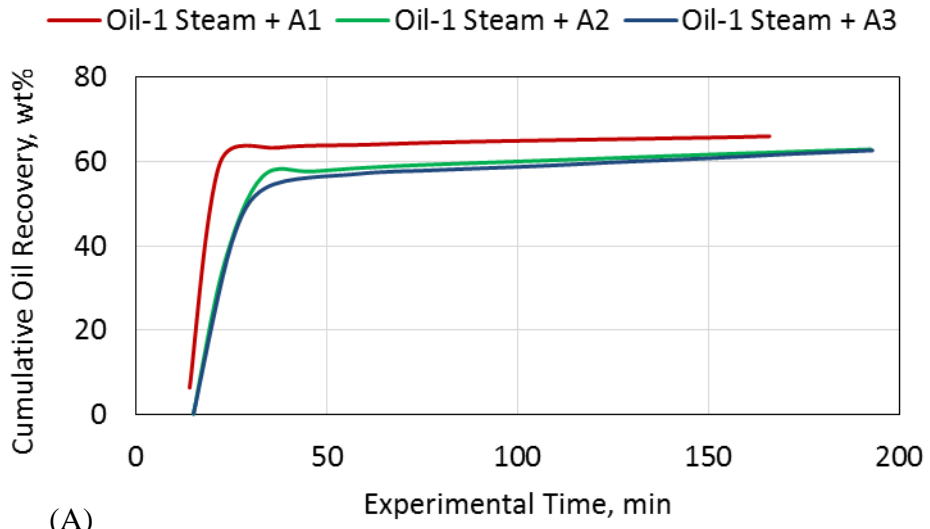


(A)

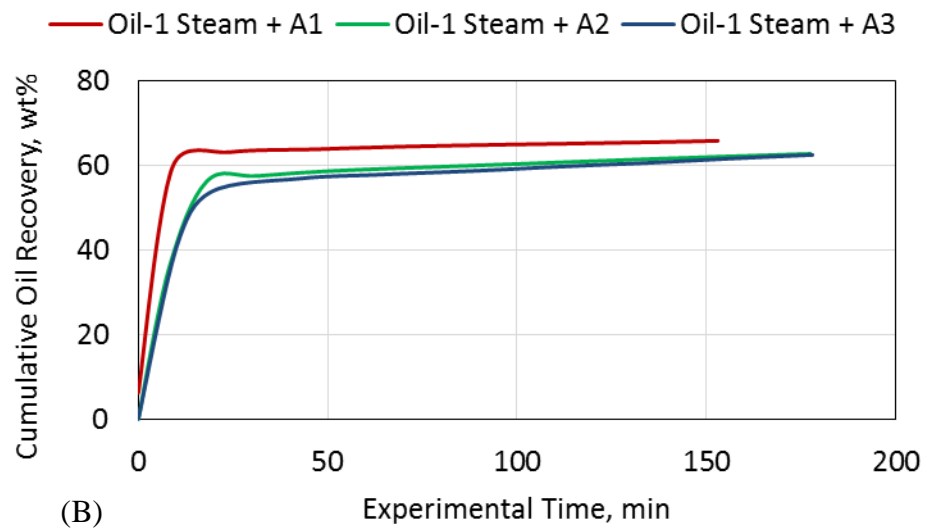


(B)

Fig. C.1 - Cumulative oil recovery for flooding experiments of steam injection, E1 and E11. At the top real experimental time and at the bottom oil production start time was shifted origin.



(A)



(B)

Fig. C.2 - Cumulative oil recovery for Oil 1 flooding experiments of anionic surfactant-steam injection, E2, E3, and E4. At the top real experimental time and at the bottom oil production start time was shifted origin.

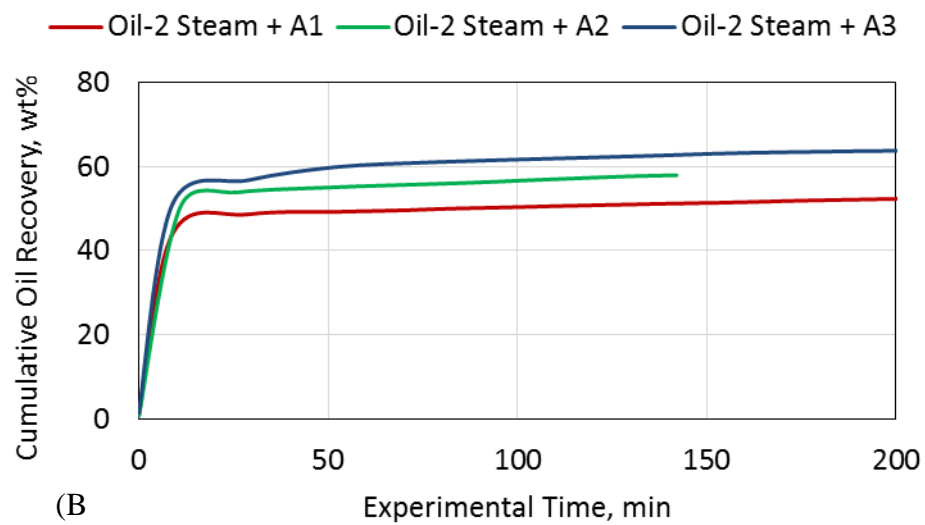
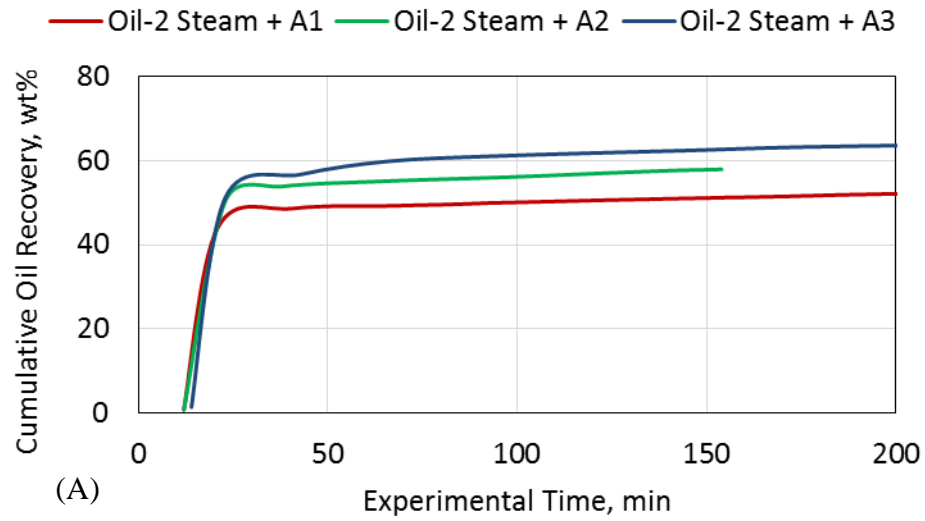


Fig. C.3 - Cumulative oil recovery for Oil 2 flooding experiments of anionic surfactant-steam injection, E12, E13, and E14. At the top real experimental time and at the bottom oil production start time was shifted origin.

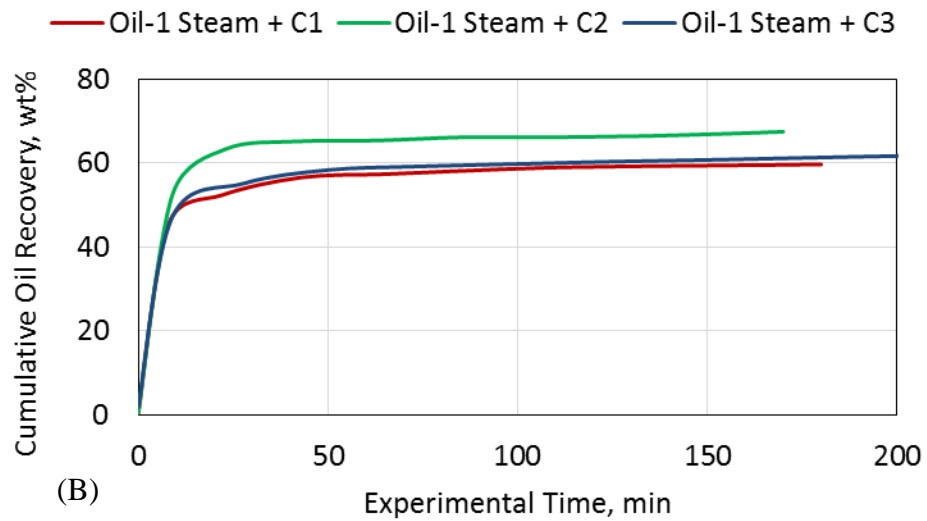
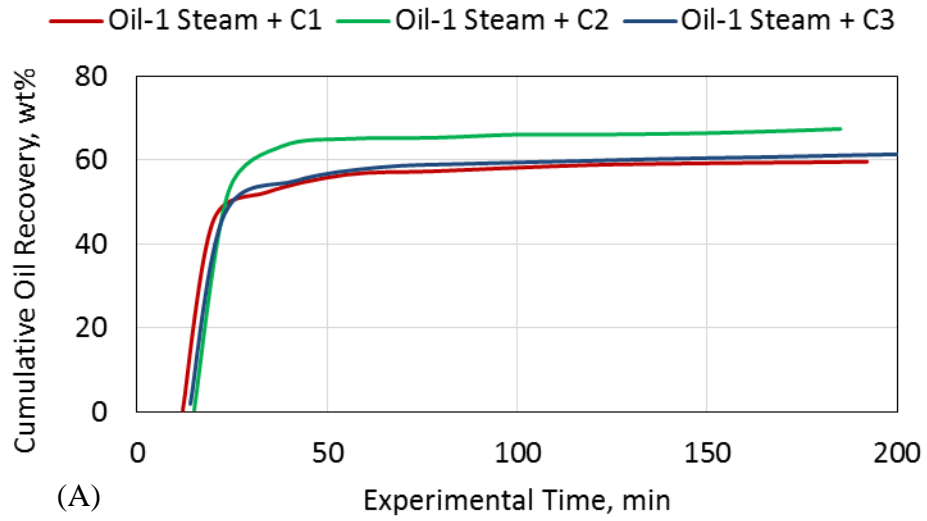


Fig. C.4 - Cumulative oil recovery for Oil 1 flooding experiments of cationic surfactant-steam injection, E5, E6, and E7. At the top real experimental time and at the bottom oil production start time was shifted origin.

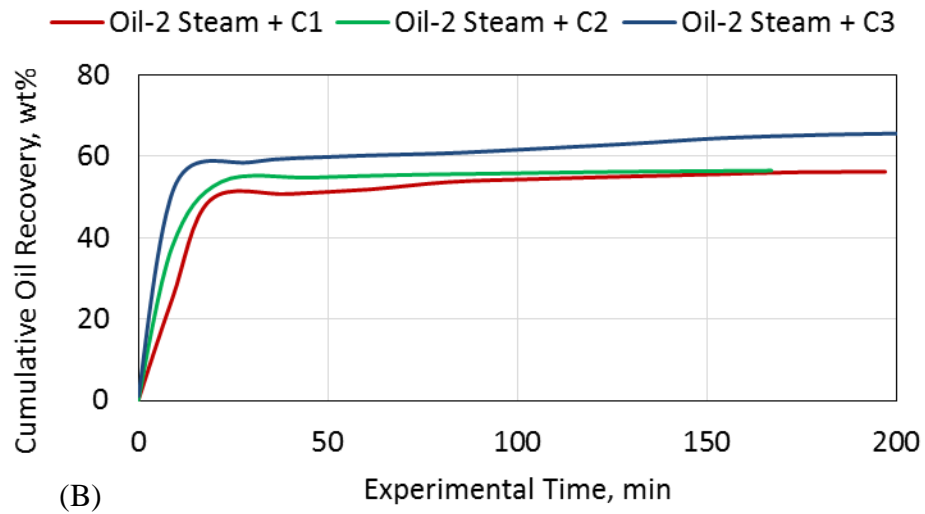
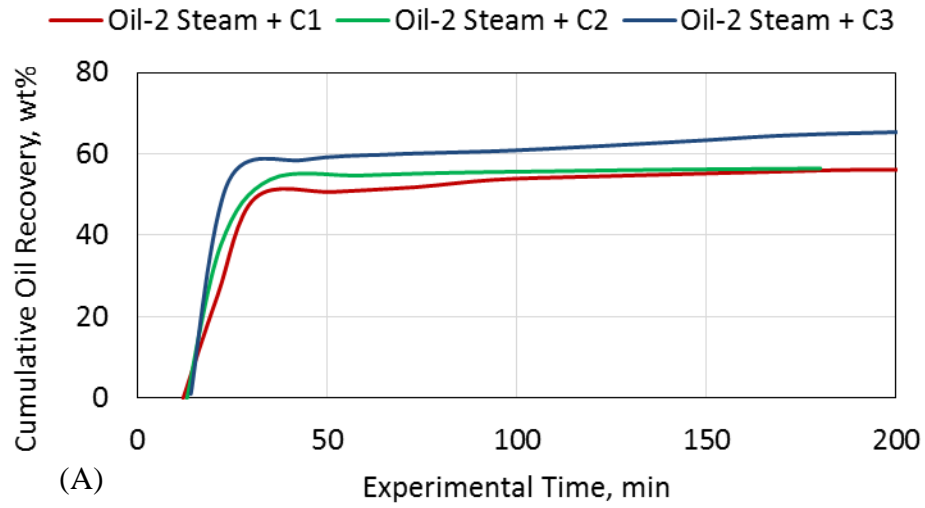


Fig. C.5 - Cumulative oil recovery for Oil 2 flooding experiments of cationic surfactant-steam injection, E15, E16, and E17. At the top real experimental time and at the bottom oil production start time was shifted origin.

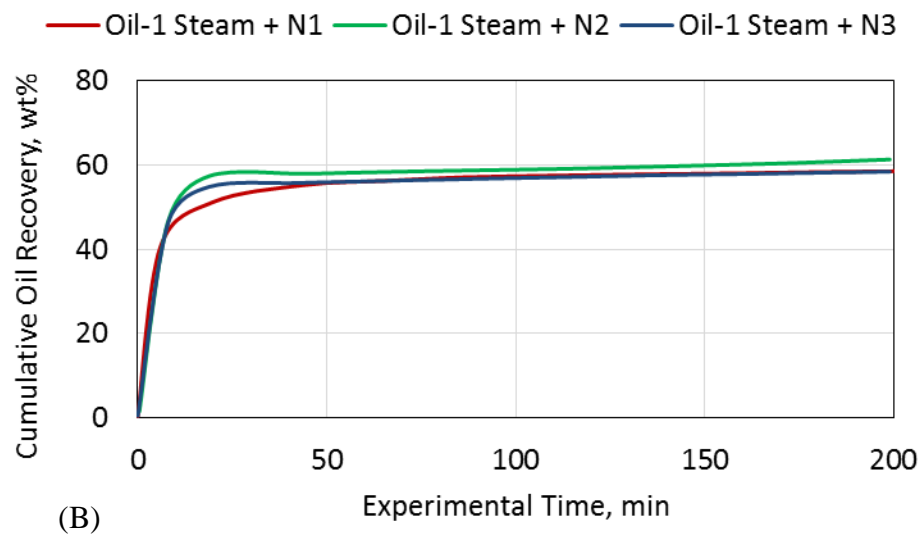
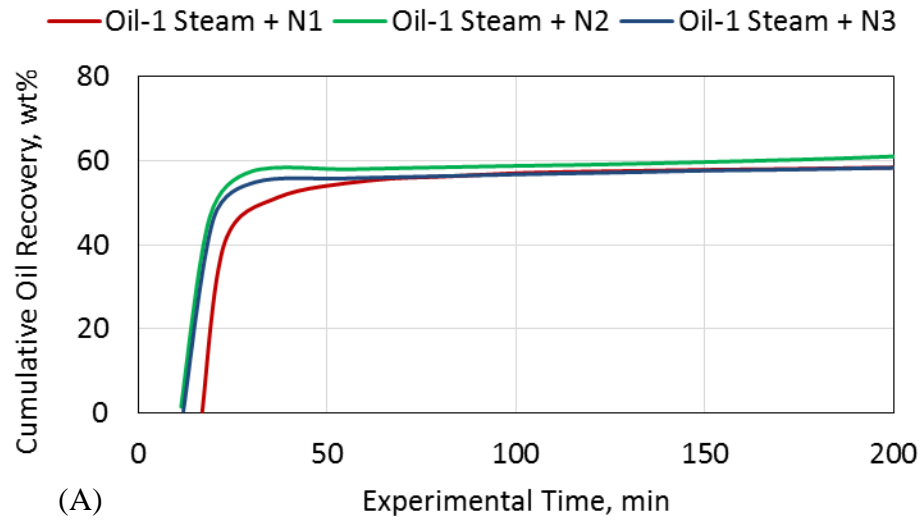


Fig. C.6 - Cumulative oil recovery for Oil 1 flooding experiments of nonionic surfactant-steam injection, E8, E9, and E10. At the top real experimental time and at the bottom oil production start time was shifted origin.

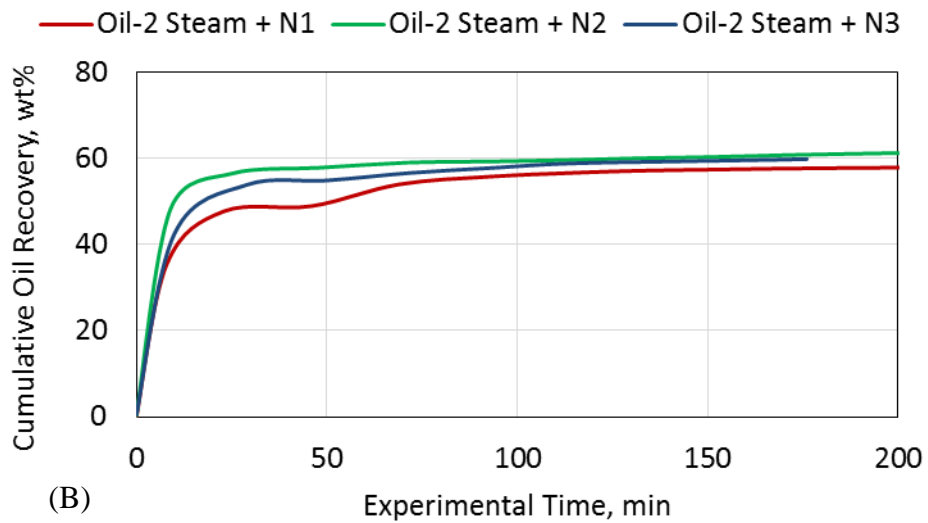
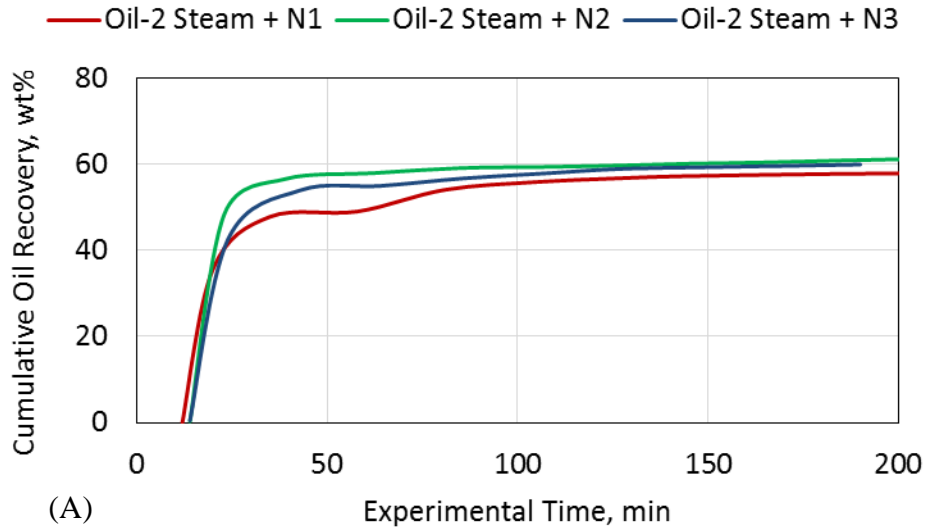


Fig. C.7 - Cumulative oil recovery for Oil 2 flooding experiments of nonionic surfactant-steam injection, E18, E19, and E20. At the top real experimental time and at the bottom oil production start time was shifted origin.

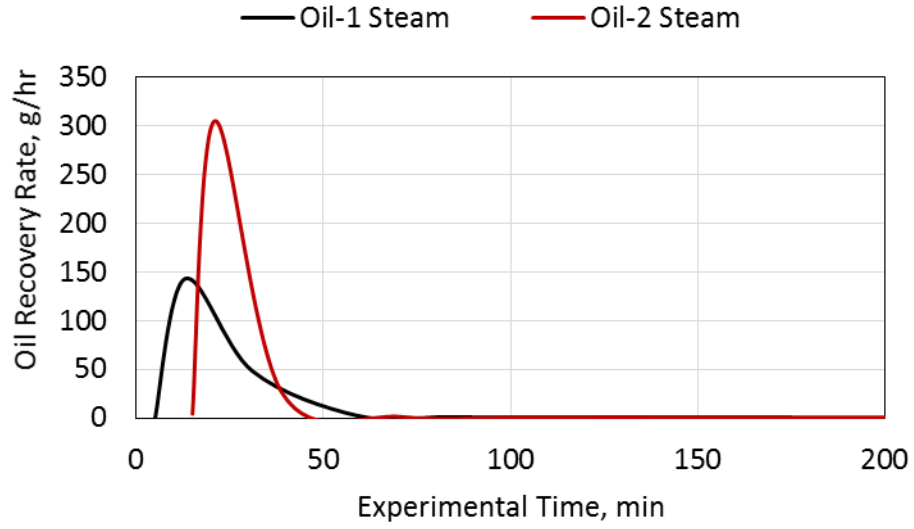


Fig. C.8 - Water recovery rate for flooding experiments of steam injection, E1 and E11

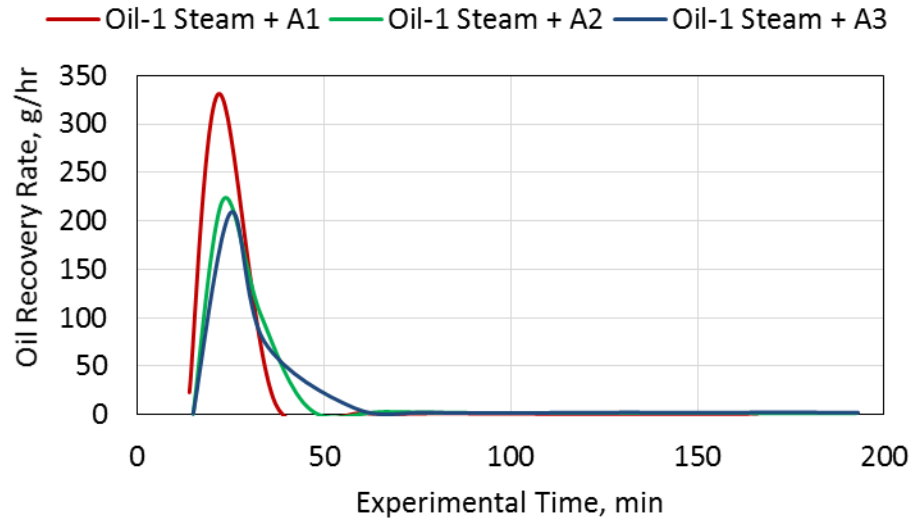


Fig. C.9 - Water recovery rate for Oil 1 flooding experiments of anionic surfactant-steam injection, E2, E3, and E4

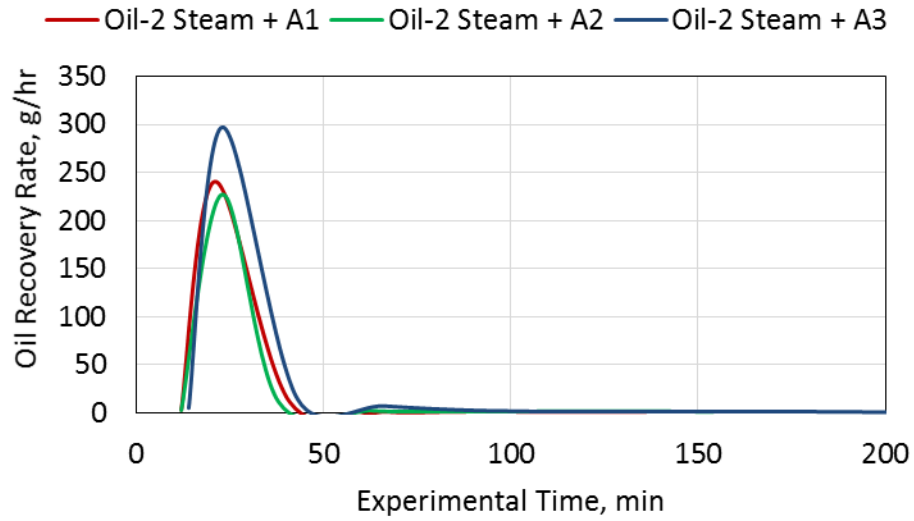


Fig. C.10 - Water recovery rate for Oil 2 flooding experiments of anionic surfactant-steam injection, E12, E13, and E14

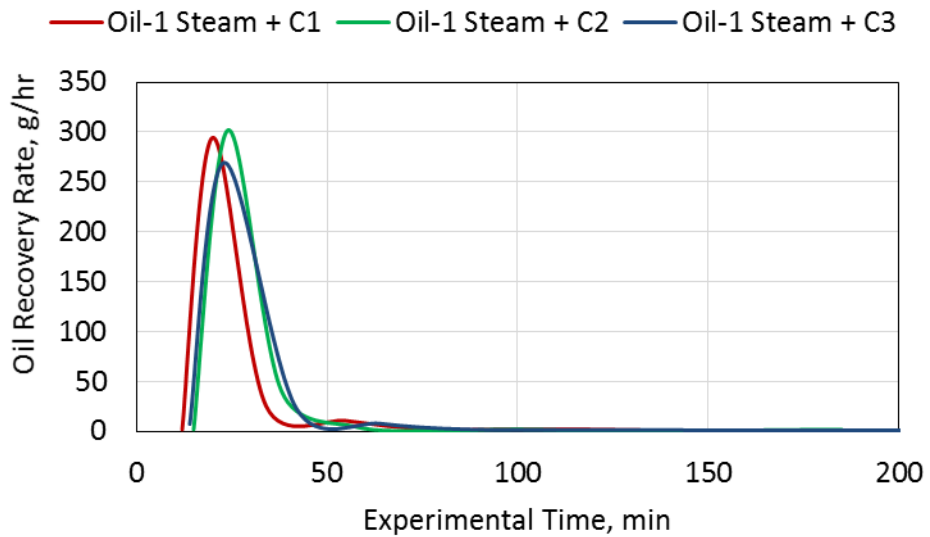


Fig. C.11 - Water recovery rate for Oil 1 flooding experiments of cationic surfactant-steam injection, E5, E6, and E7

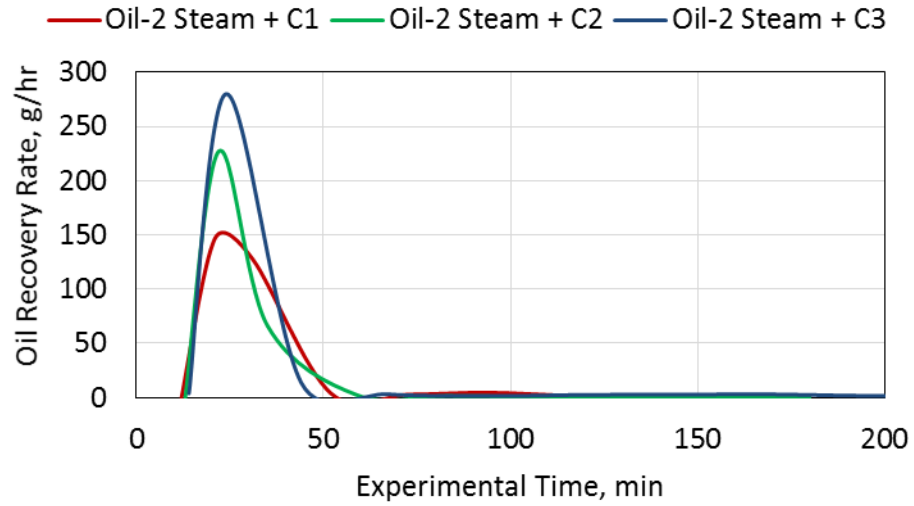


Fig. C.12 - Water recovery rate for Oil 2 flooding experiments of cationic surfactant-steam injection, E15, E16, and E17

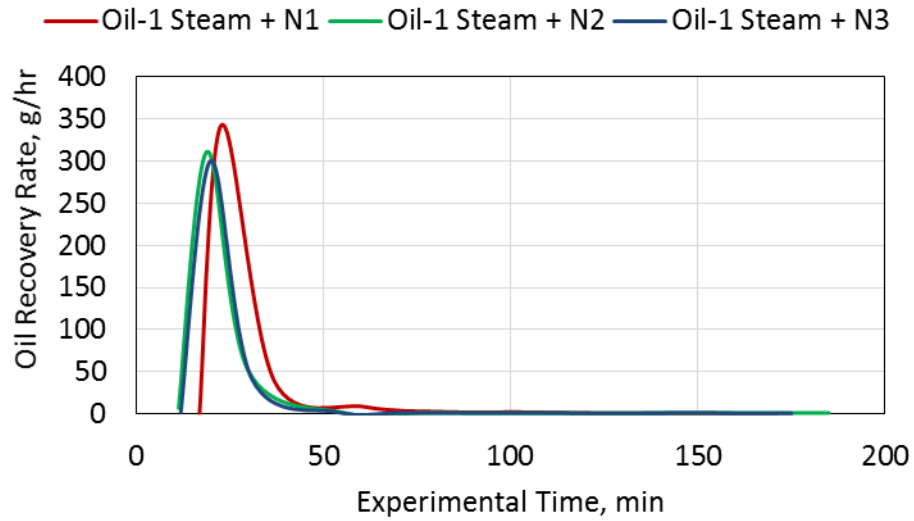


Fig. C.13 - Water recovery rate for Oil 1 flooding experiments of nonionic surfactant-steam injection, E8, E9, and E10

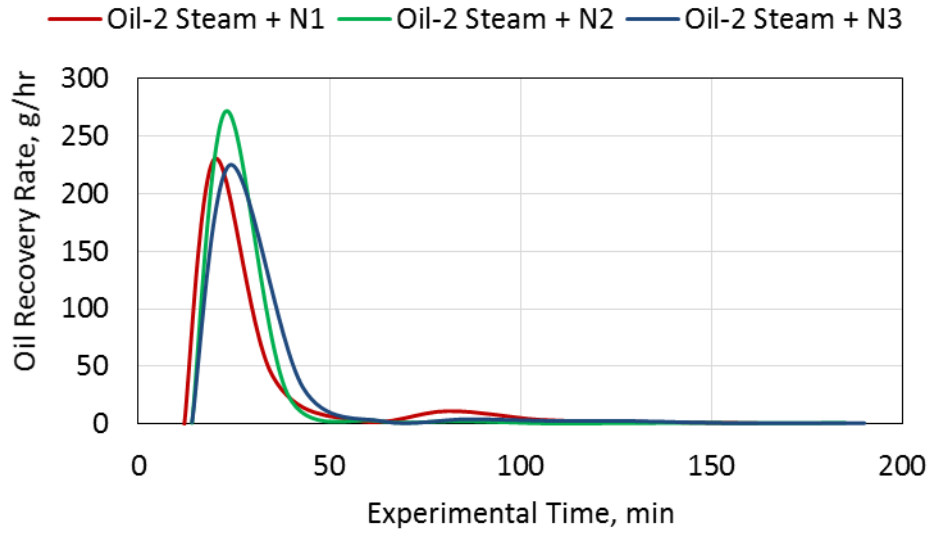


Fig. C.14 - Water recovery rate for Oil 2 flooding experiments of nonionic surfactant-steam injection, E18, E19, and E20

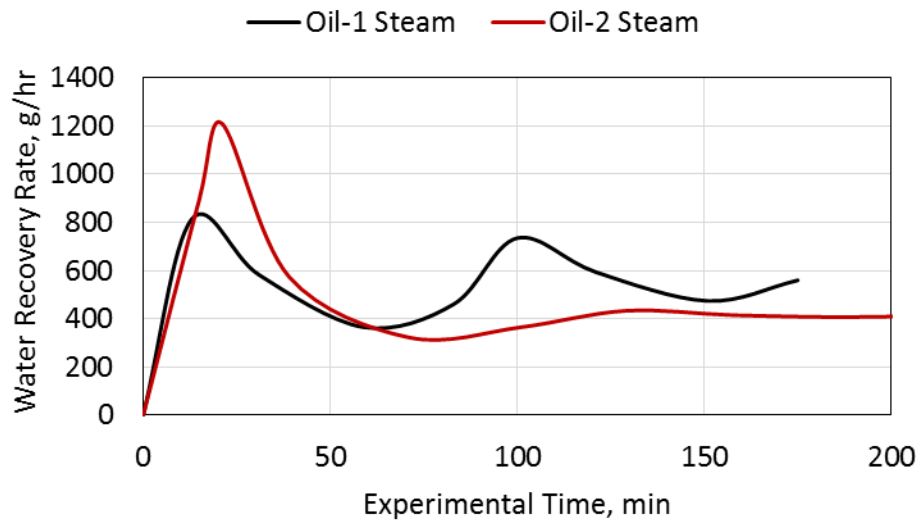


Fig. C.8 - Water recovery rate for flooding experiments of steam injection, E1 and E11

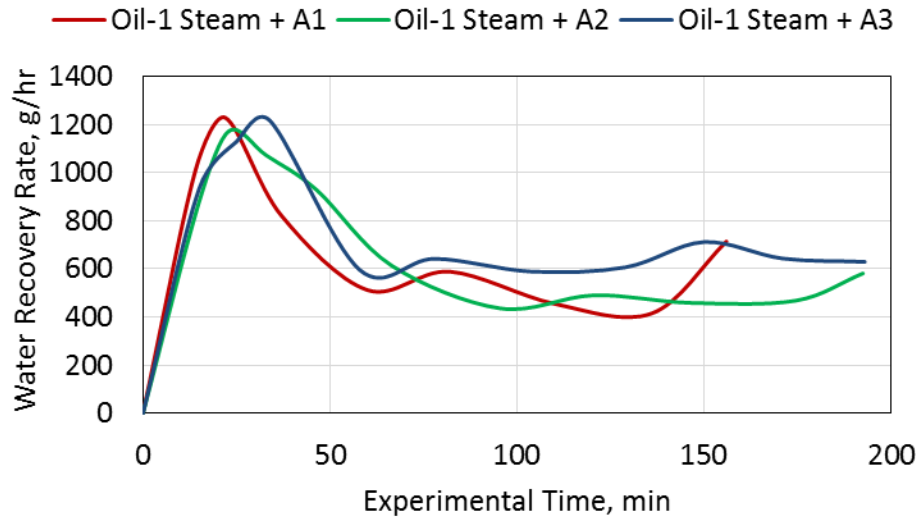


Fig. C.9 - Water recovery rate for Oil 1 flooding experiments of anionic surfactant-steam injection, E2, E3, and E4

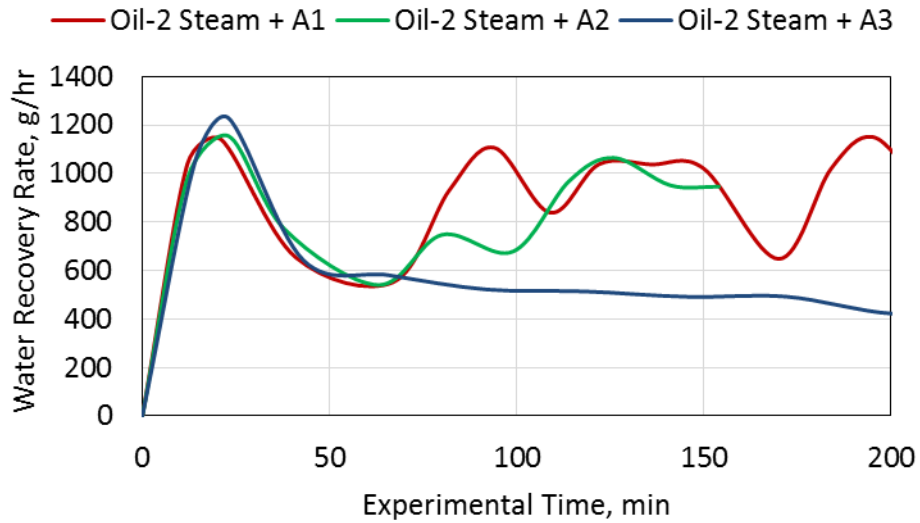


Fig. C.10 - Water recovery rate for Oil 2 flooding experiments of anionic surfactant-steam injection, E12, E13, and E14

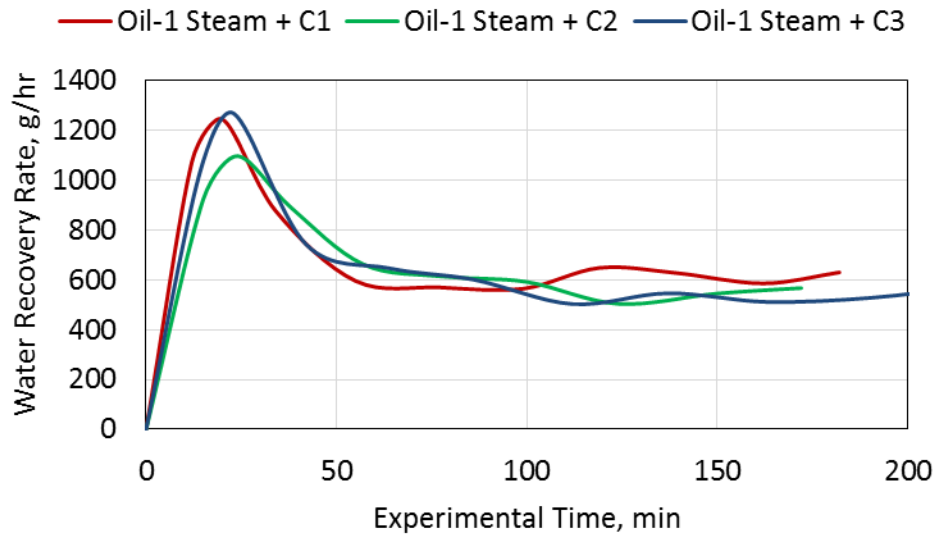


Fig. C.11 - Water recovery rate for Oil 1 flooding experiments of cationic surfactant-steam injection, E5, E6, and E7

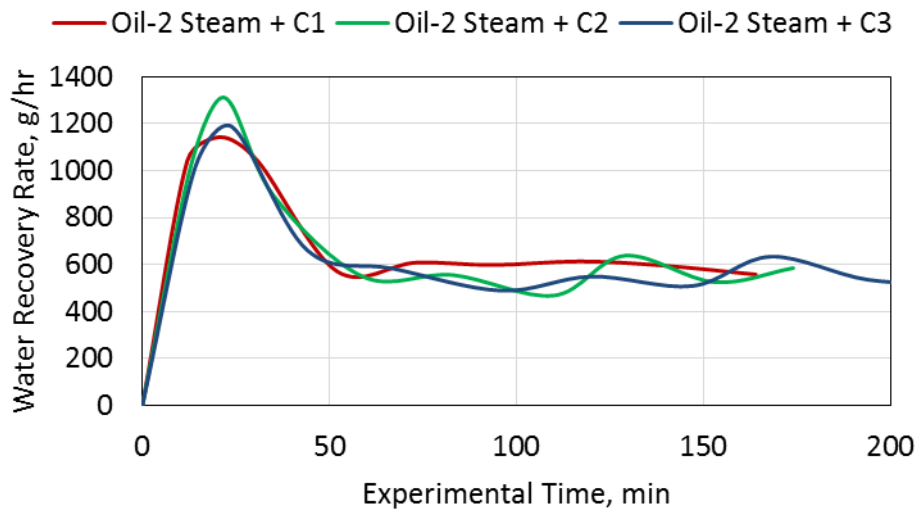


Fig. C.12 - Water recovery rate for Oil 2 flooding experiments of cationic surfactant-steam injection, E15, E16, and E17

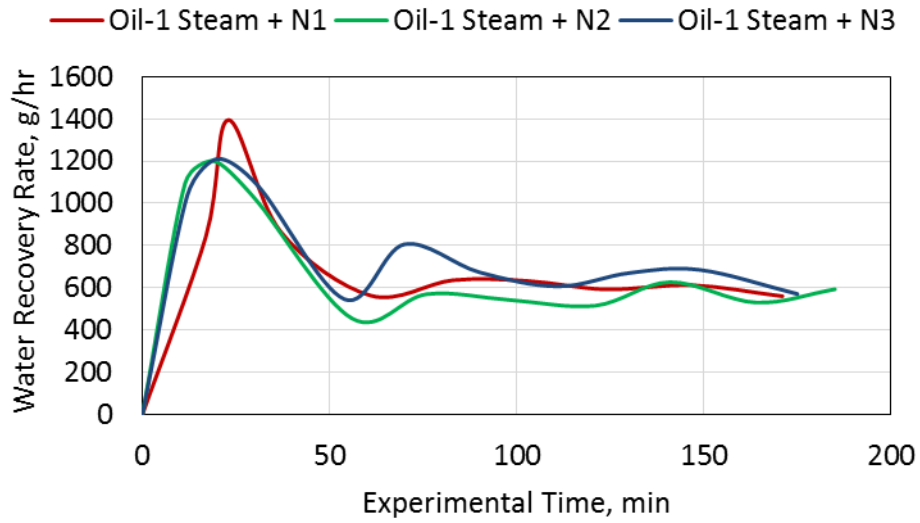


Fig. C.13 - Water recovery rate for Oil 1 flooding experiments of nonionic surfactant-steam injection, E8, E9, and E10

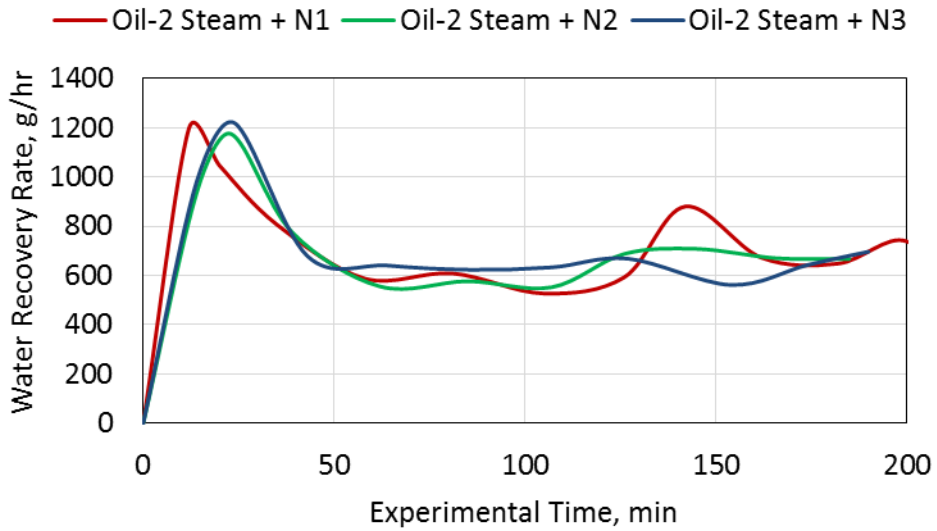


Fig. C.14 - Water recovery rate for Oil 2 flooding experiments of nonionic surfactant-steam injection, E18, E19, and E20

APPENDIX D

TEMPERATURE PROFILES FOR COREFLOOD EXPERIMENTS

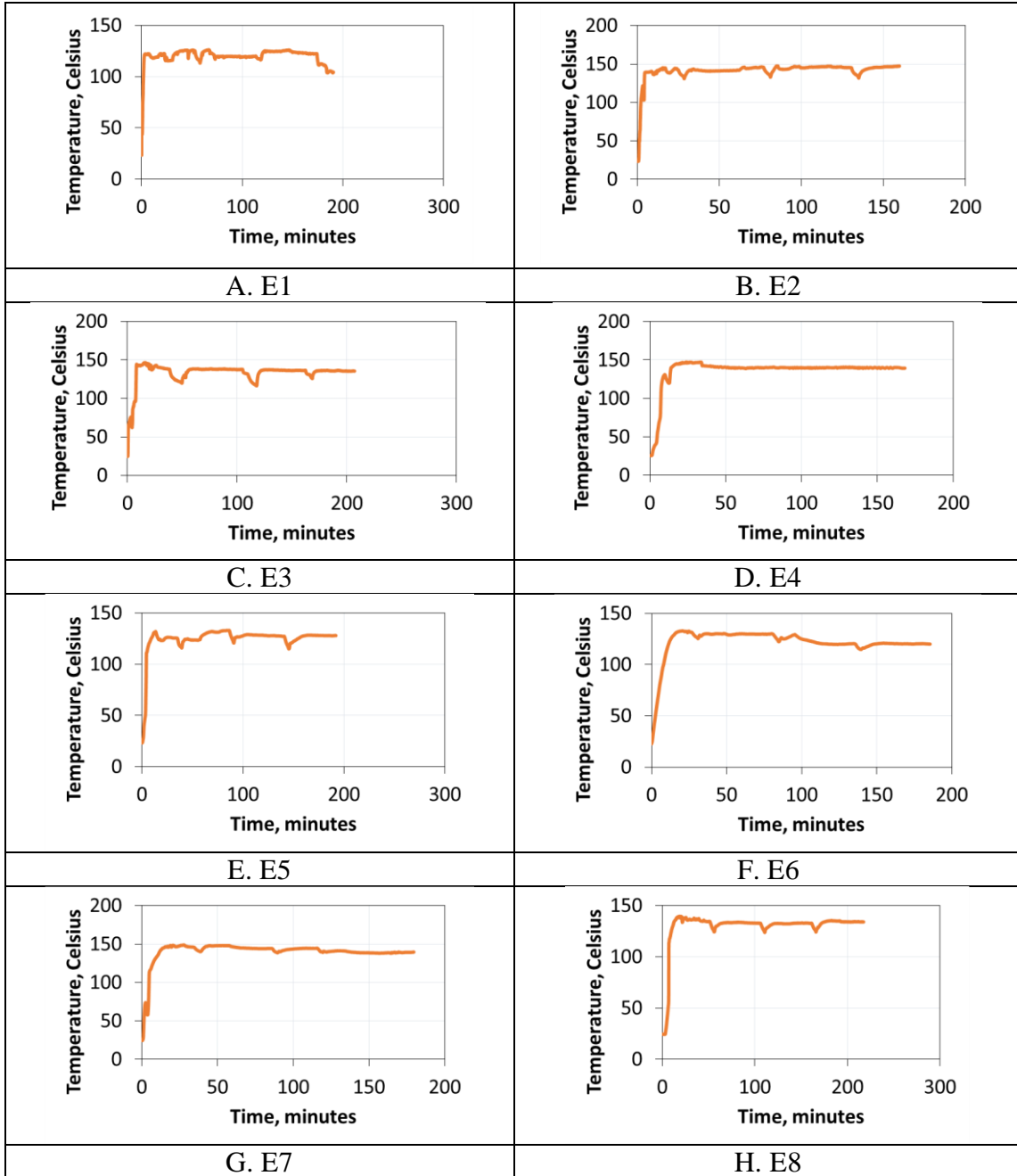


Fig. D.1 – Temperature profiles of Oil 1 steam and surfactant-steam coreflood experiments

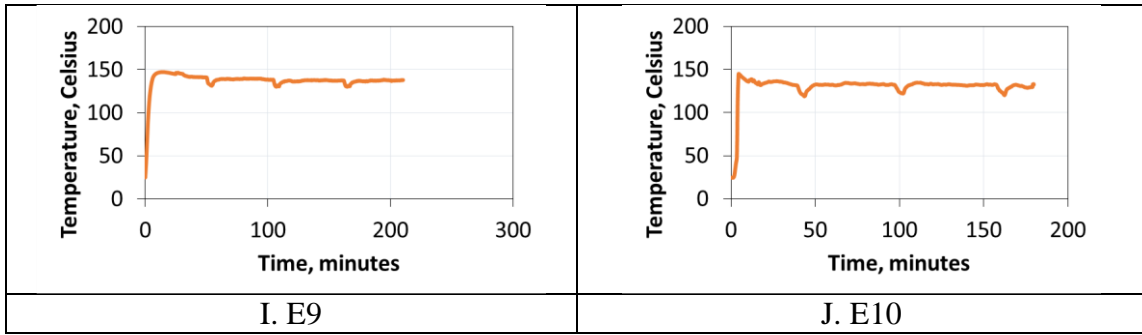


Fig. D.1 (continue) – Temperature profiles of Oil 1 steam and surfactant-steam coreflood experiments

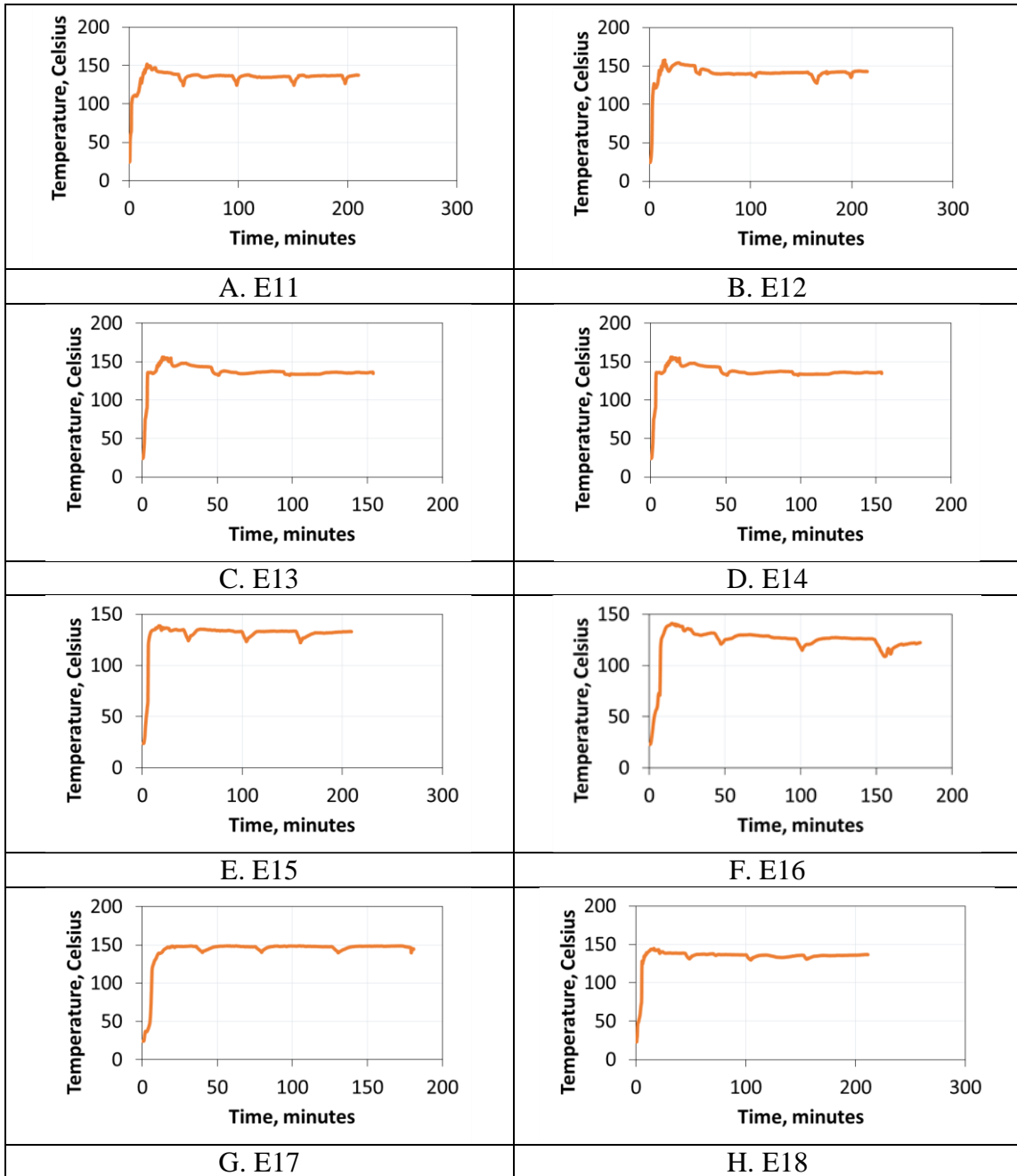


Fig. D.2 – Temperature profiles of Oil 2 steam and surfactant-steam coreflood experiments

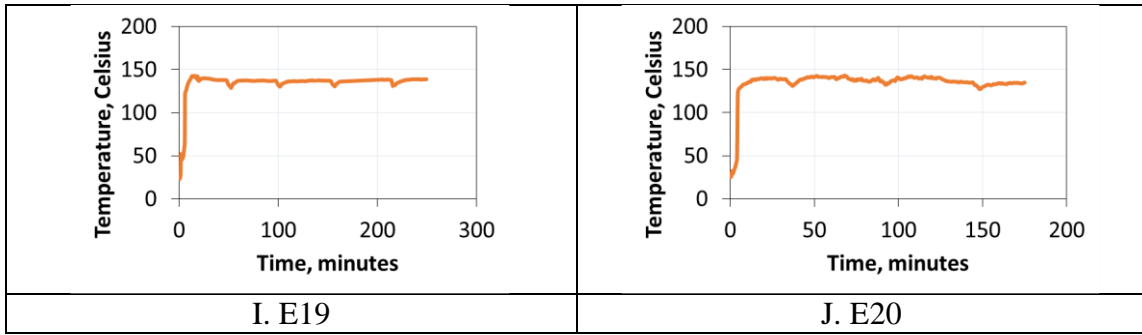


Fig. D.2 (continue) – Temperature profiles of Oil 2 steam and surfactant-steam coreflood experiments

APPENDIX E

TGA-DSC CURVES OF PRODUCED OIL

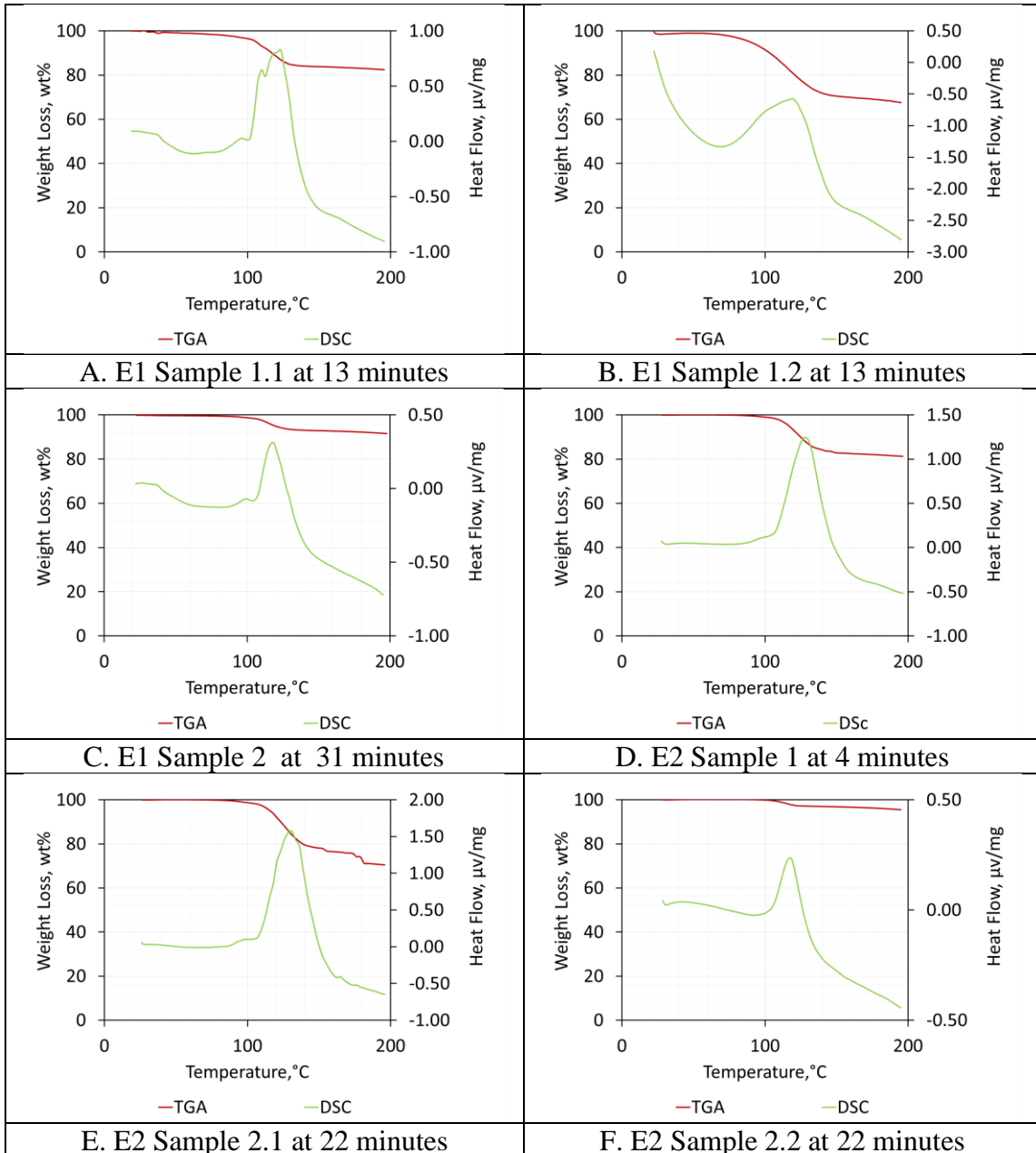


Fig. E.1 – TGA-DSC curves of produce oil samples from E1 and E2 to determine water-in-oil emulsions content.

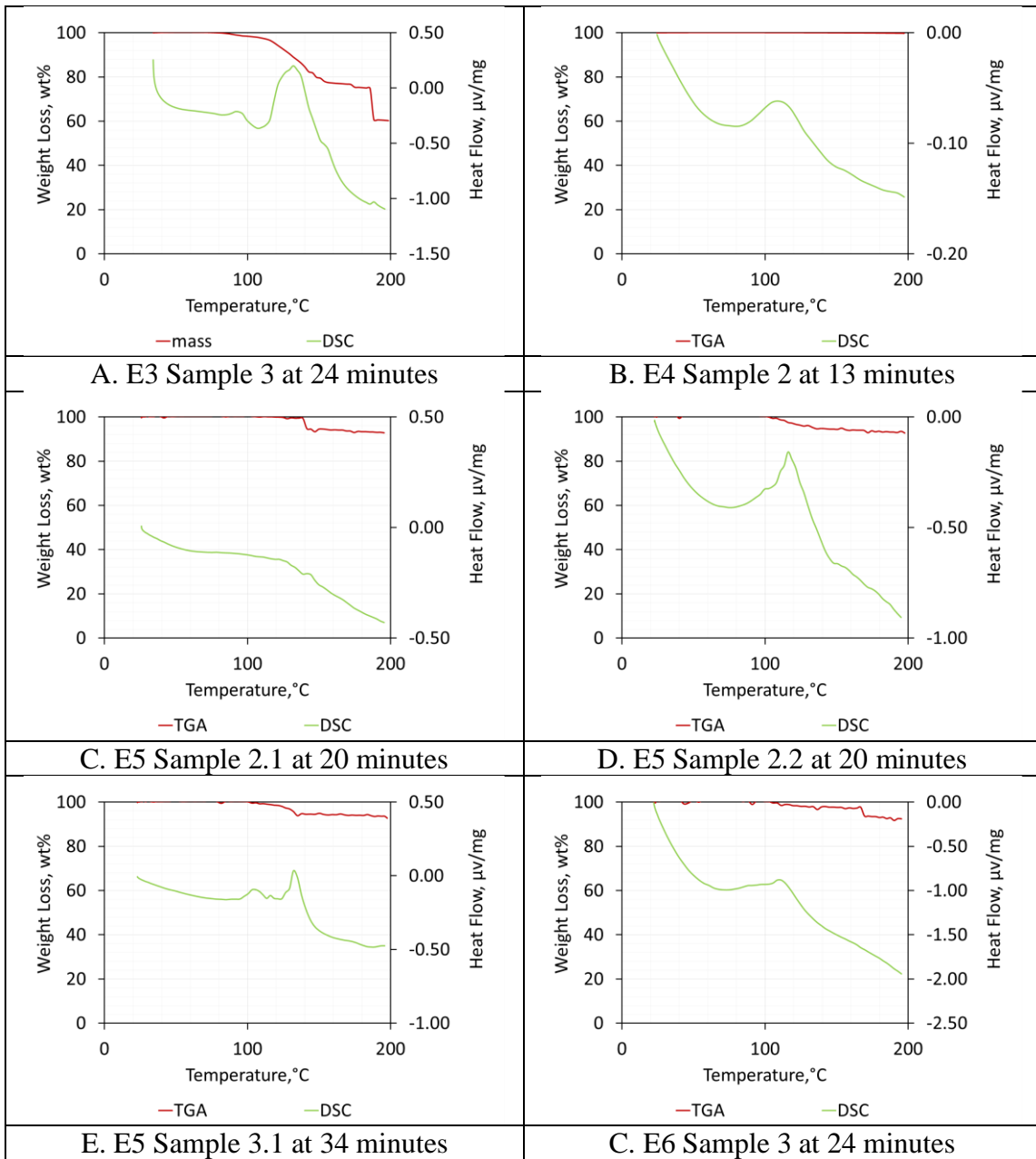


Fig. E.2 – TGA-DSC curves of produce oil samples E3, E4, E5, and E6 to determine water-in-oil emulsions content.

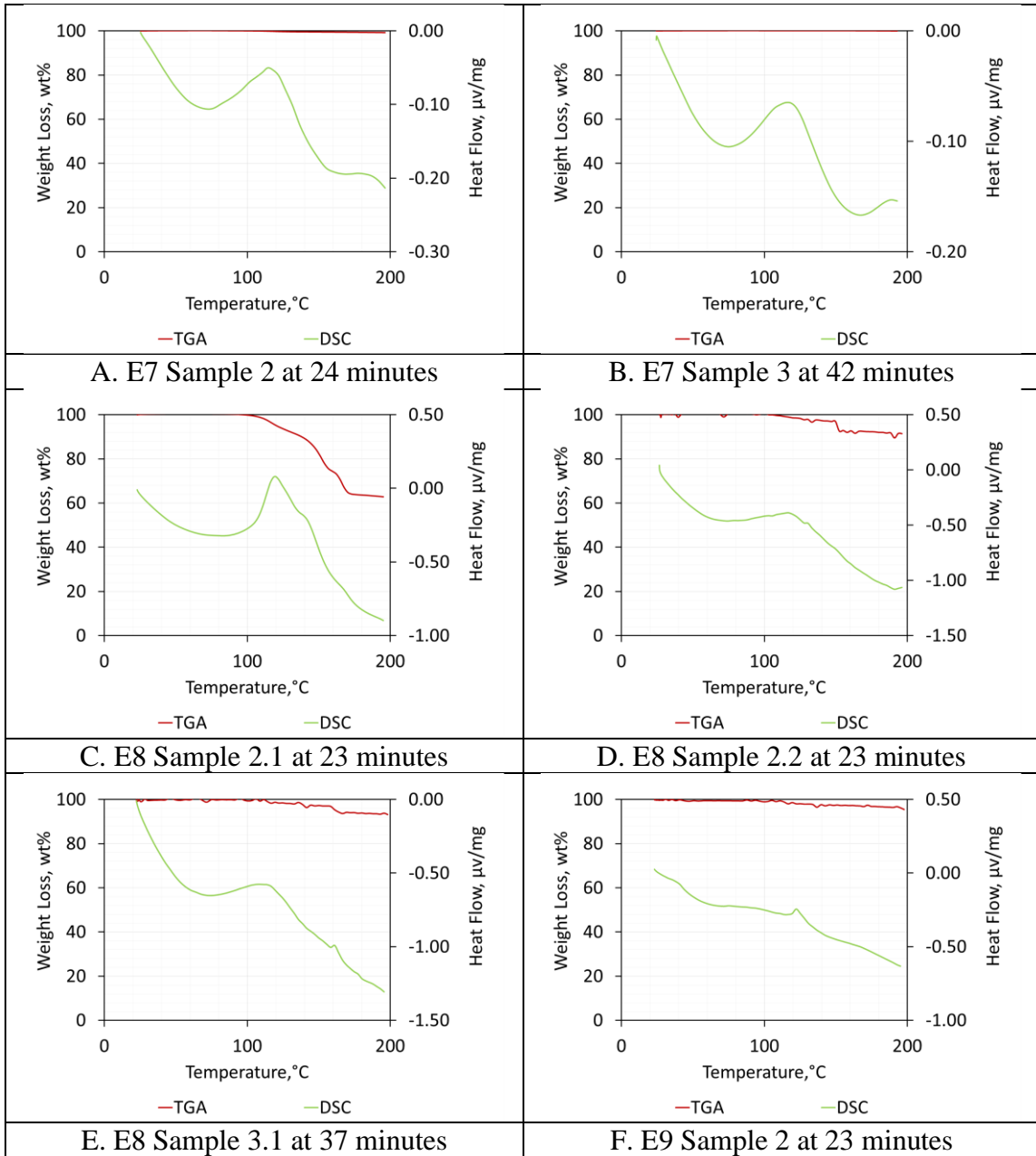


Fig. E.3 – TGA-DSC curves of produce oil samples from E7, E8, and E9 to determine water-in-oil emulsions content.

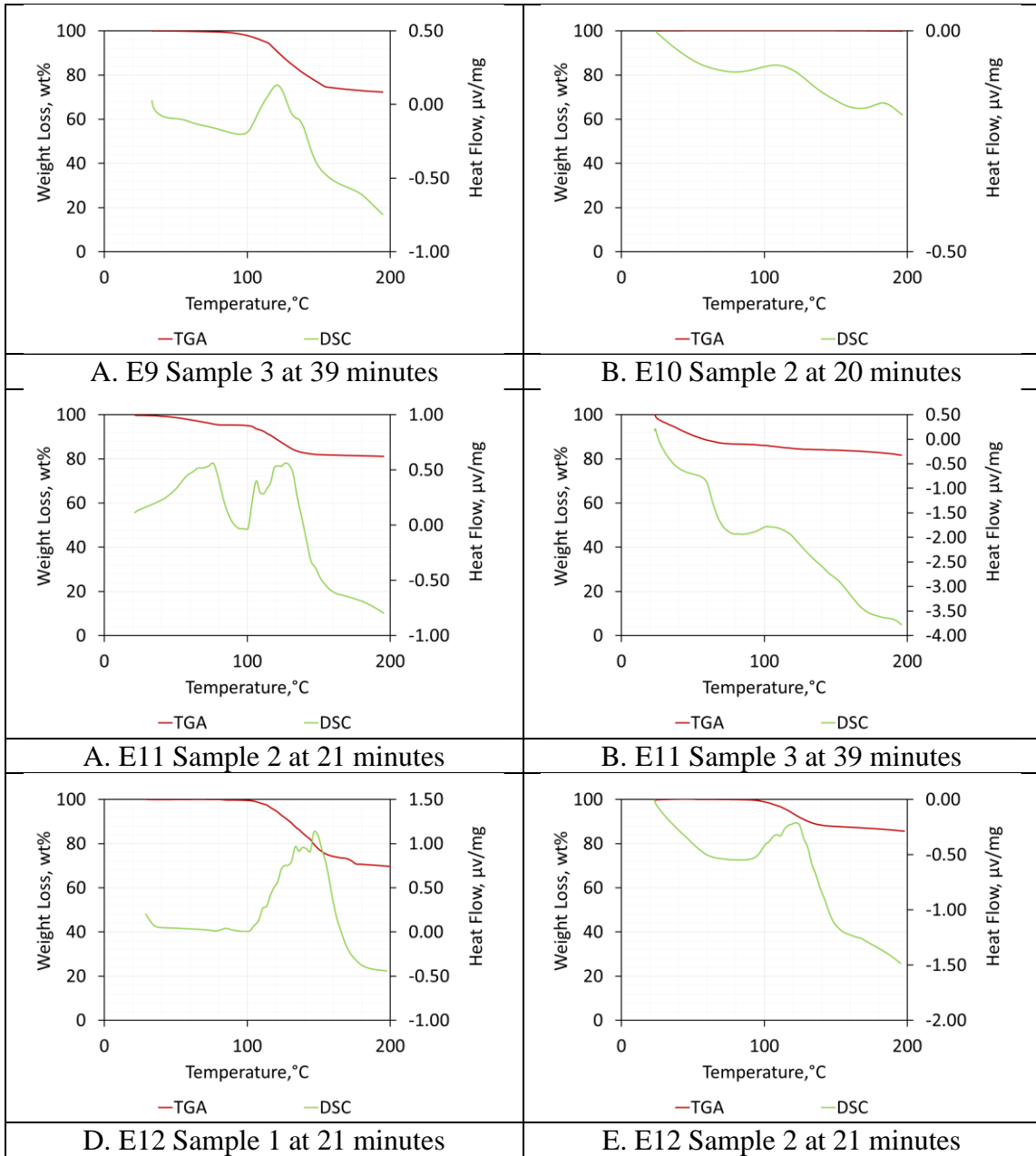


Fig. E.4 – TGA-DSC curves of produce oil samples from E9, E10, E11, and E12 to determine water-in-oil emulsions content.

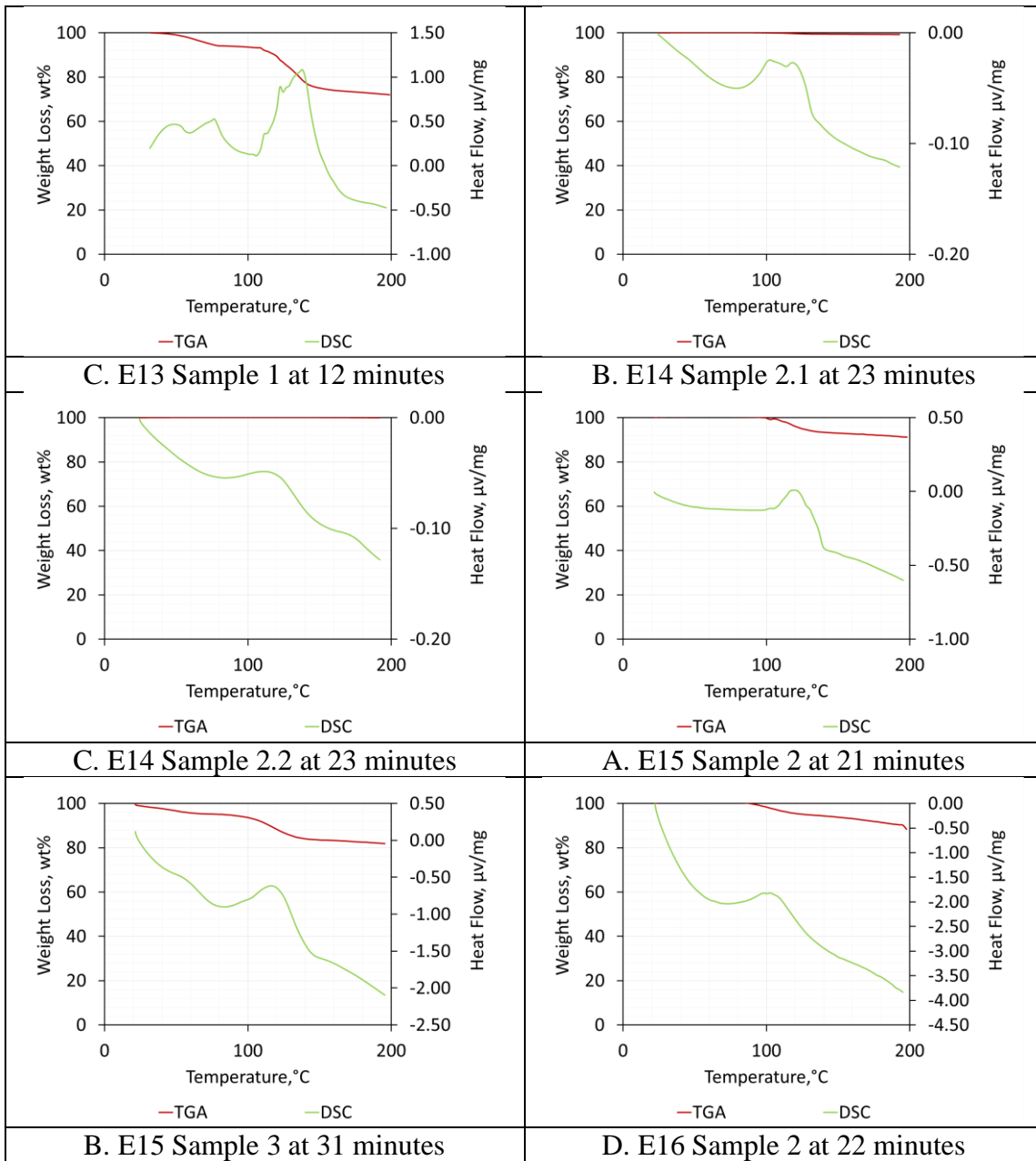


Fig. E.5 – TGA-DSC curves of produce oil samples E13, E14, E15, and E16 to determine water-in-oil emulsions content.

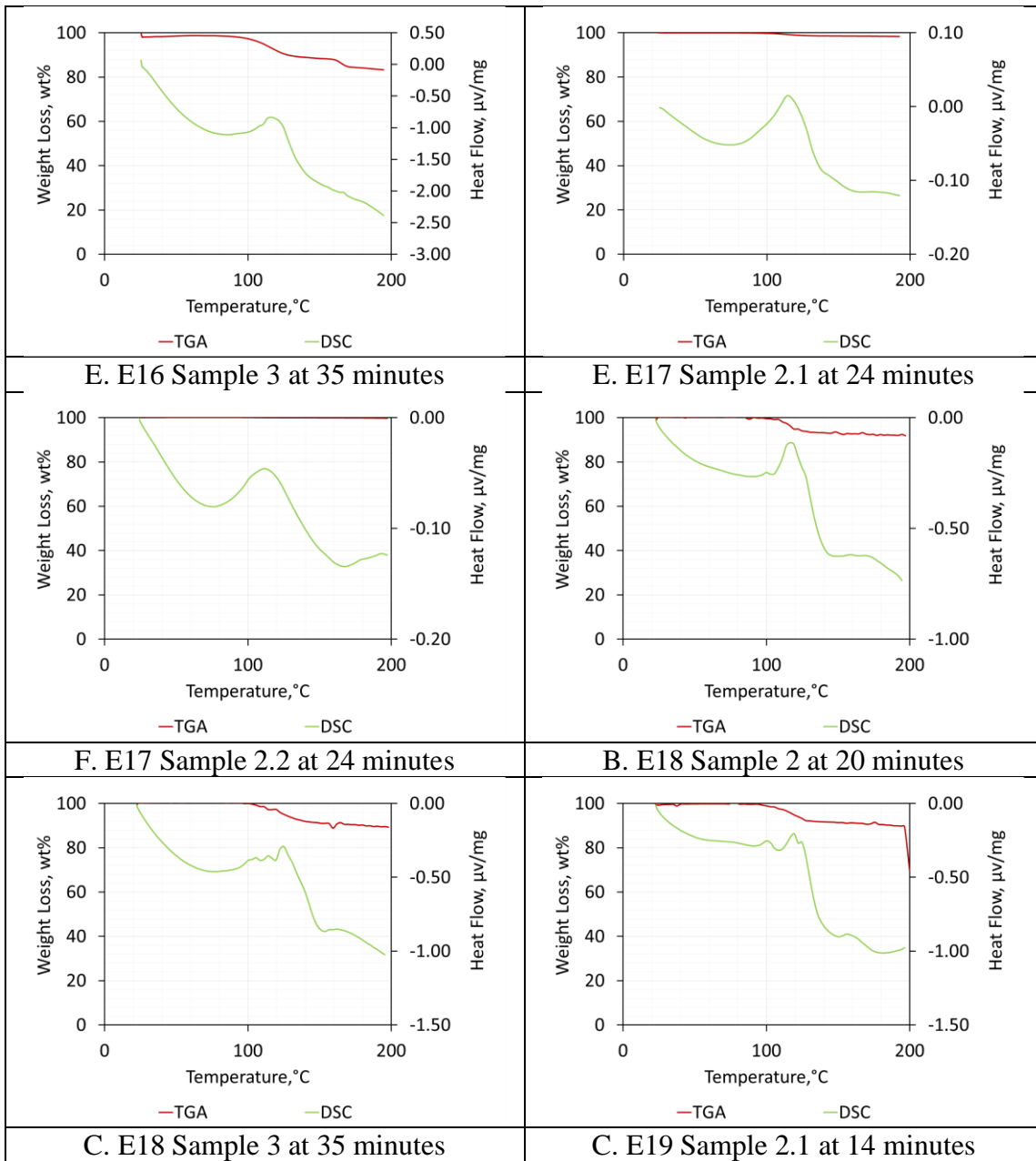


Fig. E.6 – TGA-DSC curves of produce oil samples E16, E17, E18, and E19 to determine water-in-oil emulsions content.

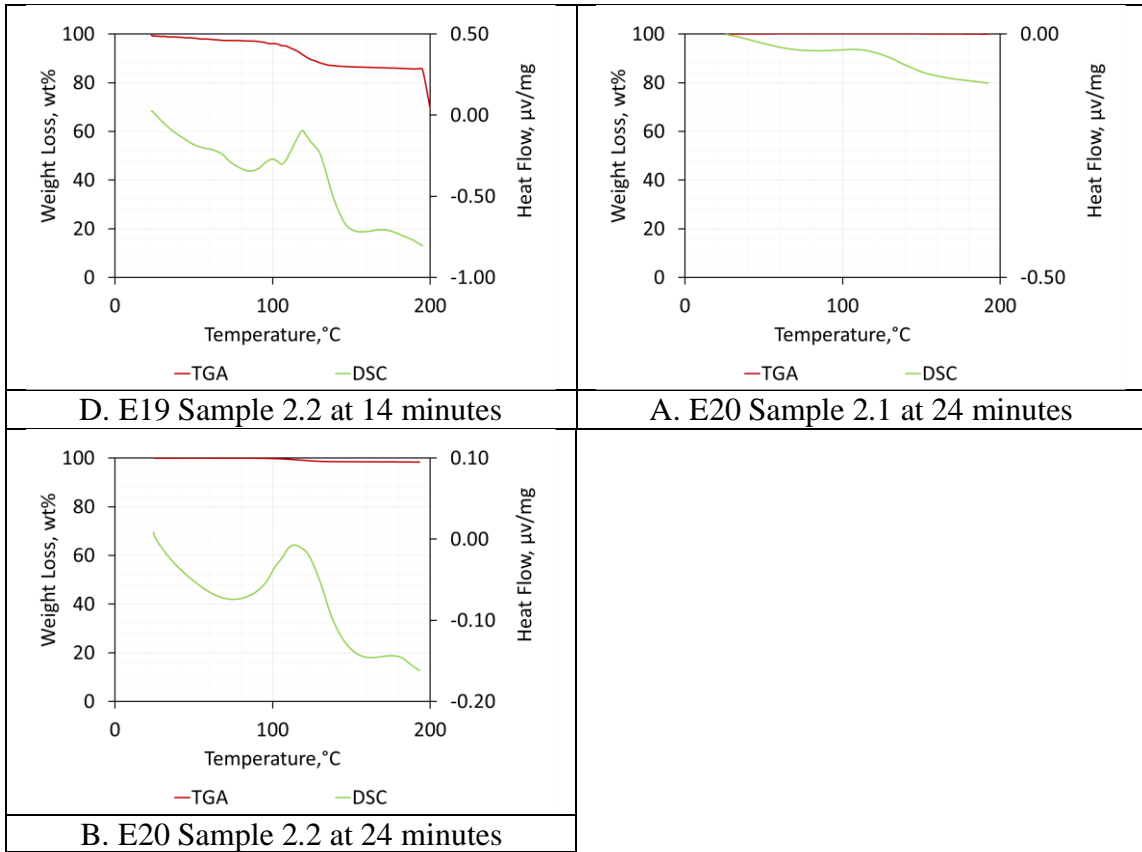


Fig. E.7 – TGA-DSC curves of produce oil samples E19 and E20 to determine water-in-oil emulsions content.

APPENDIX F

RESIDUAL OIL CALCULATION

The residual oil saturation was estimated using solvent wash method for spent rock samples (Kar et al. 2016). The residual oil saturation was estimated by weight percentage and converted to volume percentage. The below calculation is an example for 100 g of spent rock:

Sample Calculation

- A. For spent rock sample weight is 100 g, residual oil saturate in weight percentage is calculated as follow s

$$\text{Residual oil saturation wt\%} = \frac{\text{Initial sample wieght} - \text{Final sample weight}}{\text{Initial sample weight}} \quad (1)$$

$$\text{Residual oil saturation wt\%} = \frac{100 - 96}{100} \times 100 = 4 \%$$

- B. To convert residual oil saturation from weight percentage to volume percentage, the following saturation equation is used.

$$\text{Oil saturation} = \frac{\text{Oil volume}}{\text{Pore volume}} \times 100 = \frac{\text{Oil mass} / \text{oil density}}{\text{Initial oil volume} / \text{initial oil satuartion}} \times 100 \quad (2)$$

1. Pore volume of the spent rock sample (100g) can be related to the packed pore volume of the sandpack as follow.
2. Pack pore volume = initial oil volume / initial oil saturation
= (oil mass/ oil density) / initial oil saturation
= (80 g/ 0.985445 g/mL) / 0.6 = 135.3 mL
3. Pore volume of spent rock = mass of spent rock*packed pore volume/
mass of the packed sand = 100 g *135.3 mL / 720 g = 18.79 mL

Substituting into equation 2

$$\text{Oil saturation} = \frac{4/0.98544}{18.79} \times 100 = 21.6 \text{ vol\%}$$

APPENDIX G

ECONOMIC STUDY CALCULATION

To perform the economic study, the following surfactants cost is used.

Table G.1— Surfactants cost and source (Chemical 2019; Sigma-Aldrich 2019)

No.	Surfactant Name	Cost, \$/g	Source
1	Sodium Dodecyl Sulfate	0.37	Sigma-Aldrich
2	Sodium Decyl Sulphate	1.86	Oakwood Chemical
3	Sodium Octyl Sulfate	21.24	Sigma-Aldrich
4	Hexadecyltrimethylammonium Bromide	0.31	Sigma-Aldrich
5	Myristyltrimethylammonium Bromide	0.29	Sigma-Aldrich
6	Dodecyltrimethylammonium Bromide	2.77	Sigma-Aldrich
7	Triton™ X-100	0.08	Sigma-Aldrich
8	Triton™ X-114	0.07	Sigma-Aldrich
9	Triton™ X-45	0.13	Sigma-Aldrich

Sample Calculation

The following sample calculation is for surfactant-steam coreflood (E2) where sodium dodecyl sulfate is used as a steam additive. To find the surfactant cost to produce one barrel (\$/bbl), surfactant cost at maximum oil rate and oil production volume will be calculated.

- A. **Surfactant cost at maximum oil rate:** the time recorded at the oil maximum rate for E2 coreflood is 22 minutes. At this time the surfactants cost can be calculated as follows:

$$1. \text{ Surfactant solution volume} = \text{surfactant solution injection rate} * \text{Time}$$

$$= 2 \text{ mL/min} * 22 \text{ min} = 44 \text{ mL}$$

2. Surfactant weight needed = critical micelle concentration * molar mass *
solution volume = $0.00839 \text{ M} * 288.38 \text{ g/mole} * 0.044 \text{ L} = 0.1065 \text{ g}$
3. Surfactant cost at maximum oil rate = surfactant weight * surfactant cost
 $= 0.1065 \text{ g} * 0.37 \text{ \$/g} = \$0.0396$

B. Oil production volume:

1. Produced oil weight = oil rate * time
 $= 173 \text{ g/hr} * 22 \text{ min} / 60 = 63.4 \text{ g}$
2. To convert to volume oil density 0.985445 g/mL is used.
3. Produced oil volume = produced oil mass / oil density
 $= 63.4 \text{ g} / 0.985445 \text{ g/mL} = 64.4 \text{ mL}$
 $= 0.000405 \text{ bbl}$

C. To produce one barrel, surfactant injection will cost =

$$\begin{aligned} \text{Surfactant cost at maximum oil rate/ produced oil volume} &= \$0.0396 / 0.000405 \text{ bbl} \\ &= 97.8 \text{ \$/bbl} \end{aligned}$$

Table G.2— Surfactants cost to produce one barrel for Oil 1

Surf.	CMC , mM	Molar Mass, g/mol	Surf. w.t., g	Inj. Rate mL/min	Time at Maximum Oil rate, min	Solution Volume, mL	Maximum Oil rate, g/hr	Surfactant Cost, \$/g	Total Surfactant Cost, \$	Oil Recovered, g	Oil Recovered, bbl	\$/bbl
A1	8.39	288.38	0.1065	2	22	44	173	0.372	0.03960	63.4	0.000405	97.8
A2	33.2	260.33	0.2247	2	13	26	163	1.860	0.41797	35.3	0.000225	1,854.2
A3	130	232.27	0.7851	2	13	26	186	21.240	16.67494	40.3	0.000257	64,826.6
C1	0.92	364.45	0.0134	2	20	40	148	0.309	0.00414	49.3	0.000315	13.2
C2	5	336.39	0.0807	2	24	48	131	0.292	0.02357	52.4	0.000334	70.5
C3	15.6	308.34	0.2213	2	23	46	123	2.770	0.61290	47.2	0.000301	2,036.6
N1	0.9	625	0.0214	2	19	38	145	0.077	0.00165	45.9	0.000293	5.6
N2	0.2	537	0.0049	2	23	46	129	0.069	0.00034	49.5	0.000316	1.1
N3	0.1	426.59	0.0017	2	20	40	137	0.132	0.00022	45.7	0.000291	0.8

Table G.3— Surfactants cost to produce one barrel for Oil 2

Surf.	CMC , mM	Molar Mass, g/mol	Surf. w.t., g	Inj. Rate mL/min	Time at Maximum Oil rate, min	Solution Volume, mL	Maximum Oil rate, g/hr	Surfactant Cost, \$/g	Total Surfactant Cost, \$	Oil Recovered, g	Oil Recovered, bbl	\$/bbl
A1	8.39	288.38	0.1016	2	21	42	159	0.372	0.03780	55.7	0.000353886	106.8
A2	33.2	260.33	0.3976	2	23	46	161	1.860	0.73949	61.7	0.000392465	1,884.2
A3	130	232.27	1.3890	2	23	46	131	21.240	29.50182	50.2	0.000319335	92,385.3
C1	0.92	364.45	0.0141	2	21	42	76	0.309	0.00435	26.6	0.000169153	25.7
C2	5	336.39	0.0740	2	22	44	108	0.292	0.02161	39.6	0.000251822	85.8
C3	15.6	308.34	0.2309	2	24	48	132	2.770	0.63955	52.8	0.000335762	1,904.8
N1	0.9	625	0.0259	2	23	46	138	0.077	0.00199	52.9	0.000336398	5.9
N2	0.2	537	0.0043	2	20	40	113	0.069	0.00030	37.7	0.000239527	1.2
N3	0.1	426.59	0.0020	2	24	48	106	0.132	0.00027	42.4	0.000269627	1.0